Modelling and Analysis of Laser Micro-machining of Light Metal Alloys

Thesis submitted by
KAJAL KUMAR MANDAL

Doctor of Philosophy in Engineering

Production Engineering Department
Faculty Council of Engineering & Technology
Jadavpur University
kolkata, India

2018

CERTIFICATE FROM THE SUPERVISOR/S

This is to certify that the thesis entitled " MODELLING AND ANALYSIS OF LASER MICRO-MACHINING OF LIGHT METAL ALLOYS " submitted by Shri KAJAL KUMAR MANDAL who got his name registered on 05.04.2016 for the award of Ph. D. (Engg.) degree of Jadavpur University is absolutely based upon his own work under the supervision of Prof. S. Mitra and Prof. A. S. Kuar, Production Engineering Department, Jadavpur University and that neither his thesis nor any part of the thesis has been submitted for any degree or any other academic award anywhere before.

1.
Signature of the Supervisor
and date with Official Seal

2.
Signature of the Supervisor
and date with Official Seal

JADAVPUR UNIVERSITY
KOLKATA - 700032, INDIA

INDEX NO. 233 / 16 / E

1. Title of the thesis: Modelling and Analysis of Laser Micro-machining of Light Metal Alloys

2. Name, Designation & Institution of the Supervisor/s: Dr. S. Mitra and Dr. A. S. Kuar, Professor, Production Engineering Department, Jadavpur University

3. List of Publication:

- K. K. Mandal, B. Chatterjee, A. S. Kuar ,S. Mitra, "Parametric Study of Hole Taper in Laser Micro-drilling of Copper Sheet", Int. J. of Emerging Trends in Science and Technology, Vol. 03, Issue 05, May 2016, 393 – 397.
- B. Chatterjee, K. K. Mandal, A. S. Kuar ,S. Mitra, "Parametric Study of Heat Affected Zone (HAZ) Width in Laser Micro-drilling of Copper Sheet", ELK Asia Pacific Journals, Special Issue.
- K. K. Mandal, A. S. Kuar ,S. Mitra, "Taguchi-based Grey Relational Analysis of Hole Taper and Heat Affected Zone (HAZ) Width for Laser Micro-drilling of Copper Sheet", 6th Int. & 27th (AIMTDR–2016), College of Engineering, Pune, Maharashtra, ISBN: 978-93-86256-27-0,December 2016, 425 – 429.
- K. K. Mandal, A. S. Kuar ,S. Mitra, "Investigation on Kerf Width, Heat Affected Zone and Angular Deviation in Laser Micro-machining of Al 7075 Alloy", AMPT'2017, V.I.T. University, Chennai, Tamilnadu, December, 2017 – Selected for Journal publication.
- K. K. Mandal, A. S. Kuar ,S. Mitra, "Experimental investigation on laser micro-machining of Al 7075 Alloy", Optics and Laser Technology, 107 (2018), 260–267.

4. List of Patents: NIL

5. list of Presentation in National / International / Conference / Workshop:

- K. K. Mandal, B. Chatterjee, A. S. Kuar ,S. Mitra, "Parametric Study of Hole Taper in Laser Micro-drilling of Copper Sheet", Int. Conf. on Recent Issues in Engineering, Science & Technology – 2016, IER, Salem, Tamilnadu, April 8 2016, 15 - 20.
- B. Chatterjee, K. K. Mandal, A. S. Kuar ,S. Mitra, "Parametric Study of Heat Affected Zone (HAZ) Width in Laser Micro-drilling of Copper Sheet", 2nd Int. Conf. ARIMPIE-2016 ITS Engg. College, Greater Noida, UP, April 15 – 16 2016, 143 - 147.
- K. K. Mandal, A. S. Kuar ,S. Mitra, “Taguchi-based Grey Relational Analysis of Hole Taper and Heat Affected Zone (HAZ) Width for Laser Micro-drilling of Copper Sheet”, 6th Int. & 27th (AIMTDR–2016), College of Engineering, Pune, Maharashtra, ISBN: 978-93-86256-27-0, December 2016, 425 – 429.
- K. K. Mandal, A. S. Kuar ,S. Mitra, “Investigation on Kerf Width, Heat Affected Zone and Angular Deviation in Laser Micro-machining of Al 7075 Alloy”, AMPT'2017, V.I.T. University, Chennai, Tamilnadu, December, 2017 – Selected for Journal publication.

Dedicated

To

My Respected Parents Late Pradip Mandal & Late Subala Mandal

And

My Beloved Wife Tanima Mandal & Daughter Kuheli Mandal

Preface

The modern industries is urgently leading towards miniaturization of components. Many industries like, aerospace, spacecraft, biomedical, automobile, consumer electronics, etc. are seeking for micron level to sub-micron level quality characteristics at low cost and high speed maintaining its quality, accuracy and precision and complex contour. Few specific application include micro-scale batteries and fuel cells, micro-nozzles for high temperature and high speed jets, micro-holes for fiber optics, medical implants, diagnosis, micro-scale pumps/valves/mixing devices, micro-fluidic system optical lenses, deep X-ray lithography masks, etc. The above mentioned components need a rapid growth in innovative machining processes which is continuing over the years. Till now it is possible to produce complex shaped micro-components made of different types of engineering materials like, metals, alloys, light metal alloys, ceramics, composites, polymers, etc. based on their demand in the modern industries due to their excellent properties. Among various micro-machining methods, laser beam machining process can be utilized for different operations such as micro-drilling, micro-cutting, micro-channeling, micro-milling, micro-turning, micro-grooving, etc. Laser beam has the wavelength ranging between ultraviolet to infrared radiation. It is highly coherent, convergent and monochromatic beam of elecromagnetic radiation due to which it can be focused to a very narrow area with very energy density. This concentrated high energy is responsible to remove unwanted material from the workpiece by melting, vaporization and chemical degradation. Laser beam process has several advantages like, non-contact type processing, almost all materials can be processed, high productivity, elimination of further finishing operation, minimum heat affected zone (HAZ), narrow kerf width, improved quality, adaptability to automation, reduced processing cost, etc.

In this present research work, pulsed Nd:YVO_4 laser system is used for micro-machining of Al 7075 alloy to investigate the effect of processing parameters like, laser beam power, pulse frequency, scanning speed and repetition rate in searching of

better product quality in terms of kerf width, HAZ and angular deviation as well as surface roughness. This laser system has alsobeen utilized for micro-drilling of copper sheet to explore the influence of laser beam power, pulse frequency, scanning speed and number of pass on hole taper and HAZ width for finding better hole quality. Micro-channeling is fabricated on Beryllium-Copper alloy using diode-pumped fiber laser. Responses like, kerf depth, kerf width, HAZ, overcut and angle are observed and analyzed considering laser beam power, pulse frequency and scanning speed as the influencing parameters.

The author has tried heart and soul to justify the uniqueness of the present research to identify optimal parametric combination for laser beam micro-machining operation through different design of experiment, optimization and prediction technique applied for experimental analysis.

It is expected that researchers and manufacturing scientists will be benefitted from this present research work as a lot of insights and clear understanding are provided related to various feature of laser beam micro-machining with proper direction and guidance for choosing the parametric setting to meet the objectives like, minimum kerf width, minimum HAZ, minimum surface roughness, minimum hole taper, maximum hole circularity, etc.

Further, the author believes that the present research work will provide a great momentum for successful utilization of laser beam micro-machining technology for light metal alloys. The research finding can be applied in the area of aerospace, missile, spacecraft, biomedical, consumer electronics, etc. It will be very helpful for effective direction towards further research in the field of newer advanced machining processes.

ACKNOWLEDGEMENT

The success and final outcome of research work required a lot of guidance and assistance and direction from many people and I am extremely fortunate to have got this opportunity, and I do not forget to thank them.

I took the opportunity to express my sincere gratitude and indebtedness to Prof. (Dr.) Souren Mitra, Ph. D. supervisors and Prof. (Dr.) Arunanshu Sekhar Kuar, Ph. D. supervisors & Head of Production Engineering Department for their constant valuable advice, guidance and encouragement. It is because of their continuous guidance, support and valuable advice at every aspect of the problem from the developing to the developmental stage, that my thesis has seen the light of this day.

Beyond this I would like to express my grateful thanks to Mr. Nilanjan Roy and Mr. SadipKonar of the Department for their inspiring instructions and active help without which it would not have been possible to complete this thesis report.

I would like to thank my friends & other persons who for their valuable advices, suggestions and kind cooperation directly or indirectly andof course my family for their continuous support.

I also express my gratitude to Jadavpur University authority, NERIST (my home Institute) and All India Council for Technical Education (AICTE) for giving me the opportunity to do my research at Jadavpur University.

Date:_____ _____

Place:_____ **(KAJAL KUMAR MANDAL)**

Index No. 233 / 16 / E

VITA

The author, Kajal Kumar Mandal, son of Sri PradipMandal and Smt. SubalaMandal, was born on 27th Day of December 1972, in a remote Village of Sundarban Delta Region i.e., Jogeshganj, P.O. Jogeshganj, P.S. Hingalganj (Recenly, Hemnagar Coastal), Dist. North 24 Paraganas, West Bengal, Pin Code - 743439. INDIA. He passed Madhyamik (10) Examination from Jogeshganj High School (HS) under WBBSE Board in 1988 and Higher Secondary (10+2) Examination under WBCHSE Board from the same School in 1990.

The author has obtained his B.M.E degree from Jadavpur University, Kolkata in the year of 1995 through WBJEE. He received his M.Prod. E. degree in 1998 from the same university through GATE.

He was engaged on research from that time i.e. 1998 onwards in the Department of Production Engineering, Javadpur University, as a Technical Project Assistant. In the year of 2000, he joined as a Senior Research Fellow in the same Department.

The author accepted the offer of appointment as a Lecturer, Mechanical Engineering Department of North Eastern Regional Institute of Science and Technology (NERIST), Nirjuli (Itanagar) 791109, Arunachal Pradesh in the year of 2001 and he joined on 10.07.2007. At present, he is serving this Institute as an Assistant Professor. He is involved various academic activities related to the Institute as well as his career. He has published research papers in reputed International Journals. He has also published and presented several research papers in different National and International Conferences.

List of Tables

List of Figures

TABLE OF CONTENT

Chapter 1

INTRODUCTION

From the very beginning of aeronautic industry, aluminium, copper and their alloys have played a crucial role in its development. Nowadays, different aluminium alloy families are the base material of aerospace vehicles and automotive industries also. They are also used simultaneously in miniature components like sensors, circuit board. At present, the materials that serve as the base of the principal light metal alloys are made of aluminium, copper, titanium and magnesium.

Laser beam machining (LBM) is one of the best thermal-energy based un-conventional and non-contact (between tool and job) type advance material processing technique. It can be utilized for almost all types materials, i.e. metal, non-metal, plastics, ceramic, composite, alloy, super alloy, etc. Also this process gets its importance for light metal alloy, specially aluminium alloys (due to huge demand in aeronautic industry, versatility and improved finish), machining for small sizes

application. Focused laser beam is applied to remove unwanted material through melting and vaporizing from the workpiece. It is also applicable to produce complex profile with miniaturization of sizes. In the year of 1960, first working Ruby laser was invented by Dr. Theodore Maiman. Even 58 years later from the invention of laser, a continuous development for new, better and compact laser set-up has been observed. During the last decade, number of ways/techniques were developed and modeled to analyze and optimize the process parameters and quality characteristics for the betterment of laser beam machining performance. Nowadays the interest is put on precise machining of sheet material, specially for reflective material like aluminium, copper and their alloys. As the shorter pulses reduce the chances of damage due to heating effect, it is used for micro-machining application and the accuracy become nanometer range. Also, by reducing wavelength very small feature sizes can be produced due to better absorption of heat by the material and reduction in reflectivity of the incident radiation.

Laser beam machining is utilized for different applications like making of mould, manufacturing of automotive, aerospace, biomedical, electronics, etc. industries. Nd:YAG and CO_2 laser are the most established laser among different type of laser available. Few others are Excimer, ND:YVO_4, Ti:Sapphire, etc. To enhance the laser efficiency, diode laser is used for pumping to other lasers. Recently, fiber laser with diode pumping facility is getting more importance due to comparatively high efficiency, easy to control and compactness.

For efficient and economic cutting, selection of cutting parameters with workable range should be optimum for any types of material to be processed. There are several statistical method available which are used for modelling and optimization. Design of experiment, modelling, optimization and prediction of process parameters and quality characteristics are to be performed by using different types of statistical methods. Recently, hybrid i.e. coupled methodology/technologies are getting more importance to the manufacturing engineers for better performance.

1.1 LIGHT METAL ALLOYS: CHARACTERISTICS AND APPLICATIONS

The growing demand of spacecraft, automotive and aerospace industry leads towards the lightweight structure as well as lightweight design principle to improve energy efficiency and sustainability. Due to the high specific strength and durability, light metals alloys act as real security relevant light weight components. Light metal alloys have become of great importance in several industries. They yield to plastic working, find extensive application in the automotive, railway engineering, machine-building, aerospace and aviation industries, etc. due to reduction of weight of the components. Under plastic worked condition, light metal alloys additionally offer advantageous fatigue characteristics. Few examples, light metal alloys are aluminium alloys, copper alloys, titanium alloys, magnesium alloys, etc. [1, 2].

Aluminium Alloy: About 60% of aircraft structure is fabricated from aluminium alloy. The Al 2017 alloy (T451) is excellent for bending and press-forming work with enough resistance against corrosion and has good strength. It is mostly used to produce automotive components, aviation & aerospace industries, precision machine parts and aircraft structure.

Al 7075 alloy is strong, can be compared to steel with good fatigue strength, average machinabilty properties. It contains roughly zinc 0f 5.6 to 6.1%, magnesium of 2.1 to 2.5 %, copper of 1.2 to 1.6%, silicon < 0.5%, and very amount of iron, manganese, chromium, titanium, etc. Al 7075 alloy has a density of 2.81 g/cc. It's mechanical properties are greatly dependent on the temper of the alloy as follows:

Al 7075 - 0 temper (without heat treatment): Tensile strength is as high as 280 MPa and maximum yield strength may be up to 140 MPa. It shows elongation before failure of 9 - 10% and highly corrosion-resistant property.

Al 7075 - T6 temper: It shows tensile strength in the range of 510 to 540 MPa and yield strength more than 430 MPa, elongation at failure 5 - 11 %. This alloy is

obtained homogenization of Al 7075 casting at a temperature of 450^{o}C for 6-7 hrs followed by quenching followed by ageing at 120^{o}C for a day.

Al 7075-T651 temper: Tensile strength may be as high as 570 MPA with yield strength up to 500 MPa and elongation at fracture condition is 3 - 9 %.

Al 7075-T7 temper: Tensile strength may be as high as 505 MPA with yield strength up to 435 MPa and elongation at fracture condition is up to 13 %. This alloy is achieved by two successive ageing of Al 7075 alloy at 100 - 120^{o}C for several hours followed by 160 - 180^{o}C for more than 24 hours. T7 temper is made of very fine micro-structure which allows grain growth along the boundaries and thereby chances of better stress corrosion cracking.

Al 7075 alloys are widely used in automotive, aerospace, missile, aviation, marine and transport application mainly because of very good strength/weight ratio. Even, airframes for hang glider, equipment for rock climbing, frames for inline skating are also manufactured from Al 7075 alloys. High quality M16 rifles and mould tools are manufactured from this alloy due to high strength, low density, highly polishing property and good thermal properties. Al 7075 alloy may also be used to produce a further refined alloy, like 7020 and 7050 [1 - 4].

Copper Alloy: Copper and zinc is used to form brass and looks like yellow in colour. Amount of zinc may be 0 - 40 %, however to maintain good corrosion resistance properties, it is limited by 15 %. Brass is sensitive to leaching corrosion under certain condition; during leaching from the alloy a spongy copper structure is formed. Brass is used in musical instrument, antimicrobial container, etc.

When copper as the base metal is mixed with other element (most of the cases it is tin; it may be aluminium, phosphor or silicon) except zinc, they are generally named as bronze. Aluminium bronze has higher strength and corrosion resistance than other types. Aluminium forms a thin passivasion layer on alloy surface. It can be used for molding & trim shapes, thread plates, decorative parts, marine parts, bush and bearing, aircraft engine parts, etc.

Beryllium-copper (BeCu) or copper-beryllium (CuBe) alloy is also known as beryllium bronze or spring copper. It contains about 0.5 - 3 wt. % of beryllium and small amount of other element like nickel and cobalt in addition copper [5]. It has high strength, ductility, weldable, metal working, forming and machining properties, non-magnetic and non-sparking qualities. It is highly resistance to non-oxidizing acids, plastic deformation, abrasive wear and galling. After heat treatment its strength, durability and electrical conductivity can be increased. The attainable strength may be as high as 1400 MPa and thermal conductivity may reach up to 62 Btu/ft-deg. F-H. It is used specialized application of tools working within hazardous environment, musical instrument devices, bullets, aerospace & aviation, load cells, spring wire, oil rings, etc [1 – 5].

Titanium Alloy: One of the well known Ti6Al4V is a two-phase precipitate strengthened titanium alloy. It is used due to very good synchronization between plastic properties & strength and easy formability. By hyper-quenching and ageing processes, its tensile strength can be improved on simultaneous decrease of plastic properties. This alloy is widely used to make components of racing cars, aviation, aerospace, landing flaps, machine-building, railway industries, chemical industries like hydraulic and pneumatic tubing, etc [3, 4].

Magnesium Alloy: Magnesium alloy contains the other element with variable quantity. However, commercial magnesium alloy is made of 3 to 13 wt.% aluminium, 0.1 to 0.4 wt. % manganese and sometimes 0.5 to 3 wt. % zinc. They can be hardened by heat treatment. AZ31 alloy is characterized by good mechanical properties and low cost. Due to its light weight, its application is seen in automobile, aerospace, aviation industries. Properties of alloys are far better than that of casting alloys. AZ63 and AZ92 alloys are generally used for sand casting parts, AZ91 alloy is used for die casting parts and AZ92 can also be employed for permanent mould casting components. On the other hand, forged and extruded components are manufactured from AZ61 and AZ80 due to their very high strength among all magnesium alloys. The best magnesium alloy available based on all properties is Mg - Al - Zn -Mn, consists of 8 wt.% Al, up to 1.5 wt.% Zn and up to 2 wt.% Zn [1 - 4].

1.2 NEED FOR LASER MICRO-MACHINING OF LIGHT METAL ALLOYS

The term micro-machining is defined as the dimension of removed material for production of a component lies between 1 to 999 μm in general; though 1to 500 μm is recorded as the values of micro-machining according to Scientific Technical Committee of the Physical and Chemical Machining Process of CIRP [6]. The laser beam micro-machining process has several advantages over other machining processes as follows:

- It results narrow kerf width with more feasible arbitrary contours.
- Wastage of material is reduced due to narrow kerf width.
- Possibility to achieve high cutting/scanning speed.
- Narrow HAZ can be attained as the quantity of total input heat is small concentrated within the machining zone and damage of base material is avoided.
- Very little distortion effect and residual stress is observed.
- Can be applied for both very soft i.e. deformed easily as well as very hard i.e. difficult-to-cut materials.
- Complex geometric profile can be formed due to high degree of flexibility.
- Very sharp cut edge like square shape can be formed.
- There is no tool wear and mechanical force; so damage of precision components can be avoided. Also, it avoids the use of complicated job holding device.
- It is suitable for making miniature holes because of high energy density of laser beam by varying the wavelength in sheet metal of light metal alloys which may be difficult by other methods.
- In laser micro-machining, shorter pulses reduce dross formation, cracks of material which opens a new era for nano-meter accuracy with little or no collateral damage.
- Micro-machining provides high precision which need not further finishing.
- Laser beam can be paired with assist gas to make the process more efficient, by minimizing oxidation effect of the surface.

However, Laser machining process has some limitations also in spite of those advantages. The principal limitations of laser machining are the following:

- It is somewhat difficult to cut highly reflective and conductive material.
- Generally, laser is applicable for thin materials.
- Initial capital investment cost is high compared to other machining sources.
- Dangerous exhaust fumes may be produced during processing of polymers.

Light metal alloys can be machined by conventional processes using various methods. The machining is dependent not only on the type of surface to be produced but also dependent on the size (i.e. macro, micro), accuracy, precision and surface roughness values (i.e. in the range of micro-meter or nano-meter) [7]. In general the conventional machining processes are turning, drilling, milling, grinding, etc. For finishing purpose, reaming, honing, lapping may also be followed to improve the accuracy, precision and surface roughness.

However the problems encountered in these conventional processes are wastage of material, more HAZ, surface roughness is not so good, more taper, high kerf width, miniature production is difficult, etc.

Utilizing laser micro-machining, the problems during conventional machining can be overcome; even can be improved a lot. Following are the some improvements of laser micro-machining process over conventional processes:

- Miniature jobs in the range of micrometer with complex shapes can be produced easily with a minimum loss of material.
- No tool wear.
- Surface roughness is very good; in the range of nanometer.
- Very narrow cutting/kerf width is possible.
- Very small heat affected zone.
- Taper of the hole can be minimizes [8, 9].

1.3 FUNDAMENTALS OF LASER MATERIAL PROCESSING

1.3.1 Laser Beam Generation

"LASER" is an acronym for light amplification by stimulated emission of radiation, laser beam is a form of electromagnetic radiation. When electrons (within special glasses, crystal or gases) absorb the energy from electrical current become "exited"; the laser is generated. State of electron before and after the excitement is represented in Fig. 1.1. At the same time, exited electrons move from a lower energy orbit to a higher energy orbit around the nucleus of the atom. When these exited electron come back to normal i.e. "ground state", they discharge photons of same wavelength and coherent in nature in the form of light particles. Laser light is also directional and creates a very tight beam and then defused. Due to the coherency, laser can be focused for a vast distance [10].

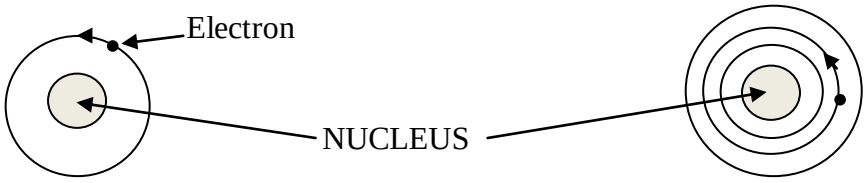

(a) Ground State (b) Excited State

Figure 1.1 State of Electrons at Different Levels

In a simple way, light can be described as electromagnetic radiation which would be visible by human eye. It has the wavelength ranging between ultraviolet and infrared radiation; about 0.37 - 0.75 μm and frequency of 10^{15} Hz. Whereas, laser has the wavelength of 0.2 - 500 μm i.e. in the range of X-ray, through ultraviolet and Infrared radiation [11]. Simply, laser generation is the effect due to emission of energy at transmission condition of electrons from a higher energy level/orbit to a lower energy level/orbit within an atom during absorbing photon. During that time, exited atom releases another photon when itself stimulated by a photon, and causes stimulated emission with same characteristics and ultimately high degree of coherence is occurred. Under thermal equilibrium condition, the rates of upward and downward

transitions are same, and the distribution of atoms at various levels of energy will follow Boltzmann's law. At a certain temperature and high frequency, rate of spontaneous emission is much higher than stimulated emission, whereas it will be opposite when frequency is low but temperature is same. The scheme of the laser generation process is represented by Fig. 1.2.

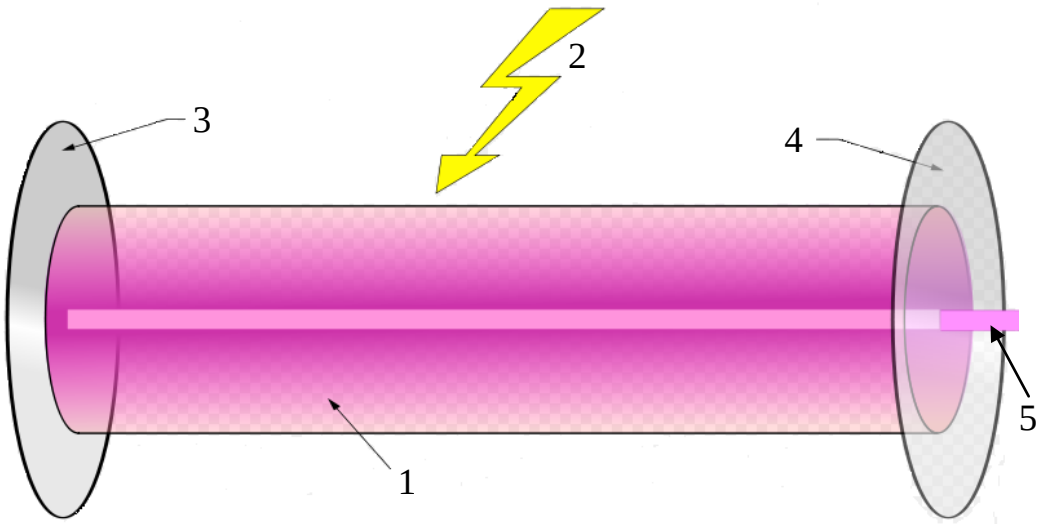

Figure 1.2 Scheme of LASER Beam Generation

1. Gain medium (rod)
2. Laser Pumping Energy (flash lamp)
3. High Reflector (fully transparent)
4. Output coupler (partially transparent)
5. LASER Beam

When laser beam propagates through an absorbing (fluid) medium, beam intensity diminishes exponentially following Beer - Lambert law. To increase the beam intensity further, population inversion is maintained at certain threshold/critical value. For this purpose, pumping is required. Pumping is the process of raising the atoms to higher energy level/orbit from lower energy level/orbit. Under extreme energy density condition, multi-photon absorption happens, and as a result incident radiation become ultrashort and pulsed. There are mainly two techniques of pumping which are optical pumping and electrical pumping [12, 13].

A. Optical Pumping

An intense source of light is used for the purpose of excitation of active medium i.e. for pumping. Generally two varieties of laser sources are utilized for optical pumping, which are (a) arc/flash lamp and (b) diode laser. One of the scheme of optical pumping system is shown on Fig. 1.3.

Arc/Flash Lamp Pumping

Arc/flash lamps are usually utilized for liquid or solid state lasers. As the output of the lamp is of broad bandwidth, large part of source energy is wasted. To minimize this lost, active medium should be of broad linewidth for efficient absorption of energy into the surface [14].

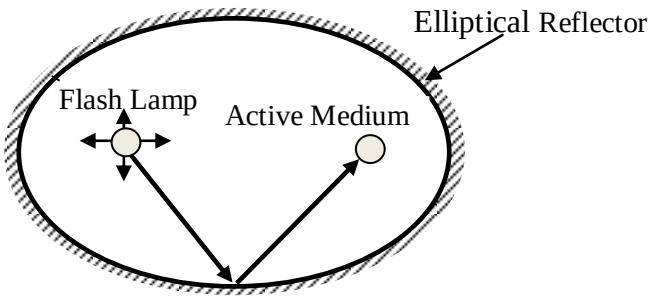

Figure 1.3 Scheme of Optical Pumping System with Elliptical Shaped Cavity

Diode Laser Pumping

Efficiency of the optical pumping system is required to increase further, which is done by using diode laser for pumping. It is seen that very little energy is wasted as the laser used for pumping charges energy at a certain specific wavelength. For this purpose, the range of output wavelength of pumping diode laser should nearly equal to absorption bandwidth of active medium being pumped. Compared to other lasers, diode lasers is very convenient and they have developed to pump other lasers. Advantages of diode laser pumping are:

- Due to relatively high efficiency, electrical power consumption requirement is low for a certain desired output power.
- Under stacked condition, they may produce high output power.
- Available with different wavelengths.

- Much smaller in size, which makes then more portable.
- Working life is more than 12,000 hours compared to arc or flash lamp.
- Efficiency of the system may be reached up to 30 - 40 % as compared to that 1 - 3 % for the lamp based pumping system.
- They require very less maintenance [14].

B. Electrical Pumping

It is convenient and generally used to semiconductor and gas lasers due to their narrow absorption bands. Electrical of 1to 2 kV at low current of 50 mA is passed through the medium and electrical discharge is created during pumping process. Kinetic energy of generated electrons is increased due to the presence of electric field and accelerated. These accelerated electrons are capable for the excitement of atoms, ions/molecules and then collide with them. Due to collision, kinetic energy of electrons is imparted to reach at higher energy level [11, 13]. One of the scheme of electrical pumping system is shown in Fig. 1.4.

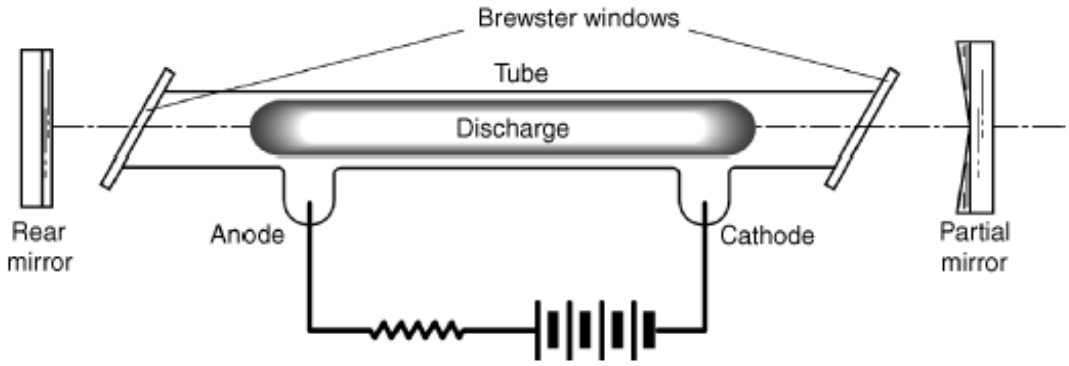

Figure 1.4 Scheme of Electrical Pumping System (Courtesy: K. A. Elijah Jr., Copyright: John Willey & Sons Inc., 2009)

1.3.2 Different Laser Sources

There are different types if laser sources with different characteristics depending on the active media utilized for laser action. Principal industrial laser, specifically used for material processing are as follows:

A. Solid-state laser

They use normally host lattice made of insulating crystal or glass embedded with dopant, active media. Dopant is usually a transition or rare earth element. In this type of laser, the form of the active medium is either like a rod or slab. Generally flash lamp is used for pumping. Rod temperature might be controlled through circulation of air or liquid around it to avoid any change of cavity dimensions and modes. Most of the solid state lasers produce pulsed beams and few of them generate continuous beams. Though they have shorter coherence length which are unsuitable for interference-based application, but significant amount of energy is available for energy-burst application. Common examples are Ruby, Nd:YAG, Nd:YVO_4 laser 12].

Nd:YAG Laser: Crystal made of yttrium aluminium garnet ($Y_3Al_5O_{12}$) is used at the host lattice. It can work on both continuous wave (CW) and pulsed wave (PW) mode. A xenon flash at medium pressure or krypton lamp at pressure may used where rod size usually within the range of 0.5 - 1.0 cm in diameter and 5.0 to 20 cm in length. The power output may vary between 150 - 6000 W for the case of CW mode and up to 50 MW for pulsed mode with 20 ps pulse duration and repetition rate of 1 - 100Hz. To get high power in case of CW mode, multi-rods, even diode laser is used for pumping. Efficiency is very, in the order of 1 to 3 %. This laser used for surgery and material processing like drilling, cutting, welding, surface modification, etc [12].

Nd:Glass Laser: Here different types glass like phosphate, silicate or fluoride with 1 to 5 % Nd^{3+} is used as the host lattice. The size of rod may be 1 meter length and diameter of 50 mm. Power output per unit volume is more and pulse width is as small as 5 ps compared to Nd:YAG laser. It can be operated at multi-mode condition due to additional inhomogeneous broadening helps in variation of ion environments. Due its low thermal conductivity, application is limited for CW mode for manufacturing operations like drilling, spot welding, very narrow hole, etc [12].

Nd:YVO_4 Laser: Here host lattice crystal is made of yttrium orthovanadate (YVO_4) doped in neodymum. It has three main sub-systems which are Laser Unit, Control Unit and Workstation which are interfaced with a computer. The typical ranges of parameter for a pulsed laser are maximum laser power of 12 Watts, wavelength of

1064±4 nanometer, spot beam diameter of 50 micrometer and pulse width of 24 - 100 nanosecond. This laser is used for drilling, marking, cutting of thin sheets [79].

B. Gas Lasers

Usually it is used for industrial application. It's power output may be few kW for CO_2 laser or few miliwatts for He-Ne laser, and they may work on both CW, PW mode at a frequency ranges from ultraviolet to infrared. Here, gas is used as the active medium with poor broadening mechanism and relatively small linewidths. As a result, the energy levels are small which requires sharp emission for excitation. Electrical pumping is commonly used for exciting the active media [13].

C. Dye Laser

Here, organic dye is used as the active medium. The dye made by some solid which may dissolved water, ethyl alcohol, methyl alcohol, etc. Different types of dyes are used for this laser, which are listed in Table 1.1. The lasing dye has two states of energy level structure. In singlet state (Si), total spin of electrons in each level is zero. Whereas, in triplet state (Ti), total spin of electrons in each level is 1. Each energy level of electrons is formed by a number of vibrational level which again consists of a number of rotational levels. During coupling with line broadening, the rotational levels essentially overlap. The output power is in the range of 10 to 100 mW for CW dye laser, while the power output for pulsed mode is of 100 W and a maximum power of 1 kW, and the pulse is of the order of few ps. The dye laser is used in the area of detection of pollution, spectroscopy, separation of isotopes, etc [14].

Table 1.1 Various Types of Dye with Corresponding Wavelength [12]

Name of Dye	Approximate Wavelength (μm)
Scintillator	Less than 0.4 μm
Coumarin	0.4–0.5
Xanthenes	0.5–0.7
Polymethine	0.7–1.0

D. Semiconductor (Diode) Laser

Semiconductor or diode laser is based on the generation of photons due to recombination of electrons in the conduction band with the holes of valence band. At absolute zero temperature, an intrinsic semiconductor is considered as an idle case when valence band is filled totally. Due to pumping, electrons are excited move from conduction band to valence band and thereafter, they drop down suddenly to the state of lower energy level within lifetime of 0.1 picoseconds. Similarly, redistribution of electrons is occurred in the valence band for filling lowest empty level which creates more holes in top of valence band. As a result, thermal equilibrium of semiconductor is disturbed though localized equilibrium in every band. Quasi-Fermi level is considered to separate the totally filled and empty levels in a band which are Fv and Fc for the valence and conduction band, respectively; whose values are dependent on number of electrons pumped to conduction band. Under equilibrium condition, Fv = Fc. When the bottom of conduction band is filled with electrons and top of valence band contains holes, then population inversion is observed between two bands. Emission of photon i.e. light wave or phonon i.e. thermal wave is dependent on the type of material during drop down and recombination with holes of electrons.

In case of silicon and germanium, no laser action can be obtained as emission of radiation is in the form of phonon. Whereas, in case of gallium and arsenide, laser action is achieved as radian is emitted in the form of light (photons). Laser action can easily be obtained for a semiconductor using diode of p-n junction due to the difference in energy levels of valence band and conduction band on the two sides of the junction. Semiconductor laser is small in size (1 mm × 1 mm × 200 μm), easily fabricated by mass production and manufacturing cost is relatively low. Narrow width about 40 μm is obtained. Wavelength may vary from 0.7 to 30 μm. Its efficiency may be as high as 50 %. During pumping of electrons from one energy level to other, absorption rate is dependent on:

- Incident radiation's density,
- Coefficient of transition,
- Probability of occupying the valence band energy level
- Probability of maintaining empties the conduction band energy level

E. Fiber Laser

Here, a core, made of optical fiber and doped with rare earth element, is used as the active media. These rear earth elements are erbium, neodymum or ytterbium. Laser pumping is required which is to be done by a diode laser in transverse or longitudinal direction. For a simple type, laser cavity is made of doped optical fiber whose two ends are cleaved & butted by dielectric mirrors. In reality, end mirrors are fabricated by fiber Bragg gratings to vary the effective refractive index, and for pumping purpose fiber coupled diodes are used. The fiber core may single –mode (used for higher quality beams with low power) or multi-mode (used for higher power but low quality beams). The power output is in the range of 100 W to few kW.

Advantages of fiber laser are as follows:

- Compact design due to coiled configuration, it is named as "briefcase laser".
- High beam quality is achieved i.e. diffraction is limited.
- It is possible to generate laser beam of ultrashort pulse with wide adjustable facility because of broadness of emission spectrum.
- It has high efficiency (50%) as compared to other lasers [15, 16].

1.3.3 Analysis of Laser Beam - Material Surface Interaction

Laser beam is only one source of heat for laser material manufacturing. Though laser is generally treated as source of light, it is a form of energy also which may be utilized as an extreme heat source if concentrated through focusing. It is possible due to the properties of laser like, monochromatic and coherent. So, laser may be utilized for heating, melting and vaporizing the material. Power density is determined by the incident power and focused beam size. According to Gaussian distribution, size of the beam is defined by radial distance where beam intensity decreases to 13.5% of peak power which is same as area which has 87.5% of total energy of beam. The power density/intensity, I can be calculated from the Eq. 1.1.

$$I = q\pi r^2 \tag{1.1}$$

where, q = laser power in watts, r = radius of beam in mm [12].

Everybody emit radiation constantly depending on their emissivity property over a range of wavelengths. Radiation heat transfer does not require a medium; in fact it reaches maximum efficiency in vacuum. Likewise eletromagnetic radiation, the incident laser beam on the surface has different physical phenomena like, reflection, absorption, transmission and scattering which are represented by Fig 1.5. On the other hand, it can be stated that during striking of radiation with the surface, some part is absorbed, called as absorption (α), part of it is reflected called as reflectivity (ρ) and part of it is transmitted called transmissivity (τ). These part of energies are related as:

$$\alpha + \rho + \tau = 1 \tag{1.2}$$

Also they can be defined as follows:

Absorption is the fraction of radiation absorbed by the surface, can be expresses:

$$\alpha = \frac{Absorbed\ Radiation}{Incident\ Radiation} = \frac{G_a}{G},\ 0 \leq \alpha \leq 1 \tag{1.3}$$

Reflectivity is the fraction of radiation reflected by the surface, can be expresses as:

$$\rho = \frac{Reflected\ Radiation}{Incident\ Radiation} = \frac{G_r}{G},\ 0 \leq \rho \leq 1 \tag{1.4}$$

Transmissivity is the fraction of radiation transmitted by the surface which can be expresses as:

$$\tau = \frac{Transmitted\ Radiation}{Incident\ Radiation} = \frac{G_t}{G},\ 0 \leq \tau \leq 1 \tag{1.5}$$

where, G is incident radiation energy on the surface, G_a, G_r and G_t are absorbed, reflected and transmitted part of incident radiation energy, respectively. G is also known as irradiance or radiation flux incident on the surface. According to first law of thermodynamics, they can be related as given by Eq. 1.6.

$$G_a + G_r + G_t = G \tag{1.6}$$

For a opaque body, electromagnetic waves are not transmitted, as a result G_t i.e. τ becomes zero. Which means, if radiation waves strike the opaque body's surface, a part is reflected and other part is absorbed up to a thin layer. So, for opaque bodies Eq. 1.2 reduces to Eq. 1.7 as given below.

$$\alpha + \rho = 1 \tag{1.7}$$

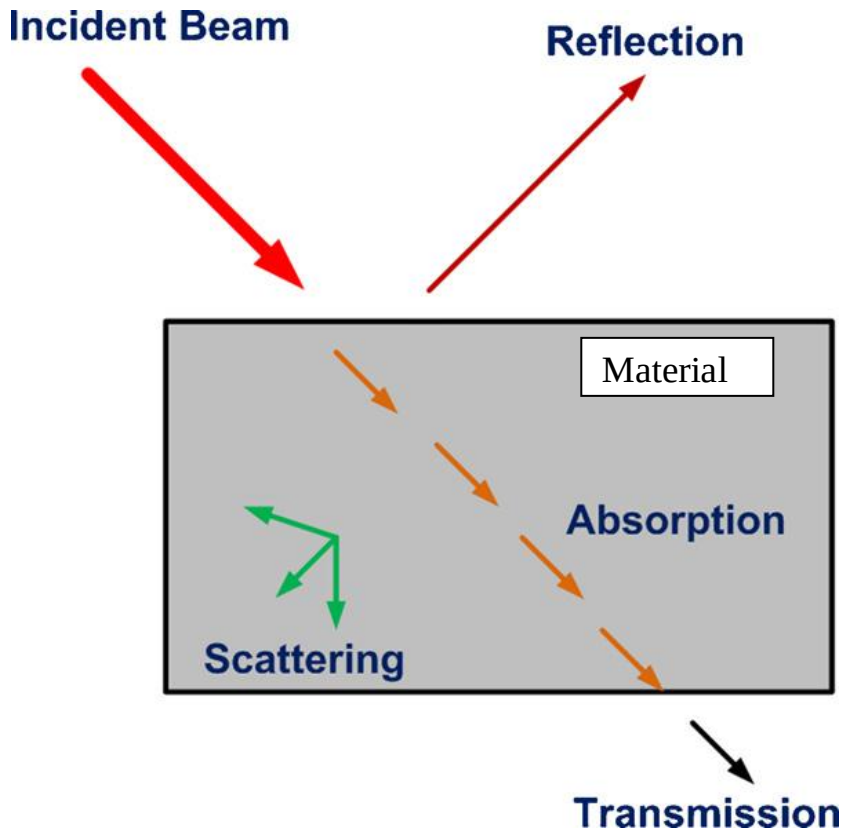

Fig. 1.5 Laser Beam - Material Surface Interaction (With permission: A.N. Samant et al., Copyright: Elsevier 2009)

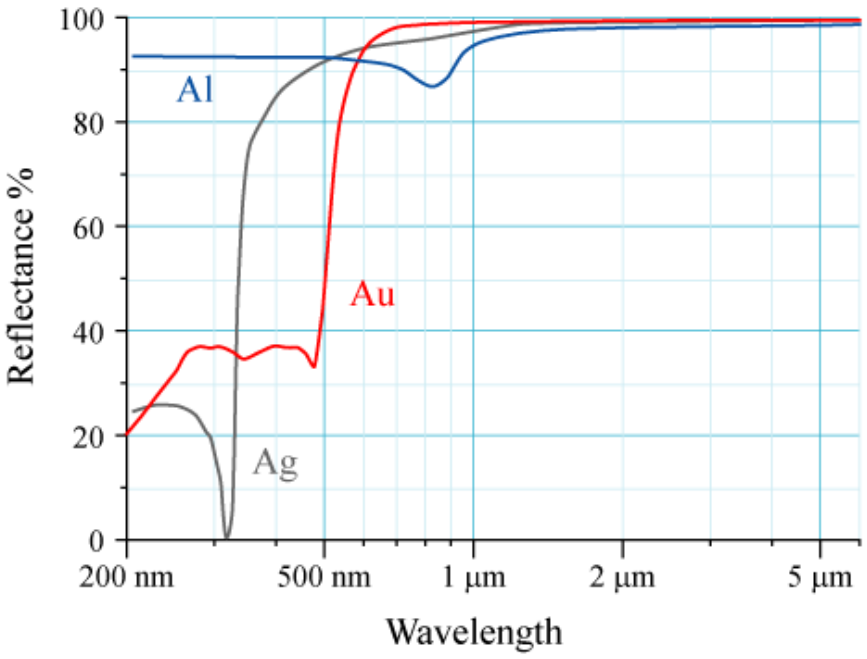

Figure 1.6 Radiation Properties of Aluminium (Al), Silver (Ag) and Gold (Au) (Coutesy: M. Bass, et all, Copyright: McGraw-Hill, 1994)

From this relationship i.e. Eq. 1.7, if any of them is known/measured, other can be determined. Actually, these definition are valid for total hemispherical properties as it is related to the radiation from all directions. So, spectral directional absorptivity and the spectral directional reflectivity of the surface are represented by Eq. 1.8 and Eq. 1.9, respectively.

$$\alpha_{\lambda,\theta}(\lambda, \theta, \Phi) = \frac{I_{\lambda,abs}(\lambda,\theta,\Phi)}{I_{\lambda,i}(\lambda,\theta,\Phi)} \quad (1.8)$$

and

$$\rho_{\lambda,\theta}(\lambda, \theta, \Phi) = = \frac{I_{\lambda,ref}(\lambda,\theta,\Phi)}{I_{\lambda,i}(\lambda,\theta,\Phi)} \quad (1.9)$$

Similarly, the spectral hemispherical absorptivity and spectral hemispherical reflectivity of the surface are represented by Eq. 1.10.

$$\alpha_{\lambda}(\lambda) = \frac{G_{\lambda,abs}(\lambda)}{G_{\lambda}(\lambda)} \quad \text{and } \rho_{\lambda}(\lambda) = \frac{G_{\lambda,ref}(\lambda)}{G_{\lambda}(\lambda)} \quad (1.10)$$

where, G_{λ} is spectral irradiation ($W/m^2\mu m$) incident on the surface, $G_{\lambda,abs}$ and $G_{\lambda,ref}$ are absorbed and reflected part, respectively.

To make it simple, surfaces are considered to reflect in a specular manner where, reflection angle is same as incidence angle of the radiation beam; or in a diffuse manner where radiation is reflected in all direction. As a result, reflection from a polished & smooth surface behaves like specular reflection while, reflection from a rough surface is nearly similar to diffuse reflection. In radiation analysis, smoothness can be related to wavelength as shown in Fig. 1.6 [13].

1.3.4 Absorption of Laser Beam Energy into the Material Surface

Absorptivity is strongly dependent on surface temperature of source from where incident radiation originates, which is evident from Fig 1.7. This figure shows that absorptivity properties at room temperature of different materials are the function of radiation source temperature. For example, it is observed that, absorptivity of aluminium increases with source temperature which is the characteristic of metal; whereas, absorptivity of white fireclay decreases with the source temperature which is

the property of white painted surface. According to physics, absorption of electromagnetic radiation is a technique by which photon energy is absorbed by the material. Then electromagnetic energy is transformed into absorber's internal energy. Due to this thermal energy, huge amount of heat energy is produced which propagates through the surface up to certain depth of layer.

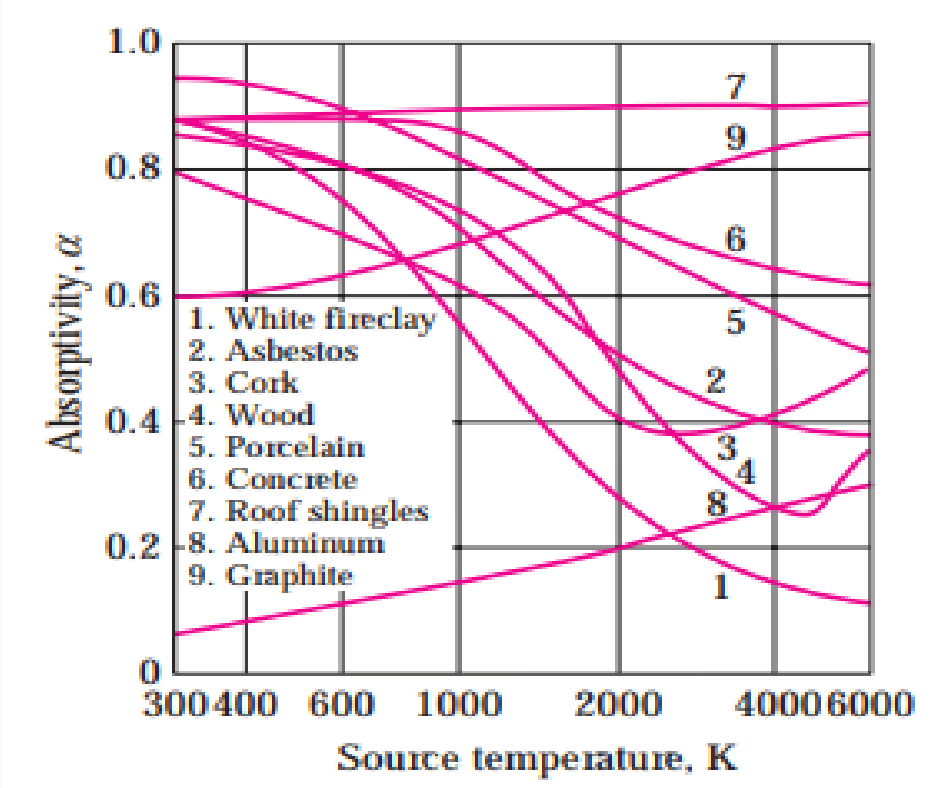

Figure 1.7 Relationship Between Source Temperature and Absorptivity

Absorption of radiation is dependent on the following:

(i) Coefficient of absorption and related parameters,

- coefficient of attenuation
- coefficient of molar extinction
- coefficient of mass extinction
- absorption cross-section and scattering cross-section

(ii) Depth of penetration and skin effect,

(iii) Constant of propagation, attenuation & phase, and complex complex wave number,

(iv) Complex refractive index,

(v) Complex dielectric constant,

(vi) Electrical conductivity and resistivity,

(vii) Absorbance i.e. optical density and optical depth/thickness ratio [15].

Absorption represents the interaction between electromagnetic radiation and material's electrons which depend both on wavelength and spectral absorptivity characteristic of material to be processed. It is also dependent on surface orientation with respect to beam direction and becomes maximum for incidence angle > 80^o. The absorbed laser energy Q_a by the material after n times reflection is given by

$$Q_a = Q\,(\beta)^n \tag{1.11}$$

where, Q is incident laser energy, β is coefficient of reflection depends on angle of incidence and n is reflection number. Again, n may be expressed by:

$$n = \frac{\pi}{4\theta} \tag{1..12}$$

where, θ is angle formed between cavity wall and normal direction to incident radiation. So, absorbed energy is dependent upon the reflectivity of material, incident laser energy magnitude, wall angle and wavelength of processed laser. This form of energy is then transformed into thermal energy and its ensuring conduction towards the material develops the temperature distribution which will affect machining time and depth of machined cavity [16].

If a plane is introduced into the machining region for describing laser power distribution for the purpose of laser absorption calculation, then laser power I(x,y) on that plane is given by;

$$I(x,y) = \frac{2E^1}{\pi\,\sigma^2 r_0^2}\exp\left\{-\frac{2r^2}{r_0 d^2 \sigma^2}\right\} \tag{1.13}$$

using the formula $I(d) = \frac{2E}{\pi\,M^2 r_0}\exp\left\{-\frac{2r^2}{M^2 r_0^2}\right\}$ (1.14)

where r_o, M and d represents laser beam radius, beam order and defocus distance, respectively. Here, d is the distance between optical axis and lattice center(x,y) on that plane which is expressed by Eq. 1.15.

$$d = \sqrt{(x_2 + y_2)} \tag{1.15}$$

Also, energy density, E_1, depends on coefficient of absorption; which is represented as given below:

$$E^1 = \frac{h(t)E}{dt} \tag{1.16}$$

where h(t) again expressed as given in Eq. 1.17

$$h(t) = \frac{1}{H} \exp \{- \frac{2(t-t_o)^2}{\omega^2} \} \tag{1.17}$$

and

$$H = \int -\frac{2x^2}{\omega^2} dx \tag{1.18}$$

Let the size and co-ordinate of the lattice be dx, dy & dz and (x,y,z), respectively at the place of irradiation. So, absorbed energy q(x,y) of m photons process at the lattice can be calculated from the Eq. 1.19.

$$q(x,y) = \int_z^{z+dz} I^m \alpha_m dxdydz \tag{1.19}$$

where I is the irradiated laser energy to the lattice and α_m is coefficient of absorption at m photon process. As a result, increase in temperature, ΔT at the lattice (x,y,z) is available from Eq. 1.20, assuming the specific heat and density of the material be C and ρ, respectively. Also, it is considered that all absorbed energy is converted to heat completely.

$$\Delta T = \frac{q}{C\rho dxdydz} \tag{1.20}$$

Again, on that plane, energy density (I) decreases at the lattice (u,v). So, decrease of energy density, dI can be calculated from Eq. 1.21 as:

$$dI = \frac{q_{sum}}{du\ dv} \tag{1.21}$$

where, q_{sum} is the summation of calculated energy of absorption for all the area where lattice (u,v) and the target lattice (x,y,z) overlapped, dudv is the size of lattice [17].

1.3.5 Heating Time Estimation for Melting of Workpiece Material

For simplicity, workpiece is considered as semi-finite solid. Due to the effect of pulsed laser action, workpice surface become hot and cold slightly simultaneously for few number of pulses, and it will be continuing up to its melting temperature. This heating process is considered as phase achieved due to pulse i. It is also assumed that initial temperature of the workpiece is of T^1_{i-1} after cooling due to (i-1) pulse. A constant heat flux (Q/A) will be developed on the workpiece surface due to continuous laser pulse, which is by equation:

$$\frac{Q}{A} = \frac{(1-r)P}{\pi r_o^2} \tag{1.21}$$

where $\frac{Q}{A}$ is heat flux i.e. power density of surface, r is reflectivity of workpiece material, P is laser power and r_o is radius of laser beam on the surface. So, heat transfer on the surface can be expressed by the Eq. 1.22 as

$$\frac{\partial^2 T_i}{\partial z^2} = \frac{1}{a_i}\frac{\partial T_i}{\partial t} \tag{1.22}$$

where, a_i is thermal diffusivity at temperature T_{i-1}. Here, initial boundary are given by Eq. 1.23 and Eq. 1.24 as:

$$T_i\,(z,0) = T^1_{i-1} \tag{1.23}$$

$$\text{and } \frac{Q}{A} = -k_i \left.\frac{\partial T_i}{\partial z}\right]_{z=0} \tag{1.24}$$

where, k_i is thermal conductivity at temperature T_{i-1}. Equation 1.23 reflects the surface temperature of workpiece after cooling due to (i-1) laser pulse, and Eq. 1.24 represents heat flux due to irradiation. The solution of Eq. 1.22 provides the temperature field $T_i(z,t)$, and it is able to analytical determination. At a condition when, $t = t_p$, laser becomes inactive and then surface temperature is determined from Eq. 1.25.

$$T_i = T^1_{i-1} + 2\frac{Q}{A}\frac{\sqrt{(a_i\, t_p \frac{1}{\pi})}}{k_i} \tag{1.25}$$

where, t_p is laser pulse duration. Due to subsequent heating and cooling, temperature is varied. However, it can be assumed that workpiece may has an uniform temperature which is equal to surface temperature, then boundary condition (through under-estimation) can be expressed by using Eq. 1.26 as:

$$T^1(z,0) = Ti \quad (1.26)$$

In addition the amount of heat conducted into the workpiece and convection heat loss are related following the Eq. 1.27 as:

$$hA(T_0 - T^1)_{z=0} = -k_i A \frac{\partial T_i}{\partial z}]_{z=0} \quad (1.27)$$

where, h is coefficient of heat transfer and T_0 is ambient temperature. During "off" time of the laser i.e. ($t = t_{off}$ i.e. cooling time) surface temperature (at z = 0) can be calculated as follows:

$$T_i^1 = T_i + (T_i - T_0)[\ 1 - [\exp \frac{h^2\, a_i\, t_{off}}{k_i^2}\ ]\ [1 - \text{erf}(\ \frac{h\sqrt{(a_i\, t_{off})}}{k_i}\ )]] \quad (1.28)$$

where, erf is the error function. This equation (Eq. 1.28) is utilized for getting number of repeated laser pulses up to the reaching of melting temperature [24].

1.3.6 Estimation of Machining Depth

After reaching the melting temperature of the workpiece, every extra laser pulse will be responsible for melting a finite volume of mass. It is considered that the shape of this mass is cylindrical with a radius of beam at irradiated erosion front surface. Now, due to propagation of erosion front into the workpiece, radius of beam changes because of defocusing of laser beam. The radius of beam can be found out from Eq. 1.29 as given below:

$$r_z = r_o\ [\ 1+\ (\ M^2\ \frac{\lambda(z+\delta_f)}{\pi r_o^2}\ )^2]^{1/2} \quad (1.29)$$

where, r_z is radius of laser beam at a depth of z below the workpiece surface, M is beam order or beam quality parameter, λ is wavelength of laser and δ_f is focal plane position w.r.t. the workpiece surface [24.

When the laser is "on" condition, the material liquefied and ejected instantly from irradiated area. So, it is assumed that there is no energy loss due to increasing the temperature of molten pool. However, some energy is lost due to convection to the surroundings and some energy for conduction from molten pool to surroundings. As a result, energy balance of molten pool is expressed by Eq. 1.30 as:

$$Q_{in} = Q_L + Q_{cond} + Q_{conv} \quad (1.30)$$

where, Q_{in} is amount of energy entered into workpiece generated from a pulse of laser beam, Q_L is energy consumed due to phase change, Q_{cond} is heat conducted into the workpiece and Q_{conv} is heat lost due to convection to surroundings. Again, Q_{in} can be expressed as:

$$Q_{in} = (1 - r)Pt_p \tag{1.31}$$

Energy consumed due to phase change is expresses by Eq. 1.32 as:

$$Q_L = m_i L \tag{1.32}$$

where, m_i is mass of cylindrical element that takes part for phase change and L is latent heat of fusion. Energy conducted into the workpiece is expressed as:

$$Q_{cond} = (k_{T= Tm} - A_{cond} \frac{\partial T}{\partial n})_{avg} \tag{1.33}$$

where, A_{cond} is area of finite element being in contact with surroundings that is responsible for heat conduction. Similarly, energy loss due to convection is as:

$$Q_{conv} = (hA_{conv} - \Delta T)t_p \tag{1.34}$$

where, A_{cond} is finite element area that can exchange heat through convection and ΔT is temperature difference between surrounding area and surface of elemental volume. Therefore, finally depth of melted finite volume can be calculated from Eq. 1.35.

$$s_i = \frac{\frac{(1-R)P}{\pi r} - k_{T=T_m} r\left(\frac{\Delta T}{\Delta s}\right) - hr\Delta T}{\frac{rL}{t_p} + 2k_{T=T_m}\left(\frac{\Delta T}{\Delta s}\right)} \tag{1.35}$$

where, s_i is the theoretical melted depth for pulse I [24].

1.4 FUNDAMENTAL FEATURES OF LASER MICRO-DRILLING

The laser micro-drilling is happened due to application of laser beam for heating the material to reach its melting/vaporization temperature. Once melting/vaporization starts, a very narrow hole is created, its absorptivity is increased which is helpful for further enlargement of size and depth of hole. Assist gas may be used to blown away molten material or vapour. When molten material and vapour are coming out into the surroundings, few of them may be condenses as scatter on the workpice surface. Narrow hole (diameter in the range of few micron) with high aspect ratio can be drilled. Laser micro- drilling is applied for fabricating jet engine turbine airfoils, injector nozzles, etc. [16, 18].

1.4.1 Types of Laser Drilling Process

By using three basic techniques, micro-holes can be produced, which are;

(i) Single-pulse (or on-centre) drilling

(ii) Multi-pulse (or percussion) drilling

(iii) Trepanning

Single-pulse (or on-centre) drilling: A single laser pulse of 1 ms pulse duration and few Joules energy though peak power is 1- to 100 kW is used for drilling a hole. The material is partly melted & vaporized and blown away with the assist gas flow and hole is formed. For deep hole drilling, excessively high laser power is required which affect on tolerance and reduces pulse frequency & productivity, plasma formation is increased which may affect the quality of hole produced.

Multi-pulse/Percussion Drilling: For multi-pulse/percussion drilling, a series of pulses of laser beam is utilized. The hole quality is improved by reducing the hole taper as required peak power reduced, and the amount of molten material & plasma formation can be controlled for a unit pulse period. Pulse duration may vary between 100 fs - 2 ms. However production rate is reduced as a series of pulses are used. The molten/evaporated material is then coming out of the produced hole by the excess gas pressure depending on beam intensity. With the increase of depth of hole, pressure of assist gas for blowing the molten material is to be increased.

Trepanning: This process is involved to drill a comparatively bigger size hole providing a relative motion (either circular or non-circular) in between workpiece and laser beam. So, basically this is a micro-cutting process. Thus, holes of large diameter can easily be drilled with improvement in hole quality and facility of repetition. Here, molten material is blown away from the lens, thereby lens lasts longer. However, this process is more time consuming; e.g. approximately 1 second to drill a hole, and hole depth is limited by 12 mm. One of the scheme for trepanning (drilling) process is shown in Fig. 1.8.

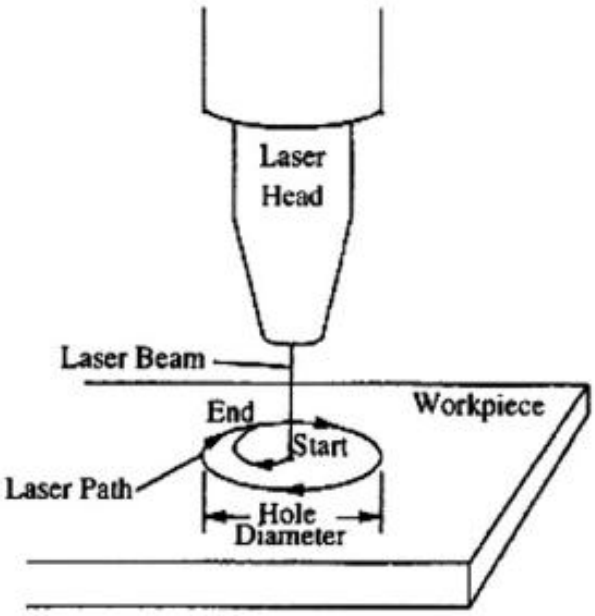

Figure 1.8 Scheme of Laser Micro-drilling (Trepanning) Operation (With permission from A.K. Dubey et al., Copyright: Elsevier 2008)

1.4.2 Process Parameters

Selection of laser for a particular application is dependent on drilling technique, workpiece material and hole geometry to be produced. The principal parameters are mainly grouped into two groups name, beam characteristics (input parameters) and process characteristics (output parameters).

A. Input Parameters

Main input parameters which affect the drilling process are laser power, pulse frequency, pulse duration and beam quality.

Laser beam power: The hole depth generally increases due to increase of laser power at higher levels. However, there is chances for more deformation at top.

Pulse : Usually, high pulse frequency is used to reduce hole taper specially for high depth/diameter ratio; whereas, for low depth/diameter ratio, low pulse frequency results a better quality holes.

Pulse duration: Generally pulse frequency for laser drilling process ranges between 100 fs - 2 ms. However, for high quality holes with minimum hole taper and lower distortion, shorter beam pulses are used.

Beam quality: Beams of moderate or high quality may be focused to very small diameter with longer focal length which is utilized to increase the depth of penetration of drilling, and improves the hole quality i.e. high depth/diameter ratio maintaining minimum possible hole taper.

B. Output Parameters i.e. Process/Drilling Characteristics

Main process characteristics of laser drilling are hole diameter and hole depth.

Hole diameter: Diameter of laser drilled hole ranges between 1 µm - 1.5 mm by using traditional lasers. however, hole diameter smaller than 12.7 µm at reasonable depth of focus is difficult. In that case femtosecond laser is recommended. Also hole diameter smaller than 1µm have to be produced by femtosecond laser. On the other hand, hole diameter more than 1.5 mm is to be drilled by trepanning technique, though it is a slow process.

Hole depth: Practically hole depth is defined by depth-to-diameter ratio which may be up to 30:1, and it is further dependent type of laser used and the focal length.

1.4.3 Process Defects

Process quality in laser micro-drilling is affected by process defects like hole taper, recast layer and micro-cracking.

A. Hole taper

Hole taper is created due to erosion of molten and vaporized material from the produced hole, and beam's conical shape. The creation taper is dependent on laser power, pulse frequency and design of optical system. This may be minimized by using longer focal length. Up to the hole depth less than 0.25 mm, taper may not be considered as a big defect.

B. Recast layer

Recast layer is formed due to resolidification of excess molten material which is not possible to remove completely.

C. Heat Affected Zone (HAZ)

HAZ i.e. heat affected zone is occurred due to overheating and/or spreading of heat around the machining zone. Due to this defect, hole circularity cannot be achieved properly, as a result oversized and/or oval shaped holes are produced.

D. Micro-crack

Micro-crack is formed, usually when brittle or hardened material is drilled, and often result due to high cooling rates or large temperature gradients [12, 18].

1.5 LASER MICRO-CHANNELING: CHARACTERISTIC FEATURES

1.5.1 Types of Laser Micro-channelling

One of the schematic diagram of micro-channeling/cutting is shown in Fig. 1.9. The distance between corner a and corner b is the length of channel. Kerf width represents the distance between corner c and corner d. Similarly, kerf depth is the distance between corner e and up to location f. Laser micro-channeling may happen by any one of the three types like, fusion cutting, sublimation cutting and photochemical ablation; which are discussed as:

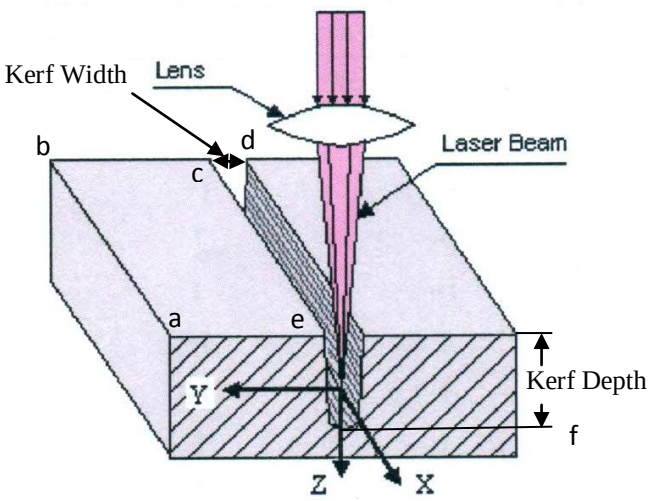

Figure 1.9 Schematic Diagram of Laser Micro-channelling (Model based on R. Biswas et al. Copyright: Inderscience Enterprises Ltd. 2008)

A. Fusion Cutting: It involves melting of base material and ejection using high-pressure assist gas. Assist gas may be inert when melting is happened entirely by laser beam. Assist gas can also be O_2 or air which does react with base material and the resulting exothermic reaction provides additional heat to speed up the process. This method is very efficient as it requires less energy per unit volume of material removal. However, fusion cutting has few inbuilt problems like, dross and striation formation.

B. Sublimation Cutting: Vaporization takes place along the cutting line from the workpiece. Pulsed beam and coaxial inert gas are utilized to get this type of cutting. Due to low energy, it's application is limited to thin sections only. However, narrower kerf and higher quality surface are main advantages of the technique.

C. Photochemical Ablation: Organic material, ceramic and difficult-to-cut materials are generally cut by sublimation cutting. The photon energy levels of laser ranges from 3.5 to 6.5 eV. This amount of energy is required to break molecular bonding e.g. C-C bond corresponds to 4.6 eV, C-H bond corresponds to 4.2 eV. Whereas, in case of CO_2 and Nd:YAG laser, corresponding photon energy is in the range of 0.12 eV and 1.2 eV, respectively. Thus, during irradiation, organic material absorbs this high energy ablation is occurred in a very thin layer of sub-micron range. The process is very fast (completed within 20 ns) and minimum thermal damage is observed. It is sometimes referred to as cold cutting due to little heat generation. Very clean and smooth cut region are main advantages.

1.5.2 Process Parameters

Main laser cutting process parameters are as follows:

A. Laser Power.

B. Characteristics of beam

C. Traverse speed.

D. Assist gas function.

E. Focal point location with respect to the workpiece.

A. Laser Power

It is the most significant parameter compared to others. Maximum thickness of cut and cutting/scanning speed of laser cut is directly proportional to laser beam power.

B. Beam Characteristics

Beam Mode - It indicates distribution of energy intensity over the beam cross-section. It is related to focusing ability of beam and equivalent to sharpness of a cutting tool. For best result, beam distribution should be as close as the fundamental mode by which smallest possible focal size with highest possible energy density is achieved. With this mode, kerf width is reduced, and cutting/scanning speed & thickness of material may be increased. Whereas, higher order or multi-mode causes larger focal size and lower energy density due to spreading of beam.

Stability - To maintain constant beam power, mode and direction, stability is required. It is also helpful to reduce variation in product output and thereby enhances the quality. When beam becomes unstable, it results poor tolerance and rough surface.

Polarization - Polarization helps in improving cut quality through maintaining narrow kerf, smooth edge and perpendicularity of beam. Because, absorption coefficient is increased, which is determined using the Fresnel relationships (it indicates that both angle of incidence and polarization affect amount of absorption). Generally, circular polarized beam is able to achieve higher scanning speed at higher power levels with narrow kerf and smooth surface. For plane-polarized beams in the cutting plane, beam is absorbed effectively at angle of incidence between 80^o and 90^o.

Beam Form - Either pulsed wave (PW) or continuous wave (CW) beams are utilized for laser cutting. In case of pulsed wave beam, quality of cut i.e. surface roughness decreases by increasing the duty cycle. Duty cycle is defined by (laser "on" time)/ (total time) ratio. Maximum attainable cutting speed is significantly reduced at low pulse rate. This is due to the fact that low pulse rate helps the material to heat and cool down substantially.

C. Traverse Speed

With the increase of workpiece thickness, maximum attainable cutting speed decreases at a certain laser power. For a certain power, two limiting curves are observed when variation of cutting speed are plotted with job thickness. Upper curve limits the maximum cutting speed beyond which cutting is incomplete. Whereas, lower curve limits the lower value of cutting speed below which self burning occurs. Self burning widens the kerf width and produces rough surface.

D. Assist Gas Functions

Assist gas serves the following functions:

- Helps to eject molten material,
- Protects lens from spatter,
- For exothermic reaction, it provides extra heat for melting,

Common gases like oxygen, inert gases, nitrogen and air are used as the assist gases. The most commonly used shape of gas nozzles include conical, convergent and convergent-divergent. Short stand-off distance (0.1 to 1.5 mm) are useful for reducing

the pressure for better surface quality and repeatability. In "clean-cut" technique, ring nozzle is used to produce drossless, oxidefree edge. The low-pressure (about 1 atm) monoxide gases flowing through inner nozzle protects nozzle; whereas, monoxide flowing through outer nozzle at high pressure (about 5 atm) removes viscous material.

E. Focal Position: It is necessary to maintain a consistency for the focal point location relative to workpiece surface. Best cutting is observed when the focal point location is either on the surface or just below the surface for thin sheet. However, for thick job, focal point location is preferred to 1/3 of the job thickness.

1.5.3 Quality of Cut Part

The quality of cut part is dependent on surface striation, dross formation and HAZ.

Striations: Laser cut surface usually has approximately periodic striation pattern which reflects as surface roughness. Processing conditions also affects striation. Striations are formed due to following reasons:

- Moving unit's vibration,
- Laser unit's fluctuation,
- Fluctuation of gas flow rate,
- Hydrodynamic property of molten metal flow.

A. Dross Formation

Some part of vaporized material become solidified due to condensation and clings to the lower edge of workpiece. It's formation is dependent on surface tension and viscosity of molten material. If surface tension and viscosity increased then formation of dross is also increased. Inert gas promotes more dross formation compared to oxygen. To avoid dross formation, high pressure above 1 MPa is required with inert gas assisted cutting.

B. Heat Affected Zone (HAZ)

HAZ i.e. heat affected zone is occurred due to overheating and/or spreading of heat around the machining zone. Due to this defect, kerf width cannot be maintained in the lower range, as a result oversized and/or defective kerfs are produced [12, 16].

Chapter 2

LITERATURE REVIEW & OBJECTIVE OF PRESENT RESEARCH

In the year of 1917, principle of laser was described by Albert Einstein, in theory of stimulated emission. Laser was invented by Arthur L. Schalow, a Bell Laboratory research person and Charles H. Towens, consultant to Bell Laboratory in 1958. Dr. Theodore Maiman invented first working Ruby laser on 16.05.1960. In 1961, Helium Neon was invented by Ali Javan, Willam Bennet Jr. and Dolald Herriot at Bell Laboratory. Semi-conductor laser was developed by General Electric Laboratory in the year of 1962. First Nd:YAG laser was developed at Bell Laboratory by J.E. Geusic, H.M. Markos and L.G. Van Uiteit in 1964. Though the concept fiber laser had come around 1970, but actually is was developed in the year of 1990 in Bell Laboratory. Afterwards, several researchers are continuously trying to fend better laser system development.

A lot of research work have been carried out till date and it is going on in the area of laser material processing, some of them are discussed shortly here with.

2.1 Study of Past Research Work

X. Zhu et al. [19] drilled less than10 µm holes in aluminium foils of 1.5 - 50 µm thickness, and 25 µm thick Mo, W, Cu, Ti, Fe, Pb & Ag foils by using femto-second Ti:sapphire laser pulses. The authors observed that drilling is effected by a combination of material properties, laser parameters and predominantly involves solid to vapour transition or small size atomic clusters of minimum droplets at micron scale. Prediction of ablation rate was predicted through a model for a range of metals.

D. Arau´jo et al. [20] experimentally observed that HAZ extension is less than 5 µm and suffers a heating between 548^0 and 596^0C with liquid phase. From Optical and SEM studies, mechanisms generating the HAZ of CO_2 laser cut Al 2024 alloy sheets can be concluded. Material initially melts partially prior to evaporation due to the presence of large α-liquid region and low laser absorption factor. Also, surface quality is degraded as high pressurized gas induces a dripping of melted material of high viscosity which leads to form a region of high stress concentration.

J. Meijer et al. [21] presented the state of art of laser beam cutting emphasizing on short and ultrashort lasers application. It is observed that, shorter pulses decreases the heat-affected damage of material and shorter wavelengths allows to produce smaller feature sizes which leads towards nanometer accuracy. They concluded that this gradual changes in miniaturization can be continued in future due to short to ultrashort laser beam machining methods.

W. Perriea et al. [22] studied the ablation rate, material re-deposition and residual surface roughness on aluminium under helium stream at ambient pressure by using 180 fs, 775nm laser pulses. Threshold fluence is ~ 0.4 J/cm^2 and ablation rate is $30 < V < 450$ µm^3/ pulse. Gas breakdown is avoided by the presence of helium above the substrate which improves surface micro-structure through minimization of surface oxidation & debris re-deposition. It was also observed that at 1 kHz, $F > 7$ J/cm^2 and power density more than 85 W/cm^2, poor surface micro-structure was formed due to residual thermal

effect and debris formation. On the other way, at low fluence ~ 1.4 J/cm^2, much better surface micro-structure is formed with negligible melt & very good surface finish ~ 1.1 ± 0.1 µm up to depth ~ 50 µm was formed with low power density ~3 W/cm^2.

L. Tunna et al. [23] reviewed the limitations in the micro machining (percussion-drilled) of aluminum by using Nd:YAG laser operated at different wavelengths e.g. 1064, 532, and 355 nm. Inter-ferometric (NT 3000TM, integrated to CAD/ CAM system) and optical methods of observation revealed that the machining depth and average etch depth/pulse are influenced highly by the wavelength & fluence and also affected by plasma generation and/or the melt produced. When wavelength is increased from 355nm to 1064 nm then maximum average drilling rate is reduced from 50 to 10 µm/pulse. A very low taper is observed.

K. Salonitis et al. (24) established a theoretical model for simulation of percussion drilling with medium irradiance laser beams considering required time to reach melting temperature and subsequent volume of material removal/pulse. This model is used to estimate specific laser beam power and maximum depth of drill. CO_2 laser of 1.8 kW laser has been used to verify the theoretical predictions and fine tuning of developed model. The authors concluded that time to reach melting temperature of job depends on the pulse frequency; maximum depth of drill attained is independent of pulse frequency for low - medium power densities, linear correction factor of 0.80 was introduced to improve the prediction accuracy.

A.K. Dubey et al. [25] reviewed experimental investigations to study Nd:YAG laser machining performance on the effect of input parameters. Authors also discussed on usefulness of various design of experiment methodologies used by different researchers to achieve optimality condition of various quality characteristics. The quality of machining mainly depends on: laser related, material related and process related parameters. Quality characteristics that are studied mainly: taper, HAZ, surface roughness, recast layer, dross & micro-crack formation. It was observed that job thickness affects more on taper, HAZ and recast layer. Inert gas improved surface quality

but poor MRR at high cost. Taper increased while surface roughness reduced with increase in spot overlap. Fractional factorial design techniques is simple and combination of all experimental trials which may be used to identify the interaction effects of all process characters efficiently for optimization purpose but it requires large number of experimentation for large number of factors. Taguchi method can reduce the process variation and hence the loss of quality, optimizes the qualitative variables but better results is possible due to insufficient machining data. RSM might be the best method for parametric optimization considering less number of experiments maintaining better accuracy of results. The study showed the utility of said laser for almost all materials' machining like high reflective and dielectric materials due to variation capability of wavelength and frequency. Micro-holes of 5 µm diameter with high aspect ratio > 20 can be drilled efficiently. 4 µm thin foils is cut successfully.

S. K. Dhara et al. [26] studied on laser micromachining of tungsten molybdenum general purpose HSS. Authors developed a prediction model for optimum parameter setting to generate maximum groove depth with minimum recast layer considering a feed-forward back-propagation artificial neural network (ANN). It was trained and then tested for reproducibility so that the model was able to predict the responses at any parametric combination. Suitability of the model is demonstrated by experimental results and optimization strategy is satisfied for practical requirements. It was found that ANN model of 4 - 25 - 2 structure can provide the best prediction among several combination. Verification test for this model showed acceptability of this model on the basis of accuracy is very good.

Y. Kuo et al. [27] proposed a multiple attribute decision making (MADM) and grey relational analysis (GRA) to solve the problem. 18 alternative layout and 6 performance were assumed in case of facility layout. 9 alternative dispatching rules and 7 performance attributes assumed for the problem to select dispatching rules. The results showed that GRA is efficient and reliable for solving MADM problem in both the cases. Also GRA provides better distinction among all the alternatives.

A.K. Dubey et al. [28] developed a hybrid approach consisting Taguchi methodology (TM) and principal component analysis (PCA) approach for multi-objective optimization during Nd:YAG laser cutting of nickel based super alloy for achieving improved cut quality. Input parameters were pulse width, pulse frequency, assist gas pressure and cutting speed. Kerf taper, kerf deviation and kerf width were optimized considering level and significance of input parameters. Responses at predicted optimum parametric level were verified by confirmation experiments. Initial parameter setting had been improved by TM and PCA combined approach.

A. Riveiro et al. [29] aimed CO_2 laser cutting of 2024-T3 plate using a novel laser cutting head with supersonic gas jet. Kerf dimension, surface roughness, microstructural characterization and grain morphology of the cuts surface has been analyzed. Produced cut edges are free of dross and cracks with negligible HAZ. These successful results leads towards application of supersonic assisting gas jet as a promising technique in the field of aerospace. Despite the disadvantages of CO_2 laser of 2024-T3 aluminum alloy such as the small absorption and the difficulties to drag out the molten material, the laser cutting process is possible by a supersonic cutting head, obtaining a very smooth cutting edge and without cracks. Besides, applying 2.500 W of laser power, it is possible to cut 1.5 mm thick sheets with speeds as high as 250 mm/ s and a good finishing quality.

A.K. Dubey et al. [30] applied Taguchi methodology for finding optimal cutting parameters for Nd:YAG laser cut aluminium alloy. Predicted kerf taper & material removal rate (MRR) are improved significantly using Taguchi methodology and verified by confirmation test. Multi-objective optimization is performed and compared to single-objective optimization which shows 1.6 % increase in kerf taper whereas MRR is unchanged for both the cases. Cutting speed has 91 % contribution on MRR, whereas pulse width affect mostly on kerf taper.

A.K. Dubey et al. [31] used Taguchi method to optimize kerf deviation and kerf width of Al alloy cutting by Nd:YAG laser. Responses are ooptimized at: gas pressure of 8 kg/cm^2, pulse frequency of 28 Hz, pulse width of 1.2 ms and cutting speed of 17.5

mm/min. It was observed that kerf quality was affected significantly by assist gas pressure and pulse frequency. However kerf width and kerf deviation had been reduced significantly compared to initial setting.

A.K. Dubey et al. [32] reviewed the previous research work both on experimental and theoretical in the area of LBM for various material including their required shapes. Author examined critically on different modeling and optimization technique used to determine optimum machining combination and discussed about the developments & trends of LBM for future research. It is stated that LBM is a powerful manufacturing process to produce complex profile, drilling microholes, machining of micro-parts in different types of materials. Micro-holes of 5 µm diameter can be drilled accurately. Even 4 µm thin foils may be cut successfully maintaining narrow kerf width. LBM performance depends mainly on laser, material and process parameters. Main output parameters were HAZ, kerf and/or hole taper, surface roughness, recast layer, formation of dross & microcrack.

U. Caydas et al. [33] stated an fruitful technique to optimize St-37 steel laser cutting parameters considering grey relational based with multiple performance characteristics. Best factor level condition are determined through Taguchi based 16 experimental runs. Laser beam power and cutting speed are optimized simultaneously for surface roughness, kerf width and HAZ width. It was seen that laser beam power has more influence on the responses compared to cutting speed. Also, performance characteristics of laser cutting responses were greatly simplified and improved together through this approach.

A. Stournsras et al. [34] experimented on the quality of CO_2 laser cut AA5083 alloy. Authors evaluated processing parameters like, laser power, pulse frequency, scanning speed and gas pressure through monitoring kerf width, surface roughness and HAZ size. Empirical models had been developed to describe input parameters' effect on the laser cut quality using regression analysis. For the validation purpose of the developed regression model, another set of experiment was conducted on AA2024. The laser beam power and cutting speed significantly influence on kerf width and HAZ due to insertion of more heat

in processing area per unit time, increases local temperature and thereby thermal effect is more. Lower values of pulse frequency at fixed scanning speed decreases laser spot overlaps and thereby increases the fluctuations on the cutting edge. Also, it was observed that more the gas pressure more the effective removal of melted material.

M.J. Tsai et al. [35] reported on optimization on quad flat non-lead (QFN) laser cutting by grey relational analysis (GRA). The most important output parameters were cutting depth, HAZ width and kerf width for both epoxy and Cu^{+} epoxy materials. Based on L9 OA best parametric condition were current of 29 Amp, frequency of 2 kHz and scanning speed of 2 mm/s. Moreover, ANOVA was also performed for determination of each control parameters' contribution. Finally, confirmation tests verified reliability of GRA predicted optimum configuration. The optimum condition obtained from both GRA and TM based on 9 experiments are same. Furthermore, ANOVA reveals, contributions of cutting parameters in descending order were frequency, current then cutting speed.

S. M. Karazi et al. [36] generated a prediction model for CO_2 laser formed micro-channel's width and depth in glass. Design of experiment (DOE) was built and experimented with laser beam power, pulse frequency and traverse speed. Three different feed-forward back-propagation artificial neutral network (ANN) models were also developed by varying the selection & training data. ANN, DoE model and experimental data were compared as a average percentage error which shows that ANN modeling method may be applied to predict micro-channel dimensions efficiently.

R. Biswas et al. [37] studied on microdrilling of gamma-titanium aluminide by pulsed Nd:YAG laser. Exit hole circularity and hole taper were observed at the expense of lamp current, pulse frequency, job thickness and gas pressure. Central composite design based on response surface methodology was used during design of experiments for achieving optimum responses. ANOVA test has been performed to check the adequacy which shows that lamp current and job thickness had significant effect on both the responses; while, pulse frequency and air had dominant effect on hole circularity. Optimum value of hole circularity had been observed at lower levels of lamp current, higher levels of job

thickness and moderate levels of air pressure and pulse frequency. While, optimum value of hole taper had been obtained at lower level of lamp current and air pressure; higher level of pulse frequency and job thickness. For both responses, optimum value is observed at moderate levels of lamp current, pulse frequency & air pressure, and higher levels of job thickness.

B. S. Yilbas et al. [38] carried out laser cutting of Al 7050 alloy sheets reinforced by Al_2O_3 and B_4C particles. Laser power & duty cycle were selected as the process parameters. SEM, EDS and the optical microscope were used to for geometry examination and to determine kerf width. It was observed that Al_2O_3 reinforced composite produced larger kerf width compared to B_4C reinforced composite. Prediction of kerf width was matched with the experimental result for both the composites. Increase of laser power increased kerf width gradually. Presence of Al_2O_3 and B_4C influenced kerf width through reducing thermal conductivity of these composites, while specific heat capacity was increased. Scattering rate of $\%\Delta w_k$ was found significant for Al 7075 alloy reinforced with Al_2O_3 than that of reinforced with B_4C. Moreover, the kerf width was more at the bottom surface as compared to that of the top surface of sample. Investigation of cut edges revealed that both particles remained as solid phase nearer to cut edges. The overall quality was influenced little bit by the laser power whereas it was not affected noticeably by the duty cycle.

K. Huehnlein et al. [39] reported on Al_2O_3 ceramic layer cutting optimization. Both CW 500W fiber laser and 200 W CO_2 laser were used to optimize and compared with cutting of 250 μm thin Al_2O_3 substrate layer. Results demonstrated the potential of DOE for the optimization of laser material processing. 46 individual experiments were performed with five individual influencing factors. It highlighted possibility to reduce overall efforts significantly required for optimization.

A. Sharma et al. [40] optimized process parameters for kerf width, kerf taper and kerf deviation of pulsed Nd:YAG laser cut nickel base super alloy. Input parameters were oxygen pressure, pulse width, pulse frequency and cutting speed. L27 OA had been

utilized to conduct experiments for both the straight and curved cut profile. It was observed that the optimal parametric levels of kerf width were equal for both profile; while, for kerf taper, they are entirely different. Experimental observations and confirmation experiment revealed that kerf taper was more in curved cut when compared to straight cut. Also, for straight cut, kerf width had been decreased from 0.363 to 0.349 mm, kerf taper from 0.2864 to 0.1227 degree and kerf deviation from 0.02 to 0.0166 mm, respectively. Similarly, for the curved cut, corresponding decreases were; kerf width from 0.43 to 0.331 mm, kerf taper from 0.368 to 0.15 degrees and kerf deviation from 0.04 to 0.036 mm, respectively.

A. Riveiro et al. [41] determined influence of input parameters and optimum combinations for CO_2 laser cutting on Al–Cu alloy (2024-T3) under both CW and pulsed mode to evaluate cutting speed and cut quality. Superior cut quality was obtained under CW mode compared to pulsed mode. Under pulsed mode, two clear processing regimes were identified varied by pulse frequency. The best result was observed at high laser beam power and frequency with moderate duty cycle. On the other way, high cutting speed is achieved in CW mode as compared to that of pulsed mode.

S.A.A.A. Mousavi et al. [42] investigated on microstructure of pulsed Nd:YAG laser welded beryllium copper sheet through tensile and hardness tests, optical microscopy, SEM and XRD. SEM images revealed three distinct solidified structure due to the variation in thermal gradient. XRD patterns showed that preferred solidification directions are as same as FCC material. Tensile strength of welded part become low than the parent metal due to precipitation during solidification. It was found that, focused bean diameter should be kept as small as possible to get weld pool of highest penetration and least width at constant pulse energy. Also, weld pool is increased if laser energy is increased.

A. Riveiro et al. [43] carried out experimental observation on effect of various assist gases on laser efficiency and thereby cut quality of Al-cu alloy. O_2, N_2 and compressed air reacted to molten material and generated large mass of oxides and nitrides which

affect cutting speed and cut quality. Other way, argon proves as more efficient assist gas for best quality and higher efficiency for processing Al-Cu alloys.

B. Adelmann et al. [44] reported on an algorithm including DoE for optimizing the laser parameters for getting burr-free cut of 1 mm thick aluminum using 500 W single mode fiber laser and compared with an 1 kW multimode fiber laser. Results demonstrated potential of optimization algorithm based on 27 individual experiments for certain speed with modulation and 26 individual experiments at maximum speed. Besides, algorithm additionally provides information about effect on individual parameter and their interactions in addition to determine variance of parameters.

L. Li et al. [45] provided an outlook on advances of nano-manufacturing methods of nanoparticles, nanowires and nanotubes fabricated by laser and 3-D nanostructure by multiple layer additive technique. Authors stated practical applications of laser in nanostructure, nano-components for different materials. Discussion on the challenges and outlooks in laser nano-manufacturing was also presented.

A. Riveiro et al. [46] performed experimental study of an Al–Cu alloy for studying the effect of input parameters on cutting speed and quality criteria using off-axial supersonic nozzle. Reduction in cutting speed was noticed in pulsed mode comparing with continuous mode. Best results were observed at high pulse frequency i.e. f >100 Hz, due to complete exploitation of supersonic jet to remove the molten material. Maximum cutting speed was attained within the high pressure regime. Furthermore, quality cut is obtained in term if lower kerf width, average roughness, less dross and minimum HAZ.

D. Ganguly et al. [47] used Taguchi methodology and grey relational analysis for the determination of Nd:YAG laser microdrilling parameters of zirconium oxide ceramics considering multiple quality characteristics. Efforts had been made for the minimization of microdrilling defects like, hole taper and HAZ width, for the production of high quality micro-drills. The optimum result obtained had been verified by confirmatory experiment which revealed application feasibility of Taguchi-grey technique to improve

continuously. This improvement was observed as good as 16.29% for hole taper and 8.77% for HAZ width, respectively.

A. Sharma et al. [48] presented modeled to cut straight profile on Al alloy by pulsed Nd:YAG laser and optimized the cut quality. Authors selected oxygen pressure, pulse frequency, pulse width & cutting to be input parameters and kerf taper & surface roughness to be output parameters. Taguchi methodology (TM) combined with response surface analysis (GRA) was utilized for modeling while TM and GRA coupled with entropy measurement methodology was utilized for multi-objective optimization. It was also observed that Ta was influenced significantly by oxygen pressure and cutting speed.

P. Kuryło et al. [49] tested surface layer properties of MO59 copper alloy. Technological allowances were determined based hardness distribution results. Hardness distribution on two levels showed comparison for 10, 15, 20, 25, 30 and 35 as the function of distance from the upper cast wall. The tests results showed that cast wall thickness did not have a bigger impact on durability property for 10 mm thick sample due higher hardness absence of internal faults. Samples of 20, 25, 30 and 35 mm wall thickness were characterized by comparing the hardness distribution. Hardness ranges between 66 to 68 HRB on the surface showed durability properties of the alloy despite various rate of heat dissipation and sample thickness. This occurrence may be caused due to unfavorable cooling during undesired structure creation, segregation of chemical composition, etc. The bubbles formed were shallow of approximately 1 mm from the upper wall.

A. S. Kuar et al. [50] investigated on Nd:YAG microdrilling of alumina. Influence of lamp current, pulse frequency, pulse width and air pressure were observed on hole taper and HAZ width. Taguchi methodology combined with grey relational analysis (GRA) was utilized as the DoE. GRA was utilized to convert multi-response characteristics to a single quality characteristic, named as grey relational grade for optimizing input parameters. Verification with confirmation test justified application feasibility of Taguchi-grey technique for the continuous improvement of microdrilling characteristics.

K. Hock et al (51) compared between fiber laser cutting and water jet-guided laser cutting with respect to accuracy, kerf width, HAZ and productivity for thin sheets of stainless steel and brass. They attained dross-free cut with almost no HAZ and small kerf width under water jet-guided process, but small dross and notable HAZ were observed for fiber laser cutting. Results revealed that the major advantages of water-jet guided system are narrow HAZ, low dross height and narrow kerf width. On the other hand, high cutting speed and low process costs are the advantages of remote laser cutting.

S.L. Campanelli et al. [52] demonstrated on careful choice of laser and process optimization to achieve statistical analysis for ablation depth (Δz), material removal rate (MRR) and surface roughness (SR). Moreover, multi-objective optimization technique was utilized to improve surface quality and productivity. Nd:YAG laser of 1064 nm wavelength was used for experimentation on Al 5754 alloy. The effects of scanning modality, scanning speed and repetition rate on Δz, MRR and SR were analyzed from 24 combinations of the parameters. ANOVA showed very low p-values which indicates process parameters had high significance on responses. The optimization method highlighted on maximum value of ablation depth & MRR and minimum value of SR. It was observed that parallel hatching strategy is better than the mix hatching strategy.

A. Sharma et al. [53] presented a model to optimize cut quality characteristics for curved profile on thin Al alloy by Nd:YAG laser. Kerf deviation (Da) and kerf taper (Ta) were quality characteristics and the process selected were pulse width, pulse frequency, cutting speed, oxygen pressure and radius of curvature. Experiment was performed considering L27 OA. Second order response surface model based on hybrid approach Taguchi methodology and response surface methodology was developed for each Da and Ta. Response surface plot reflected that for lower Da, moderate value of pulse frequency is preferred, however, oxygen pressure had the highest significance on Da. on the other hand, to minimize the Ta significant parameters were linear effect (lower values) of radius of curvature & pulse width. Preferred operating condition for minimum Ta and Da

was found from grey relational grade as; radius of curvature 5 mm, pulse width 1.4 ms, pulse frequency 10 Hz, oxygen pressure 4 kg/cm^2 and cutting speed 12 mm/min.
R. Khettabi et al. [54] studied on particle emissions during machining of Al 6061-T6 alloy and Ti6Al4V alloy. The investigation of chip formation mode was considered as an index for particle emissions mechanism. Under certain machining condition, coarse particles disintegrated into fine and ultrafine particles. However, in case titanium alloy this fineness is more effective compared to that in case of aluminium alloy. Particle emissions by aluminium and titanium alloys were compared considering the same high speed, as these two alloys were machined efficiently at different speed ranges.

G. Tiranda et al. [55] studied on numerical modeling of laser welding under both conduction and keyhole modes to focus on effect of important welding parameters. Numerical simulation enabled thermal behavior of welded assembly for discussion based on hot cracking criterion. Results demonstrated that laser welding in keyhole mode was more likely to reduce higher cooling rates and more risk of hot cracking, but better sensitivity to the post weld age hardening treatment as compared to keyhole mode. Optimum performance in terms of corrosion resistance, strength and fatigue were highlighted as influence of process parameters.

S. Mishra et al [56] formed a coupled model consists of finite element method (FEM) and artificial neural network (ANN) for laser percussion drilling. Firstly, thermal model based on FEM was developed considering optical properties, thermal properties and phase phenomenon of aluminium. To validate the model an experiment was conducted and hole taper was compared. Secondly using this FEM model, sufficient input data and output date were generated to train and test the ANN model. For multi-objective optimization, predicted value from ANN are utilized in another coupled model consisting of grey relational analysis and principal component analysis. Predicted data from ANN shows pulse width will affect highly on hole taper and material removal rate, but pulse frequency is most significant on HAZ. Ta decreased due to increase of pulse width, pulse frequency, peak power and job thickness (more significant). At a certain thickness, MRR

increased with an increase of pulse width, pulse frequency and peak power. As job thickness increased, MRR also increased. The extent of HAZ increased with the increase of pulse width and pulse frequency (more significant), but it decreased with the increase of peak power and job thickness. ANOVA showed significance of parameter as peak power of 51.72%, job thickness of 39.89%, pulse frequency of 6.86% and pulse width of 1.53%. Confirmation test showed the improvement of responses at the same optimum parametric combination.

S. Mishra et al. [57] used a hybrid methodology combining artificial neural network (ANN) and finite element method (FEM) for developing a prediction model in laser beam percussion drilling process. At first, thermal model based on FEM had been developed considering temperature-dependent properties, optical properties, phase change phenomenon and then validated with self-conducted experimental data with respect to hole taper. This data was used further to generate a ANN model through training and testing. Multi-objective optimization based on grey relational analysis (GRA) and principal component analysis (PCA) was performed utilizing the data obtained from ANN model. ANN predicted results showed, increase of pulse width and peak power increases hole taper, material removal rate and HAZ. But, hole taper decreases due to increase of pulse frequency and job thickness. At a certain sheet thickness, material removal rate is increased due to increase of pulse width, pulse frequency and peak power. Extent of HAZ increased due to increase of pulse width and peak power but decreased due to increase of pulse frequency and job thickness. Feed-forward back propagation ANN of 4 - 9 - 3 structure became the best prediction model with average error of 2% only. The most significant parameters were pulse frequency of 43.8 %, peak power of 25.8 %, pulse width of 24.2 % and sheet thickness of 6.2 % which was also verified by confirmation test.

S. Kasman et al. [58] investigated the cutting ability of hard metal (Vanadis 10) produced by powder metallurgy which is related to laser engraving. Scanning speed, frequency, pulse frequency and laser power were interrelated with surface roughness and engraving depth through L9 orthogonal array based experimentation. It was noticed that scanning

speed was most significant on both responses to decrease. Linear regression expression had been established to estimate the responses at different combination of input parameters. The optimum level for minimum surface roughness was found at scanning speed of 800 mm/min, pulse frequency of 30 kHz and power of 25 W. Whereas optimum levels for engraving depth was scanning speed of 200 mm/min, pulse frequency of 30 kHz and power of 50 W. Predicted and confirmation experimental data were very close to each other.

G. Selvakumar et al. [59] presented experimental analysis to select the most optimum parametric condition of wire electrical discharge machining on Al 5083 alloy. Taguchi's L9 OA method was used for the experiments with pulse "on" time, pulse "off" time, peak current and wire tension to study surface roughness and cutting speed. Influence of input parameters on the output parameters output parameters was analyzed through S/N ratio and ANOVA. ANOVA shows that wire tension has no effect on both cutting speed and surface roughness.

B. Acherjee et al. [60] utilized Nd:YAG laser in micro-channel fabrication on PMMA in under-water condition. The process parameters were lamp current, scan speed, pulse width, pulse frequency. Burr height, depth and micro-channel width were the responses. Optimum parametric combination was determined by Taguchi methodology combined with grey relational analysis to satisfy multiple objectives simultaneously. Under-water laser micro-channeling had been observed as very effective to create clean and burr-free structures, reduced heat affected zone. The structure is found as clean and debris-free whose edges were straight and parallel. Experiments had been designed based on L16 OA. ANOVA revealed that the most significant parameter was pulse repetition rate. Conformation test is performed to verify the quality.

C. Leone et al. [61] investigated laser cutting of I mm thick Al 6061 T-6 alloy sheets by 150 W multi-mode Nd:YAG laser. Maximum cutting speed was measured by linear scanning utilizing maximum average power, different cutting directions and pulse duration. The results showed that cutting speed up to 700 mm/min was achievable, with

narrow kerf < 200 µm, good taper angle $< 5^0$ and low dross height about 40 µm. In another case, ANOVA was performed to analyze effects of direction of beam travel, pulse duration and cutting speed on kerf geometry. Also, pulse duration affected on taper angle and dross height.

R. Adalarasan et al. [62] reported on CO_2 laser cutting on Al 6061/SiCp/Al_2O_3 of thickness 4 mm. Kerf width, surface finish and slope of cut-edge were studied under parametric combination of laser power, pulse frequency, cutting speed and gas pressure. Experiment was conducted based on L18 orthogonal array and optimum condition was predicted based on grey-RSM of parameters. Atomic force microscopy images and p-profile graphs of machined surface were studied for the surface finish and texture characteristics. The used hybrid technique was found as adequate, fit and effective to predict the optimum parametric setting.

R. Biswas et al. [63] optimized hole diameters at top & bottom and hole taper by central composite design based on response surface methodology for micro-drilling alumina-aluminum IPC sheet by Nd:YAG laser. Single- and multi- objective optimization techniques of hole characteristic revealed that lamp current, pulse frequency, assist air pressure and job thickness could be controlled optimally to achieve desired response by this model. ANOVA had been conducted to identify the significance of input parameters. A confirmation test had been performed to validate the predicted data through ANOVA.

C. Chen et al. [64] studied on the cut front edge temperature (T_{ce}) characteristics during fiber laser cutting of AA2219 alloy. An infrared laser thermometer was used to record time domain of T_{ce}. The experimental results reflected a close relationship between T_{ce} and kerf quality. An optimal T_{ce} range of 1800 to 1950°C for accepted kerf was observed which was smooth and almost dross-free; while it became rough and mass of dross beyond T_{ce} range. T_{ce} can be increase above 1800°C and kerf quality can be improved either by increasing laser power or decreasing cutting speed. Calculated optimal T_{ce} range are very close to the experimental data.

Q. Wang et al. [65] made a detail study of femto second double-pulse laser drill on 50 µm thick aluminium and copper films. Varying the delay between two pulses drilling process was monitored through recoding the light transmitted into job and morphology of drilled hole was studied. Focal position, ambient pressure and laser fluence was varied to observe the drilling efficiency, hole shape; then compared results for two materials. It is observed the increase of pulse casus increase of number of purse. A long time-constant ~40 ps and a short time-constant ~5.6 ps were noticed along double pulse delay axis, hole diameter decreased, abnormal fluctuations were also found; though the re-deposited material's diameter was found to behave differently. Larger sized granules were observed around produced holes by pulses of shorter delay time and finer ash was noticed for produced holes by the pulses of longer delay time.

J. Li et al. [66] studied influence of input parameters on laser marked barcode produced on aluminium alloy surface by Nd:YAG laser. Barcode quality was determined from surface roughness and image quality. Surface roughness is affected by process parameters within different intervals. Two types of scanable barcodes were formed in "white" and "black" by using Taguchi methodology. Relationship between surface roughness and process parameters are established by a non-linear regression model. Statistical significance of each parameters was evaluated by ANOVA and verified by confirmation test. It was observed that surface roughness affects greatly on final image quality. The optimum parameters for "black" barcode were at fill spacing of 0.03 mm, current of 14 A, scanning speed of 10 mm/s and pulse frequency of 5 kHz, respectively. Also optimum parameters for "white" barcode were fill spacing of 0.015 mm, current of 10 A, scanning speed of 100 mm/s and pulse frequency of 1 kHz, respectively.

S.G. Irizalp et al. [67] researched on plastic deformation behavior of Al 6061-T6 alloy at high strain rate for laser shock processing (LSP). Improvement for both strength and ductility was possible due to grain refinement into nano-structured material. Near surface microstructure was observed through TEM and fracture surface was examined by SEM after tensile test. In general, it was observed that increase in strength, decreases the ductility of the material. Here, result showed that both strength and ductility were

increased, even work hardening capability was recovered. TEM revealed that deformation twins formed with increase in twin boundary which indicated the decrease in stacking fault energy.

H. Rao et al (68) investigated on microstructure in addition of mechanical properties of A357 alloy fabricated by selective laser melting (SLM). The processing parameters were optimized to obtain maximum density, fine microstructure with least number of pores. Porosity in SLMed A357 Al sample was analyzed based on relative density Vs. laser r parameters curve. Mechanical properties in terms of melt pool morphology and eutectic Si cell characteristic was influenced by substrate temperature and laser parameters. Fracto-graphic studies had been performed for tensile properties through comparison of fracture surface and microstructure features in different planes.

M.L.M. Sistiaga et al. [69] performed SLM of Al 7075 alloy leading to sub-optimum density and micro-cracking. Silicon is added by tailoring to increase the density and thereby micro-cracks were reduced significantly by the grain refining effect. Also, hardness of SLMed Al 7075 alloy could be improved by proper heat treatment processes. Addition of 4% Si could decrease melting temperature, improve fluidity of alloy and new eutectic grain refinement was observed.

Md. Antar et al. [71] investigated on drilling 0.8 mm hole at high speed by both EDM and laser on nickel baser aerospace alloy. Full factorial design was used with 2-level 3-factor for the identification of preferred operating parameters. Better results in respect of recast layer and geometry accuracy, taper specially for thick job was observed in EDM process compared to laser drilling. However, laser drilling is very fast process compared to EDM process for the thicker job. Also, recast layer thickness was affected marginally in case of EDM process.

A.M. Alahmari et al. [72] fabricated micro-channels on some aerospace alloys like Ti6Al4V, AA2024 and Inconel 718 by Nd:YAG pulse laser. Micro-channel size in Ti6Al4V increased due to increase of current and pulse frequency but by decreasing of scanning speed. Micro-channel is oversized due to increase of lamp current intensity &

scanning speed in AA 2024. For Inconel, an increase of current intensity increased the channel size; but increase of pulse frequency and scanning speed decreased channel size. Response surface methodology was developed to predict micro-channel sizes. The models were validated through confirmatory tests. For Ti6Al4V, optimum combination of process parameter were 83.57% current, 30 kHz pulse frequency and 400 mm/s scanning speed. For AA2024, optimum parametric condition were current of 83.57%, pulse frequency of 30 kHz and scanning speed of 300 mm/s. Similarly for Inconel 718, optimum parameters were 83.57% current, 37 kHz pulse frequency and 300 mm/s scanning speed. At optimized parametric setting, micro-channel sizes were observed as for Ti6Al4V → 100 µm, for AA2024 → 122.34 µm and for Inconel 718 → 102.98 µm, instead of 100 µm.

A. Bharatish et al. [74] experimented on effect of laser drilling parameters of alumina-coated aluminium substrate by 1800 W pulsed CO_2 laser. The main processing parameters were laser power, pulse frequency and piercing time; whereas responses were spatter deposition, HAZ, circularity at entry & exit and hole taper. Genetic algorithm (GA) was used for simultaneous optimization of parameters which were improved by 5.2% in hole quality. Response surface methodology identified the minimum values of the responses. The optimum values were validated by confirmatory test.

G. D. Gautam et al. (75) focused on experimental and theoretical investigation for different material by pulsed Nd:YAG laser to enhance productivity based on the work done by other researchers. Authors made the following conclusions:

1. Laser beam drilling is useful for different types of material irrespective of their mechanical properties and can produce narrow holes with high aspect ratio.
2. Performance of laser drilling is dependent on laser parameters, material parameters, process parameters and assist gas parameters.
3. Quality characteristics are hole taper, HAZ, surface roughness, circularity, spatter formation, burr deposition.
4. Various design of experiment methods and different optimization techniques are used individually or coupled condition.

5. Confirmation test is essential for all the optimization method for the validation purpose.

A. Sharma et al. (77) reviewed the study on laser cutting parameters by using Nd:YAG laser. Author also discussed on different experimental modeling and optimization technique used by different researchers. They made following conclusions:

1. Complex geometries on any sheet material including reflective sheets, Nd:YAG laser is the most suitable machine set-up.
2. It is seen that important input parameters are laser related parameters, material related parameter, process related parameters and assist gas properties.
3. Essential output parameters are kerf width, kerf taper, kerf deviation, HAZ, surface roughness, dross formation, recast layer, microcracks.
4. Design of experiment is required for proper experimental planning and optimization is also essential for the validation of experimental result.

D. J. Kotadiya et al (78) performed parametric analysis of fiber laser cut stainless steel of 3 mm thickness on surface characteristics with CNC laser cutting set-up YLR-500"-ytterbium fiber laser. Here, laser power, cutting speed and assist gas pressure were analyzed and optimized considering surface roughness and top kerf width as the responses. It was observed that laser power had most significance on responses. Laser power and cutting speed had more interactive significance with highest F-value of 28.55 on kerf width. Regression analysis was used to identify the optimized values of process parameters as 500 W laser power, 15 bar assist gas pressure and 2000mm/min cutting speed for minimum surface roughness of 4.39939 µm and top kerf width of 283.688 µm.

Laser beam machining (LBM) can be used for almost all varieties of materials. Among various types of laser used for industrial as well as academic purpose, only CO_2 and Nd:YAG are mature as they are used most of the application. CO_2 laser is used mainly for commercial sheet metal cutting except ceramics. Whereas Nd:YAG laser offers a lot of application in material processing which needs also further investigation to improve

the performance. For reflective material, Nd:YAG laser with shorter wavelength is selected to increase the absorptivity. Nowadays, diode-pumped and Q-switching technique is applied for maintaining shorter pulse as the requirement of micro-machining. However, these type of laser, being a non-conventional system, has poor efficiency and high cost. The aim of any manufacturing system is to achieve better product quality on the basis of effect of input parameters' variation on output parameters.

As a result new laser are being developed like Nd:YVO_4, fiber laser, etc. Application of these two laser are observed in a limited research. Due to high reflectivity, laser cutting on copper and it's alloys is hardly available in few research purpose. Aluminium alloy of type 2014, 2024, 5083, 6061 are used by several researchers. However, limited number of researchers used Al 7075 & 7050 alloys for laser cutting. No laser cutting is observed on beryllium copper alloy.

The aim of the present work is to express and analyze outcomes from experimental observation using different design of experiment methodologies, optimization (individually and simultaneously) techniques and prediction models on laser (Nd:YVO_4 and fiber) micro-machining, micro-drilling and micro-channeling operation of Al 7075 alloy, Copper and Beryllium-copper alloy. This is to done to identify the significant factors and their influence on quality characteristics and optimum setting of processing parameters for better responses and to model cause and effect relationship between the processing parameters and responses.

2.2 **Objectives & Scope of the Present Research**

2.2.1 **Objectives of the Present Research**

Laser processing of light metal alloys is an emerging area of research work though laser machining, applicable to all ranges of material like, metals, non-metals, soft material, difficult-to-cut materials, ceramics, composites, plastics. CO_2, Nd:YAG laser are used by most of the researchers in their work for sheet machining like cutting, drilling, channeling, etc. However, application of diode-pumped fiber laser and Nd:YVO_4 laser is very rarely seen for laser material processing.

Keeping in view the shortcomings of the past research work and the present needs of micro-machining of light metal alloys by laser beam, and for successful utilization of Nd:YVO_4 laser & diode pumped fiber laser, objective of present research work include following:

(i) To study the in-depth material removal mechanism of various light metal alloys by using Nd:YVO_4 laser and diode pumped fiber lasers,

(ii) To carryout planned experimentation and optimization following Taguchi methodology and response surface methodology,

(iii) To study, analyze and optimize influence processing parameters namely, laser beam power, pulse frequency, scanning speed and repetition rate on kerf width, heat affected zone and angular deviation for laser micro-machining of Al 7075 alloy by Nd:YVO_4 laser,

(iv) To study, analyze and optimize the effect of process parameters such as, laser beam power, pulse frequency, scanning speed and number of pass on hole taper and HAZ width during laser micro-drilling of copper sheet by Nd:YVO_4 laser,

(v) To perform experiments for in-depth analysis of the effect of laser beam power, pulse frequency and scanning speed on kerf width, kerf depth, HAZ, overcut and angle formed in micro-channeling on copper-beryllium alloy sheet by using diode pumped fiber laser following response surface methodology,

(vi) To study the surface characteristic of Nd:YVO_4 laser micro-machined Al 7075 alloy using Taguchi methodology considering laser beam power, pulse frequency and scanning speed as the influencing parameters and surface roughness is the output parameter,

(vii) To optimize the responses/output parameters and thereby identifying the optimal parametric combination of input parameters by using Taguchi methodology, grey relational analysis,

(viii) To develop mathematical model for predicting the responses at any parametric combination during micro-machining by using Taguchi methodology, grey relational analysis, response surface methodolgy,

(ix) To study characteristics of the machined surface on Al 7075 alloy using optical microscope and scanning electron microscope, etc.

2.2.2 **Scope of the Present Research**

There is huge demand of growing industries for extensive research in the area of inherent defects of laser beam micro-machining like taper formation, absence of circularity, etc during micro-drilling; wider kerf development, production of rough surface for micro-cutting/channeling, dross formation, crack development for micro-machining.

To achieve enhanced quality of micro-machining, present parametric analysis of quality characteristics like hole taper, HAZ width, kerf width, kerf depth, HAZ, angular deviation, surface roughness, overcut, etc. by using Nd:YVO_4 and fiber laser on various light metal alloys will widen the research area and serve as impetus to further studies for academic personnel.

There is huge demand of light metal processing because of superior quality in terms of finishing, machinability with miniature and complex contour, durability, etc in different industries, e.g. aerospace, spacecraft, biomedical, etc.

With the available resources, there is wide scope for research work on effective utilization of Nd:YVO_4 and diode pumped fiber laser machines for different profile cutting, drilling, grooving, micro-channeling, marking, etc. operations for analyzing quality characteristics like kerf width, kerf depth, kerf taper, HAZ, angular deviation, surface roughness, etc. on light metal alloys which are the present need of fabrication of micro-components in different industries, specifically, aerospace, aviation, spacecraft, electronics industries.

Chapter 3

EXPERIMENTAL INVESTIGATION AND OPTIMIZATION OF LASER MICRO-MACHINING OF Al 7075 ALLOY USING Nd:YVO_4 LASER

3.1. SELECTION OF MATERIAL

It is observed from the analysis of past research that Al2024/2014 alloy have been experimentally observes and analyzed by a large number of researchers. Similarly, Al 5083/6021 alloy have also been used for the same purpose. While, a little research studies are available on Al7075 alloy. So, for the further research purpose, this newly developed alloy is utilized for the experimentation. Sumitomo Metal, a Japanese company developed Al 7075 alloy in the year of 1943 and used for airframe production. It has different trade names like Ergal, Zicral, etc.

The main alloying element of Al7075 alloy is zinc in addition to few other constituting elements like, magnesium, copper, etc. The test result on chemical composition of this alloy is listed in Table 3.1. It has the highest corrosion resistant properties among all types of aluminium alloy. Al7075 alloy can be compared with different grades of steel depending on the mechanical properties like, strength, fatigue, elasticity, elongation, density, machinability, etc. Approximate values of various properties of Al 7075 alloys are listed in Table 3.2.

Table 3.1 Chemical Composition of Al 7075 Alloy

Alloying Element	Percentage
Aluminium	89.79
Zinc	5.66
Magnesium	2.15
Copper	1.32
Silicon	0.35
Iron	0.45
Manganese	0.08
Titanium	0.05
Chromium	0.10
Others (total)	0.05

(Courtesy: K. K. Mandal et al., Copyright: Elsevier 2018)

Table 3.2 Various Properties of Al 7075 Alloy (Approximate)

Property	Unit	Value
Density	g/cc	2.81
Hardness	Brinell	15
	Rockwell A	53.5
	Rockwell B	87
	Vickers	175
Yield tensile strength	MPa	593
Shear strength	MPa	331
Break point elongation	Percentage	11
Poisson's ratio		0.33
Modulus of elasticity	GPa	71.7
Shear Modulus	GPa	26.9
Fatigue strength	MPa	159
Machinability	Percentage	70
Melting temperature	^{o}C	477 - 635
Thermal conductivity	W/m-K	130
Specific heat capacity	J/g-^{o}C	0.96
Electrical resistivity	ohm-cm	$5.15e^{-6}$
CTE, linear (250^{o}C)	µm/m-^{o}C	25.2
Annealing Temperature	^{o}C	413
Solution Temerature	^{o}C	466 - 482
Aging Temperature	^{o}C	121

(Ref: ASM Aerospace Specification Metals Inc. 800 398-4345)

It is noticed that among the listed properties (Table 3.2), mechanical property is again dependent on their temper up to which Al 7075 alloy can attain. The variation of mechanical properties based on temper is displayed in Table 3.3.

Table 3.3 Mechanical Properties of Al 7075 Alloys of Different Temper

Temper type of Al 7075	Maximum tensile strength (MPa)	Maximum yield strength (MPa)	Elongation (%)
7075-0	280	140	9 - 10
7075-T6	510–540	430–480	5–11
7075-T651	570	500	3 - 9
7075-T7	505	435	13

Further, it is observed that these variation of mechanical energy is again dependent on the form and size of the material. If the thickness of the sample is comparatively more, it exhibits lower value of percentage of elongation at breaking point and both the tensile strength and yield strength [1, 2, 4].

Generally, Al 7075 alloy is available in block form. From this purchased block, approximate 250 mm in length × 25 mm in breath × 2.5 mm in thickness sheets are cut by using Wire-cut Electric Discharge Machine. As the cut-surface is rough and cut-mark left by wire, it is then polished to remove the scratch mark left by WEDM and make them as smooth as possible. Emery papers of different grades like 120 followed 160 followed by 220, etc. are used to produce a very smooth surface by the technique of uniform, uni-directional abrasion of sample over the emery papers. To obtain a fruitful experimental result, acetone solution is used for cleaning the job surface followed by drying-up before initiating the experimental observation.

3.2. EXPERIMENTAL SET-UP

In the present research work, i.e. for laser micro-machining operation, Nd:YVO_4 laser system is utilized. It is a Q-switched, solid state laser with fundamental Gaussian mode. Q switch acts as light source, deflects the light passing through it. It is used for changing laser conditions "on" and "off" very rapidly. It is also used to generate high peak power required to mark on the job. Under fundamental Gaussian mode, a laser beam is available at maximum possible power and efficiency and can be compared with TEM_{00} in case of Nd:YAG laesr. Diode laser of 532 nm wavelength is used for pumping the main laser. Also, a laser beam scanner is used to guide the laser beam accurately with a resolution of 5 µm within speed ranges of 0.5 to 1000 mm/s and triggering permits the pulsing operation up to 250 kHz. Fig. 3.1 shows schematic view of Nd:YVO_4 laser system (Model EMS 100). The laser system has maximum power of 12 W with wavelength of 1064 nm and pulse width of 4.2 ns, spot beam diameter of 50 µm. Technical specification of this laser set-up is represented by Table 3.4. Three main sub-systems are associated with this laser system which are Laser Unit, Control Unit and Workstation, which are interfaced with a computer.

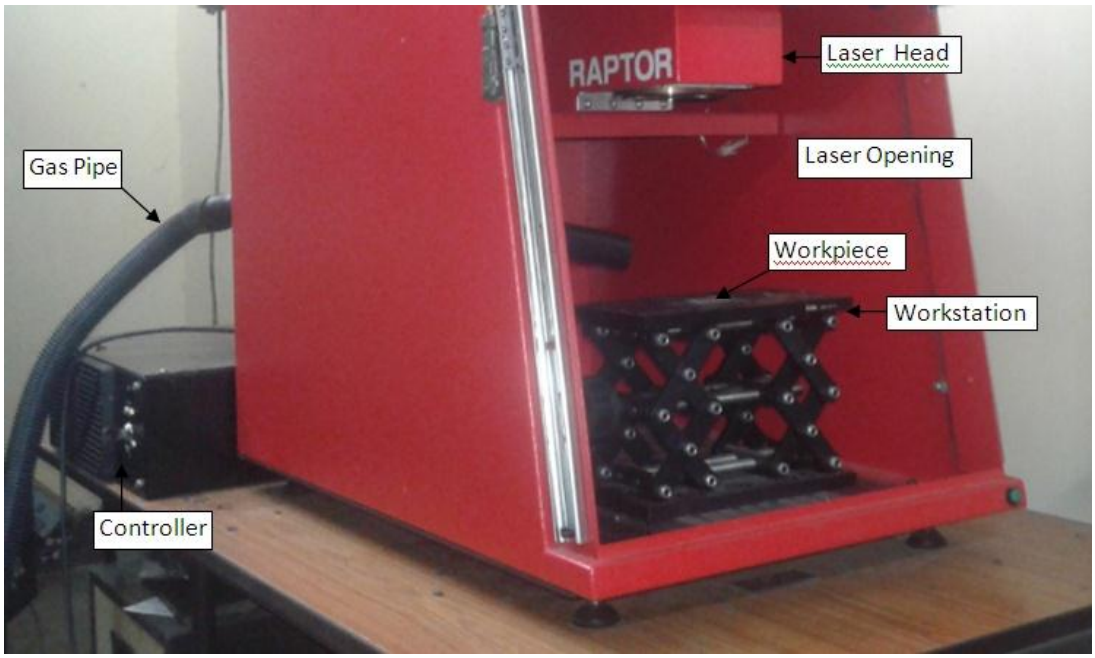

Figure 3.1 Scheme of Nd:YVO_4 Laser Set-up (School of Laser Science and Engg., JU)

Table 3.4 Technical Specification of ND: YVO_4 Laser

Laser type	Q-switched, solid state and diode pumped
Wavelength	1064±4nm
Maximum Output Power	12 W
Peak laser power	> 10kW
Pulse energy	> 0.2mJ
Beam diameter	0.8 – 1.2 mm
Beam divergence	< 2 mrad
Q-switch pulse frequency	0.1 – 250 kHz and CW
Pulse width	24-100 ns

A. Laser Unit

Laser unit consists of a "Laser Marker" machine of Model EMS 100 which is fitted with "Scorpion Rapid" and "Raptor Laser". Laser marker is used to produce different types of geometries like, lines, arcs, square, rectangle, circle, characters, etc. with variable dimensions under the control of Scriba software. According to present experiment, EMS 100 machine is served with Raptor laser. Raptor laser consists of three sub-units as follows:

(i) **Main unit**: The main unit will be located as close as possible to the laser working area. The unit is a 19" rack system which can be fitted into the use's equipment. A minimum gap of 1 meter between the unit and any wall is recommended to provide adequate ventilation. It is also necessary to allow access to the unit so that the removal of the front and top covers are easily possible. Raptor must be located sufficient air movement to avoid heat buildup.

A diode visible laser is inbuilt to the system. It produces a red light which is helpful to indicate the position of Nd:YVO_4 laser beam on the surface where actual marking is to be done accurately. Sometimes, secondary visible diode laser, attached to the Raptor safety shutter, is used as the focus finder. The coincident point of these two lasers identifies the exact positioning and focusing of component to be marked.

(ii) **Laser enclosure and laser beam scanner**: Laser enclosure is the place where laser beam is produced from the laser resonator. Laser resonator consists of two full reflectors, a gain medium and two wavelength (colour) conversion media. Here, pumping i.e. illumination of light from reflector to gain medium and energization i.e. increase of power through light amplification from gain media. The laser beam scanner is mounted on the front of the laser enclosure and positioned over the marking area. The laser enclosure should be a vibration free, leveled structure. Screwed holes are provided underneath the laser enclosure to secure the laser enclosure to the workstation. Special washers are provided to make sure that laser enclosure should not be stressed or distorted during screwed down the system.

(iii) **Controller**: The controller is attached by a short (< 2 m) lead to the control unit. It must be mounted so the user has access to it, especially the emergency stop switch on the top. The controller consists of several sub-components; few of them are as follows:

Laser I and laser O switch/LED: By pressing the laser I switch, laser system is ready to energize the laser foe power supply and commence the start up of laser diode. Yellow LED is glowing which indicates that the laser has started. For stopping the laser, laser O button is to be pressed; Yellow LED will glow and laser diode is de-energized.

Laser START switch: When yellow LED is glowing after I switch, START switch is pressed for staring the laser operation. It is used to execute (start) a part program, downloaded from Scriba program to Raptor control.

Laser STOP switch: STOP switch is used to stop the execution of the part grogram.

SHTR shutter enable switch/LED: By pressing the SHTR switch, it is allowed to open and close the shutter as and when required, commanded by the Raptor's control system and it will indicated by another yellow LED (under enable condition).

Emergency stop switch: The emergency stop switch is a red mushroom push button with yellow background, located on the top of controller. It is used when the system is to

be stopped immediately due to problems. Pressing down this switch, safety shutter is closed which stops the laser power supply and thereby prevent the generation of laser radiation. Once, this button is pressed, it is latched and remains in pressed position. To reset the switch, it is twisted clockwise a quarter turn i.e. 90^{o}.

B. Control Unit

The main switch is located at the front of the control unit to enable the mains power to be switched "put on" and "put off" with two different position for safety to the laser system. The key may only be removed in the "O" (Off) position which prevents any laser action by preventing power being applied to the unit. The "I" (ON) position is the normal position during the operation of the laser. The emission indicators located on the front of the control unit show the laser has been energized. ON/OFF switch and setting/adjusting device are inbuilt into the control unit. Control unit is shown in the Fig. 3.2.

Figure 3.2 Control Unit of ND:YVO_4 laser

C. Workstation

The workpiece is placed and aligned on the workstation which is again attached with the worktable. Workpiece material is placed on this work table which is to be micro-machined. Stand-off distance of 183 mm is maintained very carefully for placing the workpiece on the table. In the present experiment Al 7075 alloy sheet is used for studying the micro-machining. Additional options are included with work station are foot switch, fume extraction system and camera vision system. The specification of workstation is given in Table 3.5 [79].

TABLE 3.5 Specification of Workstation

Dimensions (L x W x H)	650mm 25.6” x 450mm 17. 7 x 777mm/30.6
Weight	30Kg (661Ibs)
Compatibility	Electrox Raptor & Scorpion Fibre Lasers
Construction	Welded Steel With Lift Up Door
Site Requirements	Solid level Surface
Supply requirements	Single phase + Earth, 50 or 60Hz; 100 - 240V

3.3. PLANNING FOR EXPERIMENTATION

To perform the micro-machining operation on Al7075 alloy, four process parameters i.e. laser beam power, pulse frequency, scanning speed and repetition rate are selected. Also, three levels for every process parameters are chosen by trial experiments. Here, the effect of process parameters are observed and then analyzed on the three responses i.e. kerf width, HAZ and angular deviation. Trial/pilot experiments are performed to identify the process parameters' workable ranges. This is done by varying only one parameter at a time keeping all other parameters at certain value. Thus, workable range for that parameter is selected. These steps are repeated for other parameters also. Observed workable range for these process parameters are available in Table 3.6.

Table 3.6 Ranges for the Process Parameters

Parameter	Laser Beam Power i.e. L B P (Watt)	Pulse Frequency i.e. P F (kHz)	Scanning Speed i.e. S S (mm/s)	Repetition Rate i.e. R R
Lower Value	7.5	2	0.2	1
Higher Value	9.5	6	0.6	5

After completing the trial experiment i.e. selection of ranges of process parameters, next step is to design of experiment to minimize number of experiment to be performed without loss of quality characteristics. L9 orthogonal array using Taguchi's methodology, discussed later, is followed for this purpose.

3.3.1. L9 Orthogonal Array Methodology for Design of Experiment

Ronald A. Fisher proposed a methodology for designing experiment is his innovative books: "The Arrangement of Field Experiments" in the year of 1926 and "The Design of Experiments" in the year of 1935. Individual as well as interactive effects of process parameters on the responses can be determined effectively and efficiently by design of experiment. Design of experiment also to make the design robust through full insight interaction between the design elements. Design of experiment or experimental design is basically the design of any information-gathering exercises with variation which may or may not be under the control of experimenter. It is proved that this method is effective to produce high quality products at comparatively low cost. This method has been utilized very efficiently in automobile, medical, aerospace, electronics industries of different countries [80].

One of the branch of design of experiment is the "orthogonal array" following Taguchi methodology. It is helpful to study the space parameter which is based on fractional factorial array. According to this method, he denied the interaction effects between design variables. As a result, number of experiments is further reduced as compared to a full factorial design. It can handle discrete variables also. Orthogonal Arrays, which is also popularly known as Taguchi Method, are frequently applied to study the effect of several process parameters for industrial applications. In orthogonal array type of experiment, columns of independent variable are "Orthogonal" to each other. Orthogonal

arrays are highly fractionated factorial designs. It is employed due to the following advantages:

- Validity and reliability of conclusions over the entire spanned region of control factors,
- There is a lot of saving of time and experimental effort
- Analysis and optimization become easier.

For an orthogonal array definition for further analysis, identification of following is required:

- Number of factor/variable/input parameters for which study is to be done,
- Number of levels selected for each variables,
- Estimation of specific 2-factor interaction effect [81].

In this set of experiments, as there are four influencing parameters with three levels each, so L9 orthogonal array is fitted for design of experiment. L9 orthogonal array using Taguchi methodology is displayed in Table 3.7. Table 3.8 represents the actual values of process parameters for the corresponding experiments following L9 OA by Taguchi methodology.

Table 3.7 L9 Orthogonal Array for Four Parameters with Three Levels Each

Expt. No.	Laser Beam Power i.e. L B P (Level)	Pulse Frequency i.e. P F (Level)	Scanning Speed i.e. S S (Level)	Repetition Rate i.e. R R (Level)
1	1	1	1	1
2	1	2	2	2
3	1	3	3	3
4	2	1	2	3
5	2	2	3	1
6	2	3	1	2
7	3	1	3	2
8	3	2	1	3
9	3	3	2	1

Table 3.8 Experimental Combination of Process Parameters

Expt. No.	L B P (Watt)	P F (kHz)	S S (mm/s)	R R
1	7.5	2	0.2	1
2	7.5	4	0.4	3
3	7.5	6	0.6	5
4	8.5	2	0.4	5
5	8.5	4	0.6	1
6	8.5	6	0.2	3
7	9.5	2	0.6	3
8	9.5	4	0.2	5
9	9.5	6	0.4	1

3.4. EXPERIMENTAL PROCEDURE

- Nd:YVO_4 (Neodymium-doped Yttrium Orthovanadate) laser system is set for performing micro-machining operation on Al 7075 alloy.
- Polishing by emery paper and cleaning by Acetone of the materials is done.
- Trial experiment has been performed for selecting the ranges of the parameters.
- DOE is established to get the parameter combination for experimentation. Laser micro-machining operation is performed by varying the combination.
- Measurement of the responses like kerf width, HAZ and angle is done after successful completion of the micromachining operation through optical microscope (STM 6 made by Olympus).
- From the experimental data, S/N ratio is found out on the basis of their optimization criteria.
- S/N ratio graphs are used to identify the ideal parametric combination for optimum response individually.
- ANOVA is performed to identify the most significant and non-significant parameter.
- Confirmation experiment has been performed to verify the optimum parametric combination.

- Grey relational analysis technique is utilized to identify ideal parametric combination for optimum response simultaneously.
- Confirmation experiment has been performed again to verify the optimum parametric combination obtained by GRA.

3.5 ANALYSIS OF EXPERIMENTAL RESULTS

An angular (90^o angle) pattern of 4 mm each side is opted for the experimental purpose i.e. to observe the responses more accurately. After completing the experimentation, all responses i.e. kerf width, HAZ and angular deviation are observed and measurement has taken very carefully by a precision optical microscope of model, Olympus STM 6. Scheme of this microscope is shown in Fig. 3.3. The measure are taken repeatedly on both sides to take an average of the observation for better performance. Details of the observed average result of the experiment is displayed in Table 3.9.

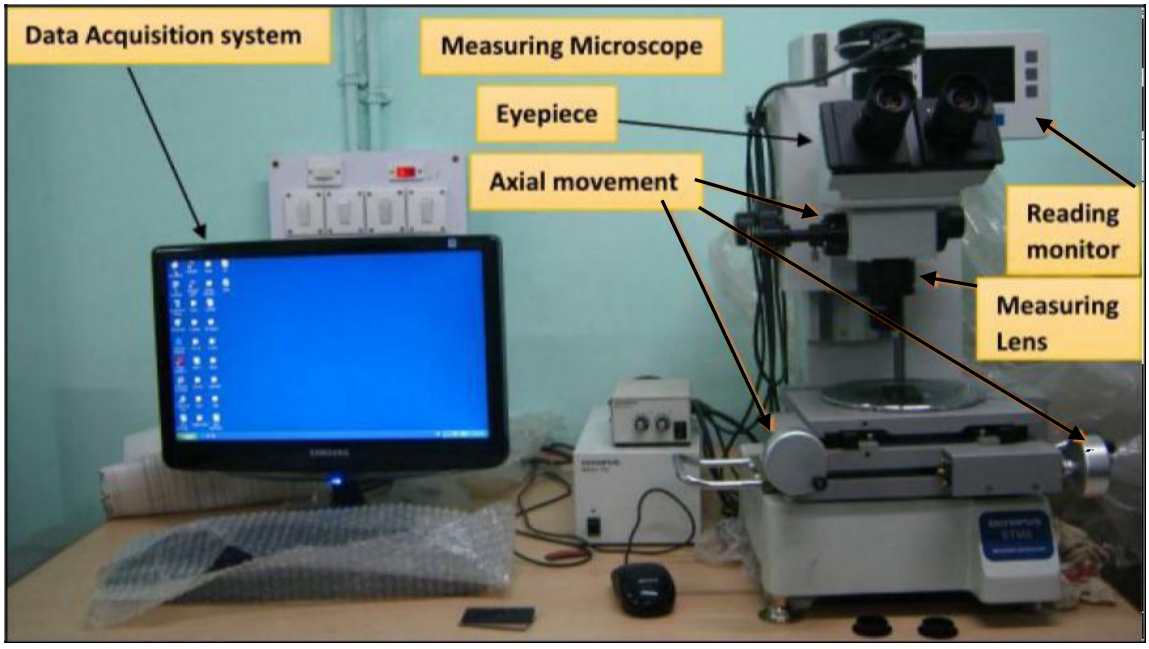

Figure 3.3 Optical Microscope (Olympus STM 6) , Production Engg. Dept., (J.U.)

Depending on the goal of the experiment, signal-to-noise i.e. S/N ratio can be chosen in absence of signal factor and fixed target for any static design. "Signal" indicates the influence of parameters on average response, while "noise" is measure of the influence on the deviations from the average response and determines the sensitiveness of the output to noise factor. Higher the S/N ratio, better will be the experimental performance.

Table 3.9 Experimental Result

Expt. No.	L B P (Watt)	P F (kHz)	S S (mm/s)	R R	Kerf Width (µm)	HAZ (µm)	Angular Deviation(^{0})
1	7.5	2	0.2	1	69.43	122.00	0.14
2	7.5	4	0.4	3	88.74	137.65	0.03
3	7.5	6	0.6	5	91.35	139.32	0.04
4	8.5	2	0.4	5	85.48	125.29	0.05
5	8.5	4	0.6	1	74.14	122.32	0.19
6	8.5	6	0.2	3	80.49	131.12	0.11
7	9.5	2	0.6	3	92.99	128.28	0.06
8	9.5	4	0.2	5	88.72	145.98	0.18
9	9.5	6	0.4	1	90.11	130.88	0.08

In this present work, as the responses are kerf width, HAZ and angular deviation which should be in the lower range. So, the criteria for choosing S/N ratio according to "the-smaller-the-better" for maximum performance of the experiment. Mean value for any level is calculated as the average of all responses obtained at that level, denoted by y_i. The y_i value is then converted to mean square deviation (MSD) or quality loss function by using the formula given in Eq. 3.1, following lower-the-better (LB) criteria. However, experimental objective decides the type of quality loss function or MSD, which are: lower-the-best (LB), nominal-the-best (NB) and higher-the-best (HB).

$$\text{MSD} = \frac{1}{n}\left(\sum_{i=1}^{n} y_i^2\right) \tag{3.1}$$

where, y_i is observed data for quality characteristic at ith trial and n is number of repetition at the same trial. The corresponding S/N ratio (η_i) is calculated from Eq. 3.2 as follows:

$$(\eta_j) = -10 \log_{10}(MSD) \quad (3.2)$$

This S.N ratio measures (expected part/unexpected part). Therefore aim is to maximize this value irrespective of nature of quality characteristics. Calculated S/N values corresponding to mean values at each level is listed in Table 3.10.

Table 3.10 Mean Values and Corresponding S/N Values of Responses

Expt. No.	Kerf Width		HAZ (µm)		Angular Deviation	
	Mean (µm)	S/N Value (DB)	Mean (µm)	S/N Value (DB)	Mean (^{0})	S/N Value (DB)
1	69.43	36.83094	122.00	41.727197	0.14	-17.07744
2	88.74	38.96239	137.65	42.775524	0.03	-30.45757
3	91.35	39.21417	139.32	42.880269	0.04	-27.95880
4	85.48	38.63729	125.29	41.958328	0.05	-26.02060
5	74.14	37.40105	122.32	41.749949	0.19	-14.42493
6	80.49	38.11484	131.12	42.353379	0.11	-19.17215
7	92.99	39.36873	128.28	42.163179	0.06	-24.43697
8	88.72	38.96043	145.98	43.285867	0.18	-14.89455
9	90.11	39.09546	130.88	42.337465	0.08	-21.93820

Mean and S/N ratio plots for every process parameters are analyzed for the assessment of influence/significance on the responses. From this analysis, optimum set of process parameters for individual response can be determined [80. 81].

3.5.1 Study of the Effect of Process Parameters on Kerf Width

A. Analysis of Kerf Width Based on S/N Ratio Plots

Fig. 3.4 is the S/N ratio plot of kerf width Vs processing parameters which reveals that initially S/N ratio increases due to increase of laser beam power gradually, but later decreases sharply. Because at the initial stage, sufficient heat is generated which is penetrated fully into the material. But, further increase in laser beam power results too

much generated heat than the requirement, more material is removed from top surface instead of penetrating into the material sufficiently and leads to increase kerf width. S/N ratio decreases continuously due to increase of pulse frequency gradually, then at faster rate. Increase in pulse frequency leads decrease of interaction time between work surface and generated heat, which results less penetration of heat rather than spreading. spreading. S/N ratio decreases steeply due to increase of scanning speed at initial stage, but later it increases gradually. Because increase of scanning speed results insufficient generated heat to penetrate enough rather the chance of spreading is increased due to less interaction between laser beam and work which result increase of kerf width. However further increase of scanning speed, chances of heat spreading is very rarely seen and the heat generation become sufficient for melting and vaporizing the material enough to decrease kerf width. On the other hand, S/N ratio increases continuously with the increase of repetition rate gradually and then at slower rate. Increase of repetition rate leads to increase interaction time between generated heat and workpiece surface, results kerf width increase. It is also noticed from the plot that optimum parametric combination is LBP_2 PF_1 SS_1 RR_1 i.e. laser beam power of 8.5 W, pulse frequency of 2 kHz, scanning speed of 0.2 mm/s and repetition rate of 1.

Fig. 3.5 (a) and (b) represent the photographs of minimum kerf width (69 µm) at two different location of machining operation at the same parametric combination, LBP_1 PF_1 SS_1 RR_1 i.e. laser beam power of 7.5 W, pulse frequency of 2 kHz, scanning speed of 0.2 m/s and repetition rate of 1, captured by Olympus optical microscope (Model: STM 6). Both the cases, though kerf width value is same but, HAZ differs (126.96 µm along X-axis, Fig. 3.5 (a) and 113.85 µm along Y-axis, Fig. 3.5 (b)) in two direction of machining. However, average will be considered for the analysis. Similar consequence may also be happed for same HAZ but different kerf width. Even, the value may differ in different location in a certain direction of machining.

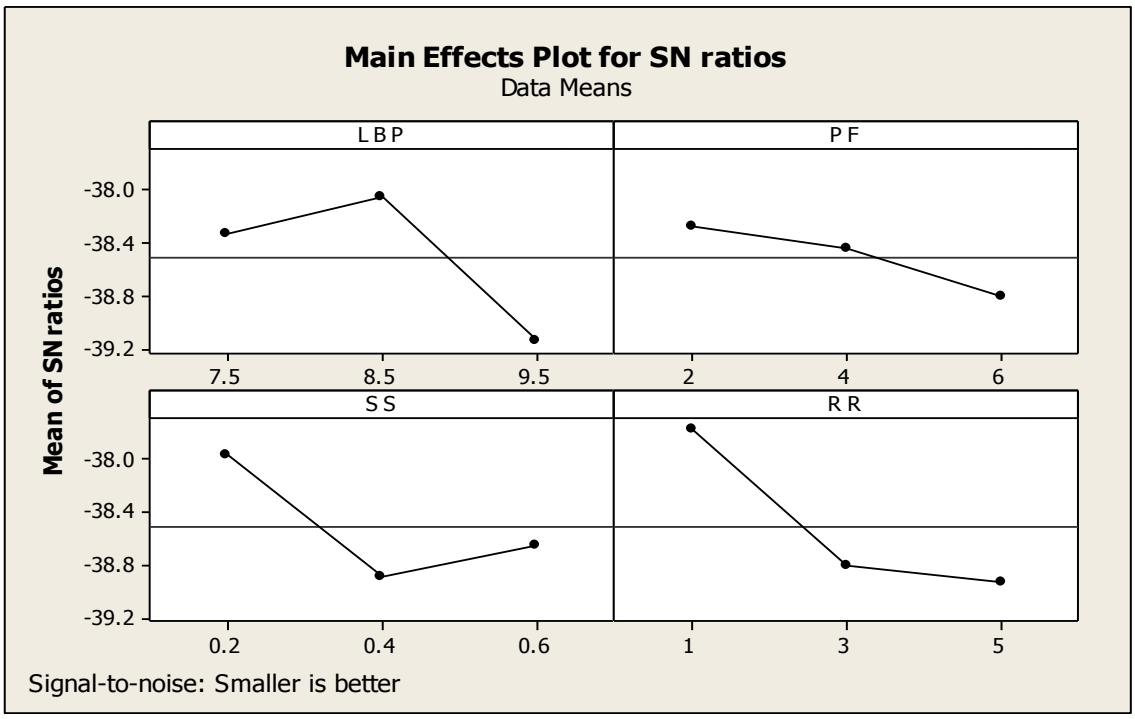

Figure 3.4 S/N Ratio Plot Depicting Effects of Parameters on Kerf Width

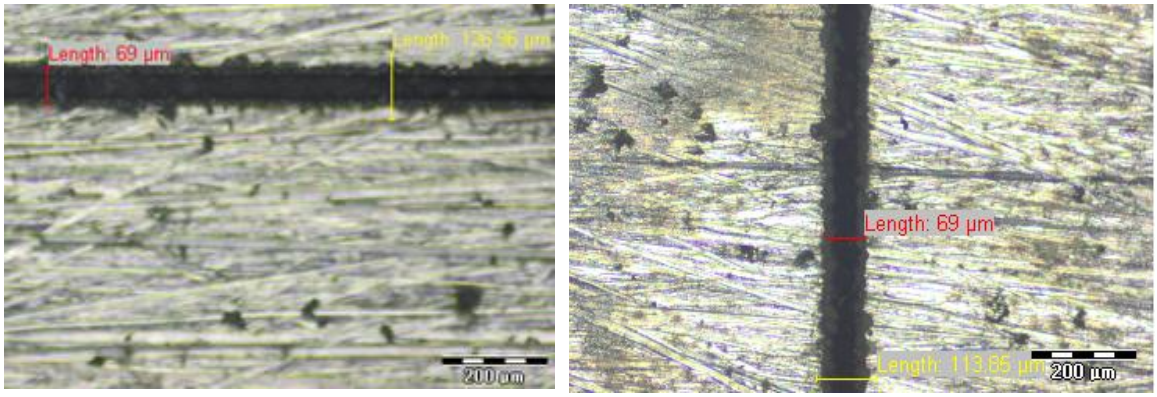

(a) Along the X-axis (b) Along the Y-axis

Figure 3.5 Microscopic Views of Minimum Kerf Width at Level LBP_1 PF_1 SS_1 RR_1

B. Analysis of Kerf Width Based on Analysis of Variance (ANOVA)

Statistical technique of ANOVA is applied on experimental data. It is a case of pulled error ANOVA to identify the significant parameters influencing the micro-machining operation. The total sum of square deviation can be determined from Eq. 3.3,

$$SST = \sum_{j=1}^{N} (\eta_j - \eta_m)^2 \quad (3.3)$$

where, N is the No. of experiments, η_m is grand mean of all the S/N ratios, which is 19.68279 (dB) in this experiment. Calculated SST is used for determining relative influence of input parameters. For every level of any parameter, there are three experiments. So, the sum of squares due to laser beam power is calculated as

$$3(\eta_{LP_1}-\eta_m)^2 + 3(\eta_{LP_2}-\eta_m)^2 + 3(\eta_{LP_3}-\eta_m)^2 \quad (3.4)$$

where, η_{LP_1} is mean of S/N ratio for LBP at level 1. By this way same will be calculated for other parameters. Mean squares are determined by dividing these sum squares by degrees of freedom. After then percentage contribution of individual factors are calculated.

ANOVA of kerf width as shown in Table 3.11, reveals that repetition rate affects mostly (39.40%) on kerf width, then after laser beam power affects (30.94%), scanning speed (22.56%) and pulse frequency (07.10%). This values indicate that repetition rate and laser beam are significant parameters and pulse frequency is insignificant parameter [80, 81].

Table 3.11 ANOVA for Kerf Width

Parameter	DF	Sum Square	Mean Square	F statistics	% Contribution	Rank
LBP	2	1.92059	0.9603	4.3579	30.94	2
PF	2	0.44071	0.22035	1.0000	07.10	4
SS	2	1.40036	0.70018	3.1775	22.56	3
RR	2	2.44530	1.22265	5.54855	39.40	1
Pooled Error	2	0.44071	0.22036			
Total	8	6.20696				

C. Confirmation Test based on Taguchi methodology and S/N Ratio Plots for Kerf Width

After determining optimum combination of process parametric combinations from S/N ratio plot and predicting optimum response from Eq. 3.5 under these conditions, confirmation test is conducted to verify adequacy of the model to determine the optimum quality characteristics. Prediction of optimum value of S/N ratio, (η_{opt}) is calculated as:

$$\eta_{opt} = \eta_m + \sum_{j=1}^{p} (\eta_j - \eta_m) \quad (3.5)$$

where, η_j is optimum level's mean S/N ratio of individual parameter, p is number of design parameters affecting quality characteristics. Confirmation result are listed in Table 3.12 in comparison with predicted value [80,81].

Table 3.12 Confirmation Test for Kerf Width

	Initial Parameter Setting	Optimum Parameter Setting	
		Predicted	Experimental
Level	$LBP_1PF_1SS_1RR_1$	$LBP_2PF_1SS_1RR_1$	$LBP_2PF_1SS_1RR_1$
Kerf width (µm)	69.43	67.111	66.2907
S/N ratio (dB)	-36.8309	-36.4291	-36.5459
Predicted Error of S/N Ratio		-0.1168	
Confidence Limit		± 0.93885	

Here, the confidence limit i.e. two standard-deviation (95% confidence interval) is estimated from relationship given in Eq. 3.6.

$$\text{Confidence limit} = \pm 2\sqrt{(\text{prediction/pooled error})} \quad (3.6)$$

3.5.2. Analysis of the Effect of Variable Parameters on HAZ

A. Analysis of HAZ Based on S/N Ratio Plots

Fig. 3.6 shows S/N plot of heat affected zone (HAZ) Vs. processing parameters. From this plot, it is clear that initially S/N ratio increases due to increase of laser beam power gradually, but later decreases sharply. This is due to the fact that at the initial stage, sufficient heat is generated which is penetrated fully into the material instead of

spreading. But further increase of laser beam power results too much heat generated than the requirement and more material is removed from top surface instead of penetrating into the material sufficiently and tends to increase the HAZ.

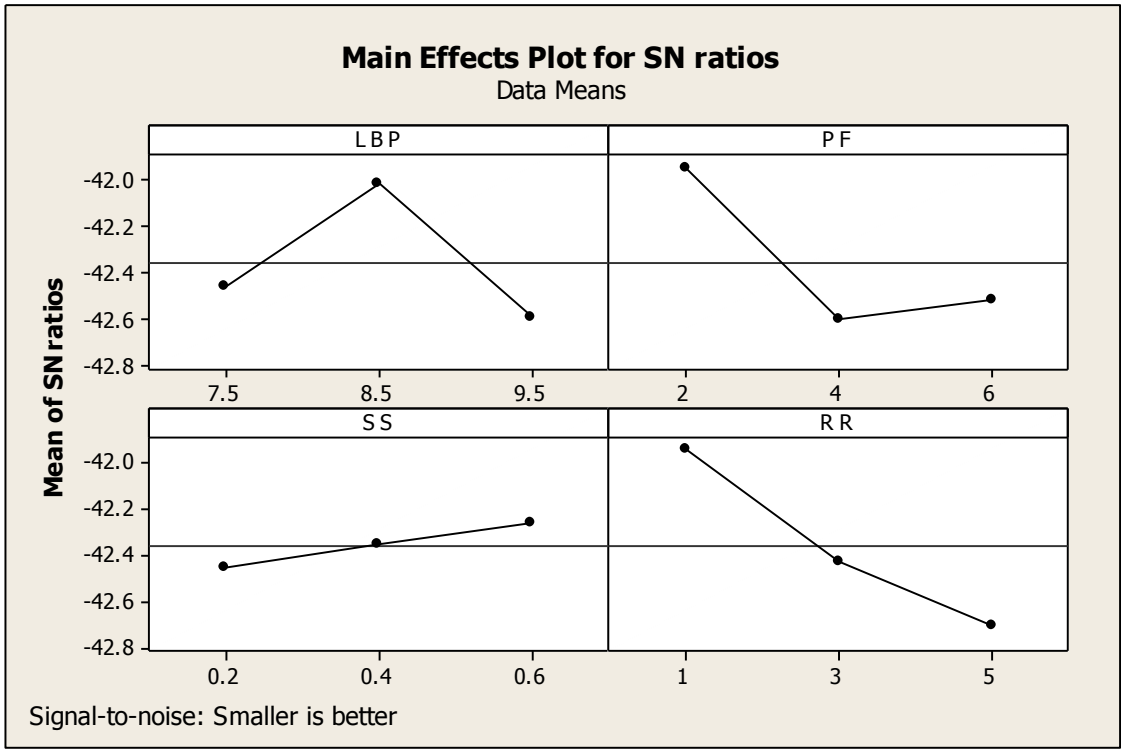

Figure 3.6 S/N Ratio Plot Depicting Effects of Processing Parameters on HAZ

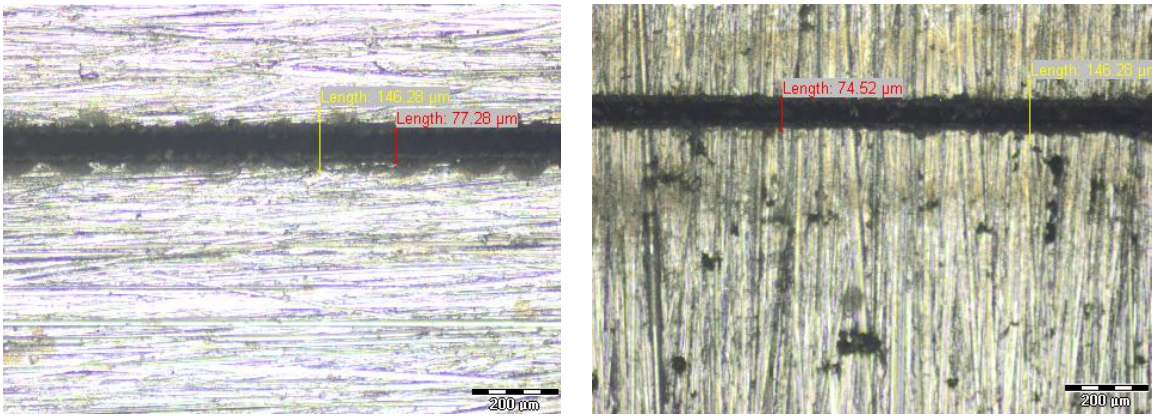

(a) Along X-axis (b) Along Y-axis

Figure 3.7 Microscopic Views of HAZ at Level LBP_3 PF_2 SS_1 RR_3

S/N ratio decreases sharply with the increase of pulse frequency at the initial stage, but later it increases gradually. Because increase of pulse frequency results insufficient heat generation to penetrate enough rather than spreading due to less interaction between laser beam and work. However further increase of pulse frequency, heat spreading is very rarely seen and the heat generation become sufficient for melting and vaporization of material enough which tends to decrease kerf width. S/N ratio decreases continuously due to increase of scanning speed. Because, generated heat is enough to meet the requirement for melting and vaporizing the material sufficiently as laser beam moves faster. Whereas, increase of repetition rate leads to increase interaction time between heat generation and job surface which results HAZ increase. Higher the repetition rate less will be HAZ. So, the plot reveals that optimum parametric combination is $LBP_2PF_1SS_3RR_1$ i.e. laser beam power of 8.5 W, pulse frequency of 2 kHz, scanning speed of 0.6 mm/s and repetition rate of 1.

Fig. 3.7 (a) and (b) represent the microscopic views of HAZ at Level LBP_3 PF_2 SS_1 RR_3 at two different direction of machining. Fig. 3.7 (a) exhibits the photographs captured along X-direction. While. Fig. 3.7 (b) is captured along Y-axis. In both the case, HAZ value is same but kerf widths are different. Opposite may also be happened that is shown in Fig. 3.5.

B. Analysis of HAZ Based on Analysis of Variance (ANOVA)

ANOVA of HAZ is done in the similar way as done in case of kerf width following Eq. 3.3 and Eq. 3.4 i.e. calculation of all the parameters related to ANOVA. The ANOVA result is tabulated in Table 3.13 which reveals that repetition rate affects mostly (40.12%) on HAZ, then after frequency (33.62%), laser beam power (23.85%) and scanning speed (22.33%). This result indicates that repetition rate is most influencing parameter, whereas scanning speed is least significant parameter.

Table 3.13 ANOVA for HAZ

Parameter	DOF	Sum Square	Mean Square	F statistics	% Contribution	Rank
LBP	2	0.54217	0.27108	9.88279	23.85	3
PF	2	0.76434	0.38217	13.93256	33.62	2
SS	2	0.05486	0.02743	01.0000	02.41	4
RR	2	0.91233	0.45618	16.63015	40.12	1
Pooled Error	2	0.05486	0.02743			
Total	8	2.27370				

C. Confirmation Test Based on Taguchi methodology and S/N Ratio Plots for HAZ

Once the optimum combination of process parametric conditions from S/N graph and prediction of the optimum response using Eq. 3.5 under these conditions are completed, confirmation test is conducted to verify adequacy of the model to determine optimum quality characteristics. Table 3.14 shows the result of confirmation test which are in very close agreement with the predicted value.

Table 3.14 Confirmation Test for HAZ

	Initial Parameter Setting	Optimum Parameter Setting	
		Predicted	Experimental
Level	$LBP_1PF_1SS_1RR_1$	$LBP_2PF_1SS_3RR_1$	$LBP_2PF_1SS_3RR_1$
HAZ (µm)	122	113.446	112.193
S/N ratio (dB)	-41.7272	-41.0958	-40.9993
Predicted Error of S/N Ratio		0.0965	
Confidence Limit		± 0.33124	

3.5.3. Analysis of Influence of Process Parameters on Angular Deviation

A. Analysis of Angular Deviation Based on S/N Ratio Plots

Fig. 3.8 is S/N ratio plot for angular deviation Vs processing parameters. It is observed from this plot that initially S/N ratio decreases at faster rate due to increase of laser beam power, later it increases slightly. Because, increase of laser beam power results more generated heat than the requirement; some portion is heat is able to penetrate into the

surface and most of the part is spread which produces a poor quality surface. However when saturation condition is reached, the generated enough heat is penetrated into material; causes slight decrease of angular deviation. S/N ratio decreases initially at faster rate due to increase of pulse frequency, later it increases gradually. Because, increase of pulse frequency leads to decrease in interaction time between heat generation and job surface and results more spreading of heat rather than smooth removal of material. As a result S/N ratio decreases. Bur, further increase of pulse frequency produces smoother surface due to sufficient heating, which increases S/N ratio. Whereas, S/N ratio increases gradually due to increase of scanning speed at initial stage but later decreases gradually. Because, generated heat becomes sufficient for melting and vaporizing the material through penetration enough as laser moves faster which helps to remove material smoothly. Further increase of scanning speed results spreading rather than more penetration into the material of heat. Initially, S/N ratio increases gradually due to increase of repetition rate but later decreases gradually. Because generated heat is sufficient for melting and vaporizing the material enough for less number of pass. But further increase of repetition rate results further melting and vaporization from the same region. Therefore there is a chance of less penetration of generated heat into the material again rather than spreading. Also, t is concluded from this plot, optimum parametric combination is noticed at $LBP_1PF_1SS_2RR_2$ i.e. laser beam power of 7.5 W, pulse frequency of 2 kHz, scanning speed of 0.4 mm/s and repetition rate of 3.

Fig. 3.9 (a) and (b) represent the photographs of angle formed for a target angle of 90^o at two different combination of machining parameters. Angular deviation is difference between angle formed and target angle. Fig. 3.9 (a) represents the photographs for angle produced at Level LBP_2 PF_2 SS_3 RR_1 and the value is 89.75^o, so, angular deviation is (89.75^o - 90^o) i.e. - 0.25^o. Similarly, the angular deviation at Level LBP_2 PF_3 SS_1 RR_2 is (90.10^o - 90^o) i.e 0.10^o.

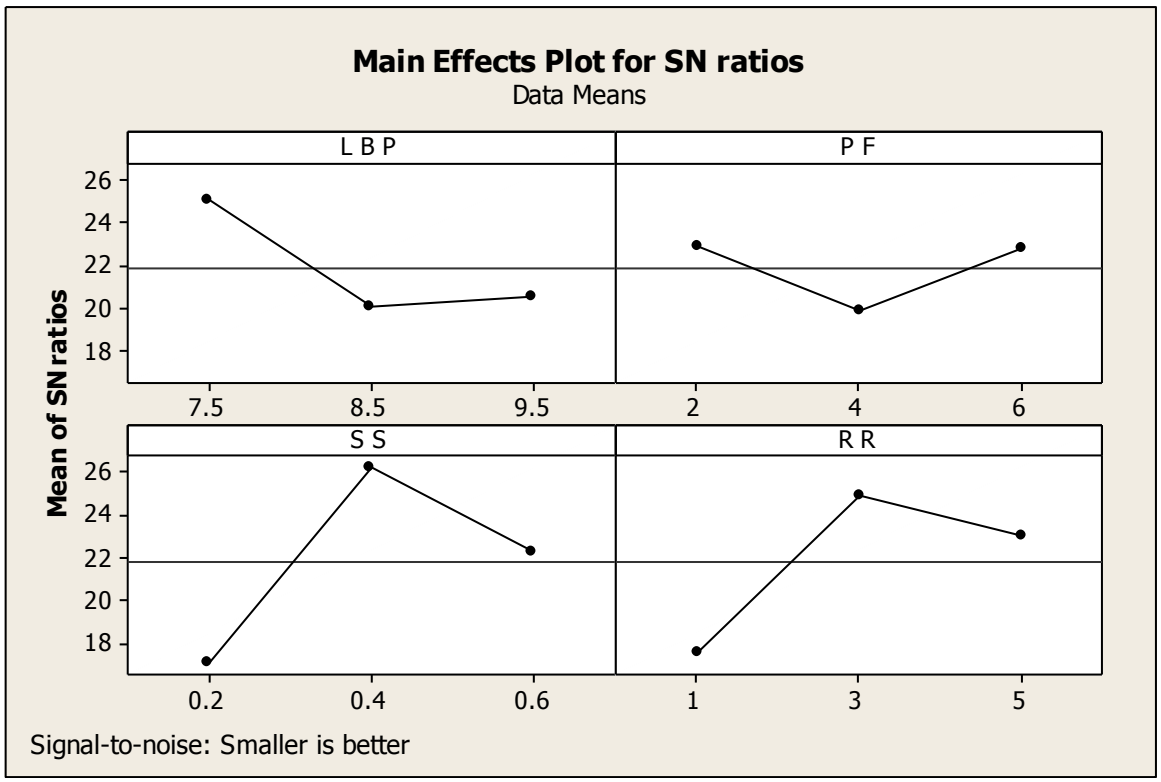

Figure 3.8 S/N Ratio Plot Showing Effects of Parameters on Angular Deviation

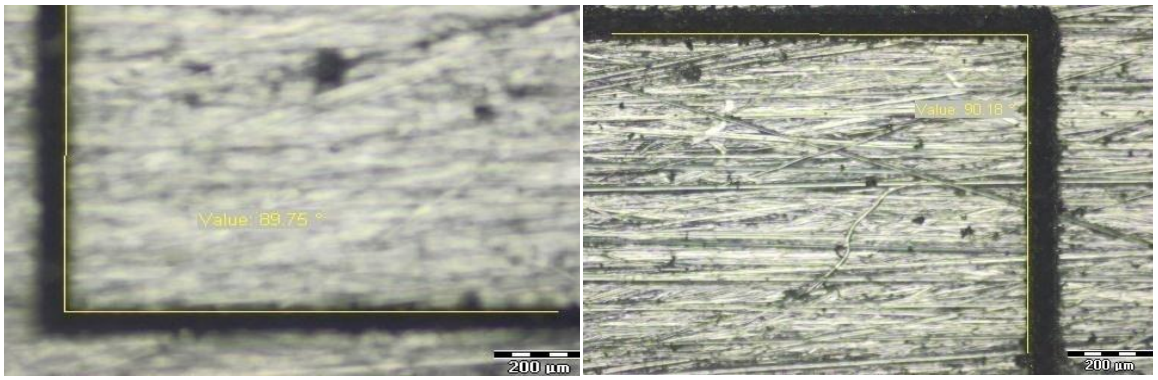

(a) at Level LBP_2 PF_2 SS_3 RR_1 (b) at Level LBP_2 PF_3 SS_1 RR_2

Figure 3.9 Microscopic Views of Angle Formed at Different Levels

B. Analysis of Angular Deviation Based on Analysis of Variance (ANOVA)

ANOVA of angular deviation is calculated by using Eq. 3.3 and 3.4 which are represented in Table 3.15. It is clear that scanning speed affects mostly (45.66%) on angular deviation, then after repetition rate (31.30%), laser beam power (16.62%) and at last frequency (06.42%). The ANOVA result reveals that scanning speed is most significant parameter and pulse frequency is least insignificant parameter.

Table 3.15 ANOVA for Angular Deviation

Parameter	DOF	Sum Square	Mean Square	F statistics	% Contribution	Rank
LBP	2	45.524	22.762	2.59045	16.62	3
PF	2	17.574	8.787	1.00000	06.42	4
SS	2	125.053	62.526	7.11853	45.66	1
RR	2	85.730	42.865	4.87824	31.30	2
Pooled Error	2	17.574	8.8787			
Total	8	273.881				

C Confirmation test based on Taguchi methodology and S/N Ratio Plots for Angular Deviation

Confirmation experiment has been performed to verify the optimum parametric combination obtained from S/N ratio graph and also by comparing experimental optimum value with predicted optimum value from Eq. 3.5. Confirmation test result is shown in Table 3.16.

Table 3.16 Confirmation Test for Angular Deviation

	Initial Parameter Setting	Optimum Parameter Setting	
		Predicted	Experimental
Level	$LBP_1PF_2SS_2RR_2$	$LBP_1PF_1SS_2RR_2$	$LBP_1PF_1SS_2RR_2$
Angular Deviation (degree)	-0.03	-0.0212	-0.0233
S/N ratio (dB)	30.4576	32.6529	33.4653
Predicted error of S/N ratio		0.8124	
Confidence limits		±5.95942	

3.6. OPTIMIZATION OF LASER MICRO-MACHINING OF Al 7075 ALLOY

3.6.1. Optimization of Process Parameters by Grey Relational Analysis (GRA)

Grey theory was established by Dr. Deng. This theory consists of grey relational analysis (GRA), grey modeling, prediction and decision making for a system. It provides an useful solution for multi-responses/decisions of the uncertainty, number of inputs and discrete data problem. Pre-processing of all data i.e. grey relational generating is done by the following steps:

(a) Mean values or S/N ratios are converted into normalized value in the range 0 to 1 to obtain a comparable sequence. Normalization is done by using Eq. (4.6) for 'lower-the-better' quality characteristics as follows:

$$x_{ij} = (\max_j y_{ij} - y_{ij}) / (\max_j y_{ij} - \min_j y_{ij}) \quad (3.6)$$

where, y_{ij} is ith quality characteristic in the jth experiment. Lager normalized value represents the better result.

(b) Relationship between ideal value and actual experimental result are expressed by grey relational coefficient, ζ_{ij}, which are calculated from the expression no 3.7,

$$\{\min_i \min_j (x_i^0 - x_{ij}) + \zeta \max_i \max_j (x_i^0 - x_{ij})\} / \{(x_i^0 - x_{ij}) + \zeta \max_i \max_j (x_i^0 - x_{ij})\} \quad (3.7)$$

Where, x_i^0 is ideal normalized value for ith quality characteristics and ξ is a distinguishing coefficient, whose value ranges between 0 and 1.

(c) Finally, grey relational coefficients are integrated to grey relational grade of every experimental value using weighting method as:

$$\gamma_i = 1/m \Sigma w_i \zeta_{ij} \quad (3.8)$$

Where γ_i is grey relational grade for the jth experiment, wi is weighting factor for ith quality characteristics and m is the number of quality characteristics. Here, weighting factor for all the quality characteristics is set as 1:1:1. The results of GRA are provided in

Table 3.17. Higher grey relational grade means experimental result is very closer to ideally normalized value of responses. responses [27, 82].

Table 3.17 Grey Relational Co-efficient, Grade and Rank of Experimental Result

Expt. No	Kerf Width		HAZ		Angular Deviation		Grade	Rank
	(µm)	Coefficient	(µm)	Coefficient	Degree	Coefficient		
1	69.43	1	122	1	0.14	0.4285714	0.80952	1
2	88.74	0.3789299	137.655	0.4337438	0.03	1	0.60422	4
3	91.35	0.3495838	139.317	0.4091475	0.042	0.8730158	0.54392	6
4	85.48	0.4233153	125.296	0.784399	0.047	0.8291457	0.67895	2
5	74.135	0.714615	122.323	0.9737707	0.195	0.3333333	0.67391	3
6	80.487	0.5158614	131.123	0.5679273	0.109	0.5108359	0.53154	7
7	92.993	0.3333333	128.276	0.6564390	0.056	0.7603686	0.58338	5
8	88.72	0.3791738	145.983	0.3333333	0.178	0.3579176	0.35681	9
9	90.11	0.3629376	130.883	0.5744568	0.083	0.6088561	0.51542	8

The effect of machining parameters in terms of grey relational grade at different levels is summarized in Table 3.18 which shows the optimum parametric combination. The optimal values of laser micro-machining process parameters to maximize grey relational grade are identified as laser beam power at level 1 (7.5 W), pulse frequency at level 1 (2 kHz), scanning speed at level 3 (0.6 mm/sec) and repetition rate at level 1 (1) for minimizing the kerf width, HAZ and angle deviation simultaneously.

Table 3.18 Grey Relational Grade at Different Levels of Processing Parameters

Processing Parameters	Grey Relational Grade			Main Effects (Max - Min)	Rank	Sum of Squares
	Level 1	Level 2	Level 3			
Laser Beam Power	**0.65255**	0.62813	0.48520	0.16735	1	0.0163
Pulse Frequency	**0.69062**	0.54498	0.53029	0.16033	2	0.0157
Scanning Speed	0.56596	0.59953	**0.60040**	0.03444	4	0.0008*
Repetition Rate	**0.66628**	0.57305	0.52656	0.13972	3	0.0101
	Grand Mean Value of Grey Relational Grade: **0.5886**					*** Error**

3.6.2. Confirmation Test Based on GRA

Confirmation experiment is carried out to verify the feasibility and reproducibility of the model. The estimated optimum grey relational grade, using the optimal level of process parameters is calculated from Eq. 3.9 as follows:

$$\gamma_{opt} = \gamma_m + \sum_{i=0}^{p}(\gamma i - \gamma m) \quad (3.9)$$

where γ_m is the grand mean of the grey relational grade, γ_i is the mean of the grey relational grade at the optimal level and q is the number of micro-machining parameters

The result of confirmation test is tabulated in Table 3.19.

To judge the closeness of the observed and predicted optimum results, variance of prediction error is determined as:

$$\sigma^2_{pred} = [1/n_0]\ \sigma^2_e + [1/n_r]\ \sigma^2_e \quad (3.10)$$

Where n_0 is the effective sample size, n_r is the sample size in the confirmation experiment, and σ^2_e is the error variance.

Here, effective sample size can be computed from Eq. 3.11.

$$n_0 = n/(1+ DOF_{factor}) \quad (3.11)$$

where, n is the total number of trials and DOF_{factor} is the total degrees of freedom that are associated with the factors. Here, $n_0 = 1$.

Finally, the error variance is estimated as:

$$\sigma^2_e = SS_{error} / DOF_{error} \quad (3.12)$$

where, SS_{error} is the sum of squares due to error.

Table 3.19 Result of Confirmation Test Based on GRA

Parameter/Level	Initial Parameter Setting	Optimal Parameters	
		Prediction	Experimental
	$LBP_2PF_1SS_2RR_3$	$LBP_1PF_1SS_1RR_1$	$LBP_1PF_1SS_1RR_1$
Kerf Width	85.48		65.66
HAZ	125.296		111.21
Angular Deviation	0.047		0.03
Grey Relational Grade (GRG)	0.67895	0.80952	0.89733
Improvement of GRG	0.21838		
Prediction Error	-0.06781		

3.6.3. Comparison of Optimum Values Obtained by Taguchi Methodology and GRA

Table 3.20 shows the optimum level results of responses obtained by Taguchi methodology (TM) and grey relational analysis (GRA) . It is observed that kerf with and HAZ are improved noticeably, but angular deviation is disproved slightly under grey relational analysis as compared to Taguchi methodology because of different combination of experiment.

Table 3.20 Comparison Between Optimum Values Obtained by TM and GRA

Parameters	Taguchi Methodology		Grey Relational Analysis	
	Value	Level	Value	Level
Kerf Width	66.2907	$LBP_2PF_1SS_1RR_1$	65.66	$LBP_1PF_1SS_1RR_1$
HAZ	112.193	$LBP_2PF_1SS_3RR_1$	111.21	$LBP_1PF_1SS_1RR_1$
Angular Deviation	-0.0233	$LBP_1PF_1SS_2RR_2$	0.03	$LBP_1PF_1SS_1RR_1$

3.7. CONCLUSIONS

Micro-machining on Al 7075 alloy has been performed successfully using pulsed Nd:YVO_4 laser. L9 orthogonal array using Taguchi's methodology is applied in design of experiment. S/N plots predict the optimum levels of machining for individual output i.e. kerf width, HAZ and angular deviations. ANOVA is done for studying significance of each machining parameter i.e. laser beam power, pulse frequency, scanning speed and repetition rate on the responses. ANOVA shows that repetition rate has most significance on kerf width, whereas pulse frequency has very little significance. ANOVA also represents that repetition rate hast most significance on HAZ, whereas scanning speed has very little significance.

On the other side, scanning speed is the most significant parameter to affect on angular deviation, whereas pulse frequency has very little significance. Confirmation experiment is performed to verify the predicted values at optimum levels. Corresponding optimized parametric combinations are $LBP_2PF_1SS_1RR_1$ laser beam power of 8.5 W, pulse

frequency of 2 kHz, scanning speed of 0.2 mm/s and repetition rate of 1, $LBP_2PF_1SS_3RR_1$ i.e. laser beam power of 8.5 W, pulse frequency of 2 kHz, scanning speed of 0.6 mm/s and repetition rate of 1, $LBP_1PF_1SS_2RR_2$ i.e. laser beam power of 7.5 W, pulse frequency of 2 kHz, scanning speed of 0.4 mm/s and repetition rate of 3; for kerf width, HAZ and angular deviation, respectively.

In addition to this Kerf width, HAZ and angular deviations are optimized simultaneously using a single character called grey relational grade for all the experiment as well as at all the levels. Further confirmation test has been performed to verify this optimum level. The optimized parametric condition is $LBP_1PF_1SS_1RR_1$i.e. laser beam power of 7.5 W, pulse frequency of 2 kHz, scanning speed of 0.2 mm/s and repetition rate of 1. Confirmation experiment for both the cases improved the machining quality sufficiently compared to the initial machining parameter setting. However, there is no improvement of angular deviation.

Chapter 4

PARAMETRIC STUDY AND OPTIMIZATION OF Nd:YVO_4 LASER MICRO-DRILLING OF COPPER

Copper & its alloys are widely used for a variety of products that enable to enhance the everyday life due to their excellent properties. Though they are highly reflective in nature, they can be laser micro-machine with short to ultrashort laser with shorter wavelength. Here, Nd:YVO4 pulsed laser is utilized for micro-drilling operation. Fig. 4.1 shows the scheme of micro-drilling operation. Hole quality is analyzed, optimized and predicted by using different statistical and mathematical techniques.

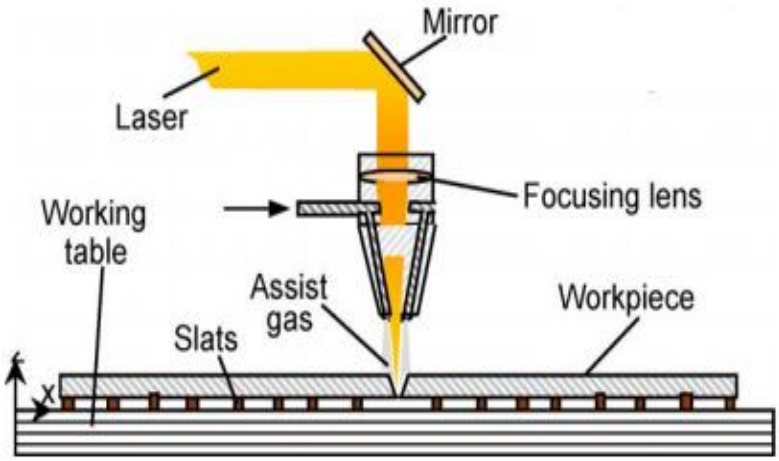

Figure 4.1 Scheme of Laser Micro-drilling Operation (Courtesy: A Stournaras et all., Copyright:Elsevier, 2009)

4.1 EXPERIMENTAL SET-UP

A typical solid state laser, diode pumped, Nd:YVO_4 (EMS 100) of maximum beam power of 12 W, wavelength of 1064 nm is utilized for laser micro-drilling operation. The laser system has main three parts which are laser unit, control unit and work station. The laser unit consists of EMS 100 laser marker compatible with Scorpion Rapid and Raptor Laser. The control unit consists of ON/OFF switch, device for setting the process parameters. A working station is used for placing and aligning the workpiece for the perfection of operation. Experimental set-up used for the present work i.e. laser micro-drilling of copper is shown in Fig. 3.1. Also, the details about the laser machine is discussed in section 3.2.

4.2 PLANNING FOR EXPERIMENT

Copper & its alloys are widely used for a variety of products that enable an enhance the everyday life. They have very good electrical & thermal conductivity, good strength &

formability and exhibits outstanding resistance to corrosion & fatigue. They are very good for micro-fabrication and micro-machining. Due to these properties they are used in the field of micro-electronics, printed circuit board, robotics, bio-medical application, aerospace & aircraft industry, automobile industry, etc. Copper sheet of 30 mm length, 20 mm breath and 0.2 mm thick is used as the workpiece for the experimental investigation. Laser micro-drilling (trepanning) process is performed to produce micro-hole of 800 µm diameter. Major properties of copper are shown in Table 4.1.

Table 4.1 Major Properties of Copper

Properties	**Unit**	**Value**
Electrical Conductivity	Siemens/mm	58.5
Thermal Conductivity	W/mK	390
Density	gm/cc	8.96
Yield Strength	MPa	70
Ultimate Tensile Strength	MPa	220
Melting Point	Degree Celsius	1084

In the present research, four processing parameters i.e. laser beam power (LBM), pulse frequency (PF), scanning speed (SS) and number of passes (NP) with three levels each are considered as the input parameters. Whereas, experimental investigation is performed to observe, analyze, optimize and predict the effect of input parameters on the responses i.e. HAZ width and hole taper. Detail of the process parameters are shown in Table 4.2. To minimize the number of experiments, L9 orthogonal array following Taguchi's methodology (shown in Table 4.3) is applied as the design of experiment tool. Here all the influencing parameters are represented in coded form as level 1, level 2 and level 3.

Table 4.2 Detail of Process Parameters

Parameters	Unit	Level 1	Level 2	Level 3
Laser Beam Power (L.P.)	Watt	8.4	9.6	10.8
Pulse Frequency (P.F.)	kHz	6	9	12
Scanning Speed (S.S.)	mm/sec	0.2	0.4	0.6
Number of Pass (No. of Pass)		5	7	9

Table 4.3 Design of Experiments; L9 Orthogonal Array

Expt. No.	L.P. (Level)	P.F. (Level)	S.S. (Level)	No. of Pass (Level)
1	1	1	1	1
2	1	2	2	2
3	1	3	3	3
4	2	1	2	3
5	2	2	3	1
6	2	3	1	2
7	3	1	3	2
8	3	2	1	3
9	3	3	2	1

4.3 EXPERIMENTAL PROCEDURE

Setting up of the Nd: YVO_4 (Neodymium-doped Yttrium Orthovanadate) laser system is done for performing micro-drilling on copper sheet. Cleaning of the sample is done by Acetone to free it from oil/dust. Trial/pilot experiments are performed to set the working range of the parameters. Based on the working range, design of experiment (L9 OA) using Taguchi's methodology has been completed. Actual experimental operation is performed varying the parameters like laser beam power, pulse frequency, scanning speed and number of pass. Measurement of the HAZ diameter and top hole diameter & bottom hole diameter has been performed after completing the micro-drilling through optical microscope (STM 6). Experimental results are tabulated and the required calculation like hole taper and HAZ width are made using the formula as given in Eq. 4.1 and Eq. 4.2. Experimental results are analyzed through main effects and S/N ratio plots. Analysis of variance (ANOVA) has been performed for optimization of responses individually and thereby the optimum combination of the process parameters is found out. Confirmation test has been performed to compare with the predicted result. Grey relational analysis has also been performed for multi-objective optimization. Confirmation test has been performed further to compare the predicted result.

4.4 STUDY OF THE EFFECT OF PROCESS PARAMETERS ON HOLE TAPER AND HEAT AFFECTED ZONE (HAZ) WIDTH

After completion of the set of experiments, heat affected zone (HAZ) diameter, top diameter and bottom diameter of hole are measured very carefully with the help of optical microscope (Olympus STM 6).

From these observed data, HAZ width (w) is calculated using the Eq. 4.1, and the corresponding values are displayed in Table 4.4.

$$w = \frac{HAZ\ Diameter - Top\ Diameter}{2} \tag{4.1}$$

Hole taper is also calculated by using the formula given in Eq. 4.2; and the corresponding values are displayed in Table 4.4.

$$\text{Hole taper} = \frac{Top\ Diameter - Bottom\ Diameter}{Two\ Times\ the\ Thickness} \tag{4.2}$$

Table 4.5 displays the calculated values of hole taper and HAZ width with respect to the process parameters and the corresponding signal-to-noise (S/N) ratios. One of the photographic views under the optical microscope (Model: STM 6 of Olypus) of the micro-drilled hole is shown in Fig. 4.2.

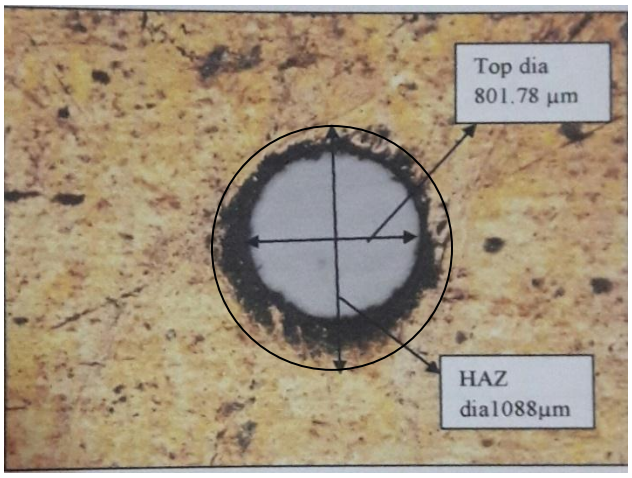

Figure 4.2 Photographic View of the Micro-drilled Hole

Table 4.4 Experimental Results and Calculated Values

Sl. No.	L.P. (W)	P.F. (kHz)	S.S. (mm/s)	No. of Pass	HAZ Diameter (mm)	Top Diameter (mm)	HAZ Width (µm)	Bottom Diameter (mm)	Hole Taper (Rad)
1	8.4	6	0.2	5	0.9627	0.8118	75.45	0.7980	0.0345
2	8.4	9	0.4	7	0.9869	0.8222	82.35	0.7977	0.0613
3	8.4	12	0.6	9	0.972	0.8125	79.75	0.7957	0.0421
4	9.6	6	0.4	9	1.0134	0.8208	96.30	0.7940	0.0670
5	9.6	9	0.6	5	0.9701	0.8123	78.90	0.7925	0.0495
6	9.6	12	0.2	7	1.0298	0.8186	105.6	0.7996	0.0475
7	10.8	6	0.6	7	1.0317	0.8158	107.9	0.7897	0.0653
8	10.8	9	0.2	9	1.0213	0.8199	100.7	0.7969	0.0576
9	10.8	12	0.4	5	1.0352	0.8236	105.8	0.7961	0.0688

Table 4.5 Calculated Values and Corresponding S/N Ratios of Responses

Sl. No.	L.P. (W)	P.F. (kHz)	S.S. (mm/s)	No. of Pass	Hole Taper		HAZ Width	
					Rad	S/N Ratio	µm	S/N Ratio
1	8.4	6	0.2	5	0.0345	-29.2436	75.45	-37.5532
2	8.4	9	0.4	7	0.0613	-24.2508	82.35	-38.3133
3	8.4	12	0.6	9	0.0421	-27.5144	79.75	-38.0346
4	9.6	6	0.4	9	0.067	-23.4785	96.30	-39.6725
5	9.6	9	0.6	5	0.0495	-26.1079	78.90	-37.9415
6	9.6	12	0.2	7	0.0475	-26.4661	105.6	-40.4733
7	10.8	6	0.6	7	0.0653	-23.7017	107.9	-40.6645
8	10.8	9	0.2	9	0.0576	-24.7916	100.7	-40.0606
9	10.8	12	0.4	5	0.0688	-23.2482	105.8	-40.4897

4.4.1 Analysis of the Effect of Variable Parameters on Hole Taper [70]

I. Analysis of Hole Taper Based on Main Effects Plot for Means

The main effects Plot for Means of the process parameters on hole taper are shown in Fig. 4.3. The figure is drawn with the help of Minitab Software using Taguchi analysis.

It is observed from the main effects plot for means that hole taper increases uniformly with the increase of laser beam power. Because more the laser beam power more will be quantity of heat input to the drilled region and more will be the material melting as well as vaporization from the top surface relative to the bottom surface. So, in such case heat input is in excess than the requirement for proper drilling.

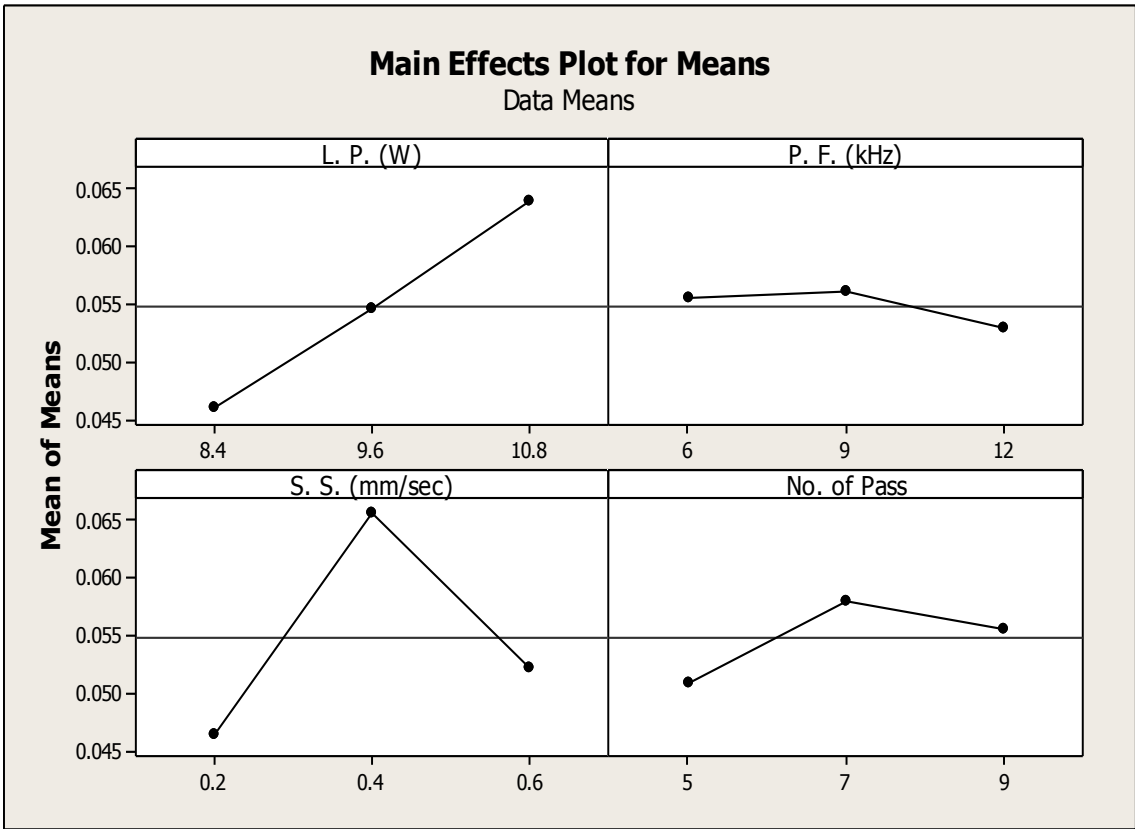

Figure 4.3 Main Effects Plot for Means of Hole Taper

Hole taper increases slightly at the initial stage with the increase of pulse frequency because duration of heat input is decreased which results insufficient heat conduction to fulfill the requirement for through hole drilling. But it decreases uniformly with further increase of pulse frequency due to the sufficient heating to the drilling zone which tends to nearly proper drilling.

Initially, hole taper increases very fast, reaches a certain value but it decreases again quickly with the increase of scanning speed. Because at the initial stage heat energy is not sufficient to overcome the material removing speed. After a certain while, heat input becomes sufficient as duration of heat is decreased and may fulfill the demand of through hole drilling.

Also, hole taper increases up to certain value at the initial stage however it decreases again uniformly with the increase of number of pass. Reason is that due to the increase of number of pass, duration of heat input is increases rapidly; so the excess heat may not be transported too fast. Whereas further increase of number of pass may not affect too much as it is already drilled and the excess heat is passed away through the hole.

From the plot for Means, it is observed that optimal combination of input parameters for minimization of hole taper is obtained at low value of means of taper which are laser beam power of 8.4 Watts, pulse frequency of 12 kHz, scanning speed of 0.2 mm/s and number of pass of 5. At this optimum process parameter, the predicted value of hole taper (mean) is 0.0317 and S/N Ratio is -29.5119.

II. Analysis of Hole Taper Based on Main Effects Plot for S/N Ratio

The main effects plot for S/N ratio of the process parameters on hole taper is shown if Fig. 4.4, which is drawn with the help of Minitab Software using Taguchi analysis. As the hole taper is concerned, so ‘smaller is better’ option is selected for getting the best result. The plot also shows the optimal combination of input parameters for minimization of hole taper is obtained at L. P. of 8.4 Watts, P. F. of 12 kHz, S. S. of 0.2 mm/sec and N. P. of 5.

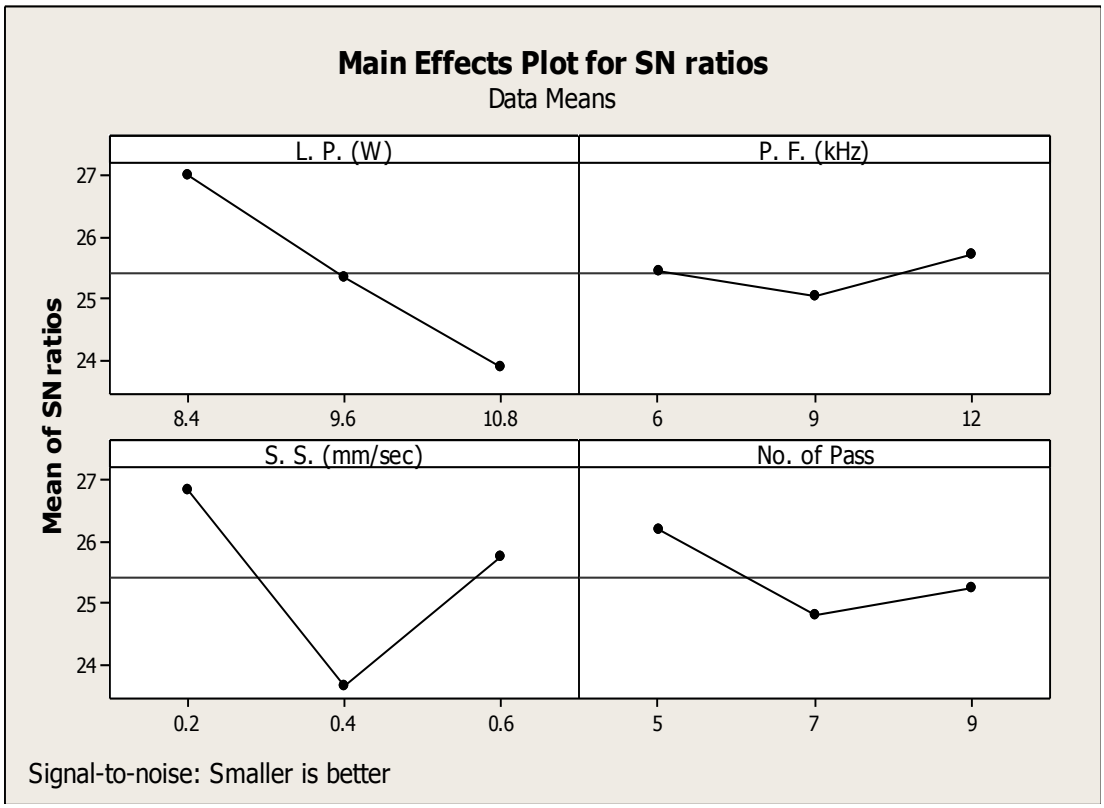

Figure 4.4 Main Effects Plot for S/N Ratio of Hole Taper

III. Analysis of Hole Taper Based on Analysis of Variance (AVOVA)

The statistical technique of ANOVA is applied on experimental data. As it a case of pulled error ANOVA to identify the significant drilling parameters influencing the hole taper, so total sum of square deviation (SST) can be determined from the formula in Eq. 33. In this experiment, the grand mean of all the S/N ratios is -25.4223 (dB). The results of ANOVA is displayed in Table 4.6. The calculated SST value is then used to determine the relative influence of the input factors. Now, the sum of squares due to factor, laser beam power is equal to the total squared deviation of the wave for that factor from line representing the overall mean. There are three experiments for every level. So, the sum of squares due to laser beam power is calculated from Eq. 3.4 for all parameters.

Mean squares are determined by dividing these sum of squares by degrees of freedom. After then percentage contribution of individual factors are calculated. It can be concluded from ANOVA result i.e. Table 4.6, that the process parameters like, scanning speed and laser beam power have greater percentage of contribution; so they are significant, whereas number of pass and pulse frequency have lesser percentage of contribution; so these parameters are insignificant [80, 81].

Table 4.6 ANOVA Result for Hole Taper

Source	DF	Sum of Squares	Mean Squares	F-Value	Percentage Contribution	Rank
Laser Beam Power	2	14.3367	7.1685	7.6212	42.45	2
Pulse Frequency	2	0.7322	0.3661	0.3892	2.17	4
Scanning Speed	2	15.6750	7.8375	8.3324	46.41	1
Number of Pass	2	3.0303	1.5152	1.6109	8.97	3
Error (Pulled)	4	3.7625	0.9406			
Total	8	33.7743				

IV. Confirmation Experiment

After determining the optimum combination of process parametric conditions and predicting the response under those conditions, final step is to conduct the confirmation experiment and verify the adequacy of the additive model for determining the optimum quality characteristics.

Predicted optimum value of S/N ratio is calculated from the Eq. (3.5). The optimum calculated value obtained is -28.41436 (dB). The calculated error variance is $0.9406(dB)^2$. The corresponding two-standard deviation confidence limits for prediction error of the S/N ratio for hole taper is ±1.93969.

Confirmation experiment with optimum parametric setting is done and compared the observed value with the predicted value. In this case the optimum process parameters are laser beam power of 8.4 Watts, pulse frequency of 12 kHz, scanning speed of 0.2 mm/s and number of pass of 5 and the predicted value of hole taper (mean) is 0.0317 Rad. The

experimental value obtained is 0.0334 Rad under the same specified optimum combination of process parameters. The corresponding S/N ratio value is -29.5119 (dB). Result shows both the values are closer to each other and within the confidence limits. The detail is shown in Table 4.7. So the model is adequate for describing the dependence of response on various process parameters [80, 81].

Table 4.7 Verification of Test Results

	Predicted Optimum	Actual Optimum
Level	LP_1 PF_3 SS_1 NP_1	LP_1 PF_3 SS_1 NP_1
Hole Taper (Rad)	0.0317	0.0334
S/N Ratio (dB)	-28.4142	-29.5119
Predicted Error of S/N Ratio	-1.0977	
Confidence Limits	±1.93969	

4.4.2 Analysis of the Influence of Process Parameters on HAZ Width [73]

I. Analysis of HAZ Width Based on Main Effects Plot for Means

The main effects plot for means of the process parameters on HAZ width is shown in Fig. 4.5. It is drawn with the help of Minitab Software using Taguchi analysis.

It is observed from the main effects plot that HAZ width increases uniformly with the increase of laser beam power. Because more the laser beam power more will be heat input to the drilled region and more will be the material melting and vaporization from the top surface. Due to the excess of heat input than the requirement for proper drilling, more HAZ is formed and spread around the drilling region.

Initially HAZ width decreases with the increase of pulse frequency because duration of heat input is decreased and most of the heat is utilized for drilling which results less chance for HAZ formation. But it increases uniformly with the further increase of pulse frequency due to the excess heating at the top compared to the heat conduction which tends to formation of HAZ.

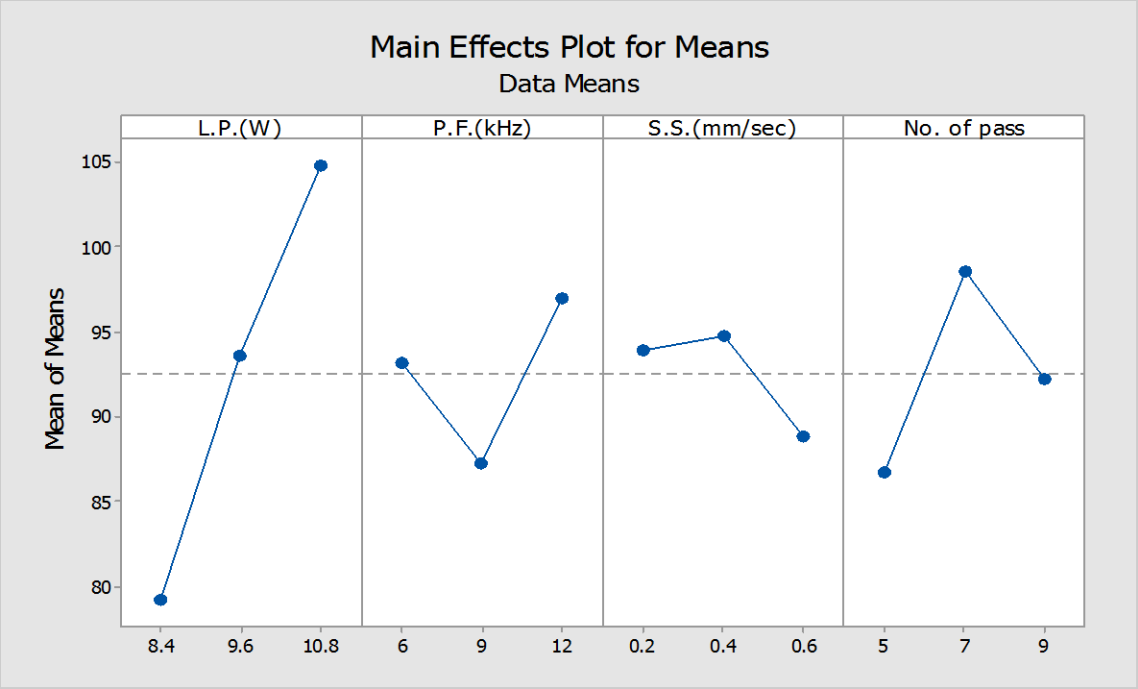

Figure 4.5 Main Effects plot of the Mean (HAZ Width)

HAZ width increases slowly at the initial stage, but it decreases again very fast with the further increase of scanning speed beyond that value. Because, at the initial stage heat input is more than the requirement for proper drilling. After a certain value heat input becomes insufficient as the duration of heat input is decreased and there is a less chance for the formation of HAZ.

Also, HAZ width increases initially however it decreases again uniformly with the increase of number of pass. Reason is that due to the increase of number of pass, duration of heat input is increases rapidly due to repeated heating effect at the top surface, so the excess heat may not be conducted too fast. Whereas further increase of number of pass may not affect too much as it is already drilled and the excess heat can be passed away through the hole.

The plot for Means show that optimal combination of input parameters for minimization of HAZ width is obtained at the lowest value of means of HAZ width which is observed at laser beam power of 8.4 Watts, pulse frequency of 9 kHz, scanning speed of 0.6 mm/s and number of pass of 5.

II. Analysis of HAZ Width Based on Main Effects Plot for S/N Ratios

The main effects plot for S/N ratio of the process parameters on HAZ width are shown in Fig. 4.6, which is drawn with the help of Minitab Software using Taguchi analysis. As the HAZ width is concerned, so 'smaller is better' option is selected. The plot also shows that optimal combination of input parameters for minimization of HAZ width is at laser beam power of 8.4 Watts, pulse frequency of 9 kHz, scanning speed of 0.6 mm/s and number of pass of 5.

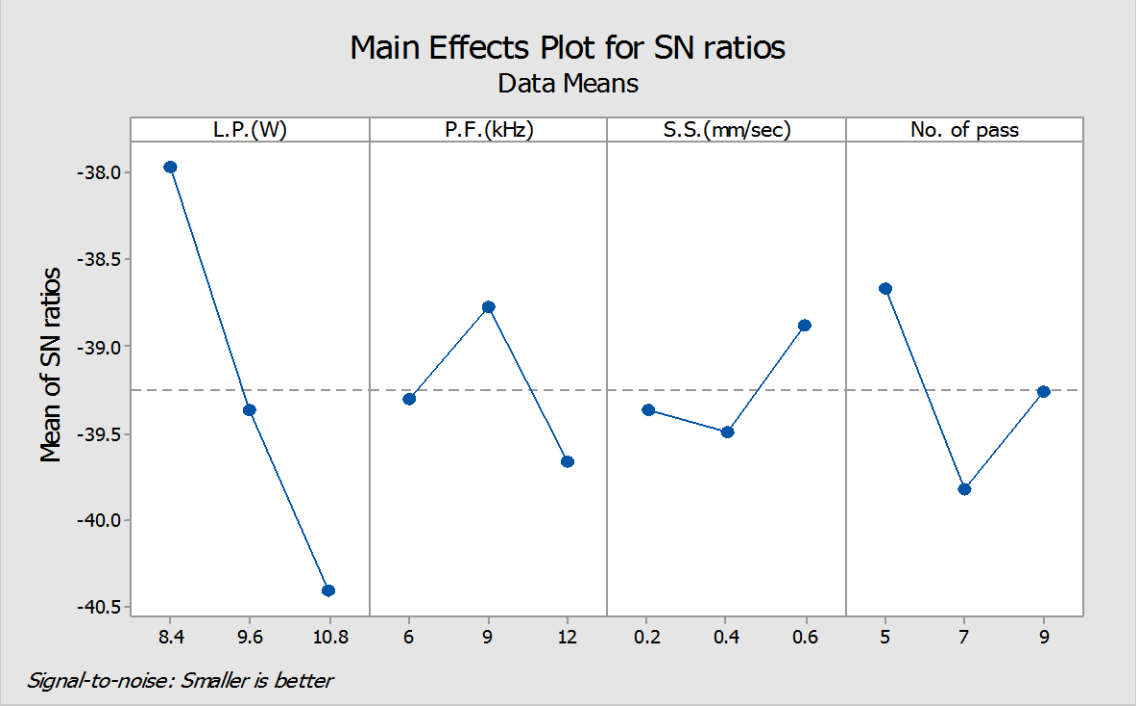

Figure 4.6 Main Effects Plot of the S/N Ratio (HAZ Width)

III. Analysis of HAZ Width Based on Analysis of Variance (ANOVA)

Analysis of variance (ANOVA) of experimental data is carried out to identify the significant drilling parameters influencing the HAZ width. The results of ANOVA is listed in Table 4.8 by comparing the F-test value of the process parameters. The total sum of square deviation can be determined from the formula given in Eq. 3.3.

Here, η_m is -39.2448 (dB). The calculated SST value is used to determine the relative influence of the factors. Now, the sum of squares due to the factor like, laser beam power which is equal to the total squared deviation of the wave for that factor from the line representing the overall mean. There are three experiments for every level. So, the sum of squares due to laser beam power is calculated using Eq. 3.4. In the similar way, sum of squares due to pulse frequency and scanning speed are also calculated.

Table 4.8 ANOVA Result for HAZ

Source	DF	Sum of Squares	Mean Squares	F-Value	Percentage Contribution	Rank
Laser Beam Power	2	8.9773	4.4887	14.4006	70.05	1
Pulse Frequency	2	1.2112	0.6056	1.9428	9.45	3
Scanning Speed	2	0.6233	0.3117	1.0	4.86	4
Number of Pass	2	2.0036	1.0018	3.2139	15.63	2
Error (Pulled)	2	0.6233	0.3117			
Total	8	12.8154				

Mean squares are determined by dividing these sum squares by degrees of freedom. After then percentage contribution of individual factors are calculated. It can be concluded from ANOVA result (Table 4.8) that the process parameters like, laser beam power has the greatest percentage of contribution; so it is the most significant, whereas number of pass and pulse frequency have lesser percentage of contribution; so they are less significant. On the other hand scanning speed has the least percentage of contribution; so it is the most insignificant. Here, residual error is zero.

IV. Confirmation Experiment

After determining the optimum conditions and predicting the response under those conditions, final step is to predict and verify the adequacy of the model for determining the optimum quality characteristics. Predicted optimum value of S/N ratio is calculated from the relationship given in Eq. 3.5.

The predicted optimum value obtained is -36.9107 (dB). So the corresponding predicted value of HAZ width (mean) will be 70.07 µm. The calculated error variance is 0.3117 $(dB)^2$. The corresponding two-standard deviation confidence limits for prediction error of the S/N ratio for HAZ width is ± 1.1166.

Experiments with optimum parameter setting are done and compared the observed value (average) with the predicted value. In this case the optimum process parameters are laser beam power of 8.4 Watts, pulse frequency of 9 kHz, scanning speed fo 0.6 mm/s and number of pass of 5 and the predicted value of HAZ width (mean) is 70.0701 µm. The experimental value of HAZ width (mean) under the same specified optimum combination of process parameters obtained is 67.1902 µm. The corresponding S/N ratio value is equal to -36.5461(dB). Result shows both the values are closer to each other and within the confidence limits. Hence it may be concluded that the model is adequate for describing the dependence of response on various process parameters. Detail of the verification experiment is shown in Table 4.9.

Table 4.9 Verification of Test Results

	Predicted Optimum	Actual Optimum
Level	$LP_1PF_2SS_3NP_1$	$LP_1PF_2SS_3NP_1$
HAZ Width (µm)	70.0701	67.1902
S/N Ratio (dB)	-36.9107	-36.5461
Prediction Error of S/N Ratio (dB)	0.3646	
Confidence Limits	±1.1166	

4.5 OPTIMIZATION OF LASER MICRO-DRILLING OF COPPER

4.5.1 Optimization of Process Parameters by Grey Relational Analysis (GRA)

Fig. 4.4 shows the main effects plot for S/N ratio of the process parameters on hole taper which is designed using Minitab Software following Taguchi methodology. 'Smaller is better' option is selected for getting the best result i.e. minimum hole taper. The plot also shows the optimal combination of input parameters for minimization of hole taper which is obtained at laser beam power of 8.4 Watts i.e. Level 1, pulse frequency of 12 kHz i.e. Level 3, scanning speed of 0.2 mm/sec i.e. Level 1 and number of pass of 5 i.e. Level 1. ANOVA result (Table 4.6) exhibits the relative importance of processing parameters on the response i.e. hole taper.

The main effects plot for S/N ratio of the process parameters on HAZ width is shown in Fig. 4.6, drawn using Minitab software by Taguchi methodology. In this case also 'Smaller is better' option is selected for getting the best result i.e. minimum HAZ width. The plot also shows that optimal combination of input parameters for minimization of HAZ width is at laser beam power of 8.4 Watts i.e Level 1, pulse frequency of 9 kHz i.e. Level 2, scanning speed of 0.6 mm/sec i.e. 3 and number of pass of 5 i.e. Level 1. ANOVA result (Table 4.8) shows the relative importance of the process parameters on the response i.e. HAZ width.

Therefore, it is observed from Fig. 4.4, Fig. 4.6, Table 4.7 and Table 4.9 that the optimum value is achieved at two different combinations of process parameters for different responses individually. To find the best combination of process parameters for both the responses to be optimized simultaneously, grey relational analysis (GRA) is carried out.

Grey theory established by Dr. Deng consists of grey relational analysis (GRA), grey modeling, prediction and decision making of a system. It provides an efficient solution for multi-responses/decisions to the uncertainty, multi-input and discrete data problem. In GRA, data pre-processing is required to transfer original sequence (very low to very high value) to a comparable sequence (ranging between 0 and 1) through normalization. Pre-processing of all the data i.e. grey relational generating is done by the following way:

S/N ratios are converted into normalized value using Eq. (3.6) for "lower the better" quality characteristics (which is the target). Larger normalized results corresponding to the better result. Then grey relational coefficient, ξ_{ij} is calculated from Eq. 3.7. Here, ξ is a distinguishing coefficient, ranging between 0 and 1.

Finally, the grey relational coefficient for each parameter of the experiment are integrated into the grey relational grade using weightage method as given in Eq. 3.8. Here, the weighage ratio (factor) for both the quality characteristics is set as 1:1. The results of GRA are provided in Table 4.10. Higher the grey relational grade means that the experimental results is closer to the ideally normalized value of the responses [82].

Table 4.10 Results of the Grey Relational Analysis

Sl. No	Hole Taper			HAZ Width			Grade	Rank
	S/N Ratio	Normalized	Coefficient	S/N Ratio	Normalized	Coefficient		
1	-29.2436	1	1	-37.5532	1	1	1	1
2	-24.2508	0.218659	0.390216	-38.3133	0.787692	0.701944	0.54608	4
3	-27.5144	0.778426	0.692929	-38.0346	0.867692	0.790754	0.74184	2
4	-23.4785	0.052478	0.345418	-39.6725	0.358462	0.438005	0.39171	7
5	-26.1079	0.562682	0.533437	-37.9415	0.893846	0.824873	0.67916	3
6	-26.4661	0.620991	0.568823	-40.4733	0.072308	0.350216	0.45952	5
7	-23.7017	0.102041	0.357664	-40.6645	0	0.333333	0.3455	8
8	-24.7915	0.326531	0.426087	-40.0606	0.223077	0.391566	0.40883	6
9	-23.2482	0	0.333333	-40.4897	0.066154	0.348713	0.34102	9

Further, the effect of machining parameters in terms of grey relational grade at different levels are summarized in Table 4.11. The optimum values of laser micro-drilling process parameters, for maximizing the grey relational grade, are identified as laser beam power at level 1 (8.4 W), pulse frequency at level 1 (6 kHz), scanning speed at level 1 (0.2 mm/s) and number of pass at level 1 (5) for minimizing both the hole taper and HAZ width, simultaneously.

Table 4.11 Grey Relational Grade at Different Levels of Machining Parameters

	Grey Ralational Grade			Main effects	Rank	Sum of
Parameters	Level1	Level2	Level3	(Max – Min)		Squares
L.P.(LP)	**0.76264059**	0.5101286	0.249949834	0.512690757	1	0.242817
P.F.(PF)	**0.57907015**	0.5446872	0.514127899	0.064942249	4	0.006334*
S.S.(SS)	**0.62278188**	0.4262715	0.58883187	0.196510367	3	0.066195
No. of Pass	**0.67339265**	0.4503659	0.514126682	0.22302671	2	0.079172
	Grand Mean Value of Grey Relational Grade **0.545962**					*** Error**

4.5.2 Confirmation Experiment Based on GRA

To verify the feasibility and reproducibility of the proposed method, confirmation experiment is carried out. The estimated optimum grey relational grade, using the optimal level of process parameters is calculated from Eq. 3.9., which is found as 0.96689.

The predicted values of grey relational grade and that from confirmation tests are shown in Table 4.12. To judge the closeness of the observed and predicted optimum results, variance of prediction error is determined by using Eq. 3.10. Finally, error variance is estimated by using Eq. 3.12, which is equal to 0.003167.

As the variance of prediction error is equal to 0.004222. So the two-standard deviation will be $\pm 2\sqrt{(0.004222)}$ i.e. ± 0.129959.

Table 4.12 Verification of Test Results

	Initial Parameter	Optimal Parameters	
		Prediction	Experiment
Level	$LP_1PF_3SS_3NP_3$	$LP_1PF_1SS_1NP_1$	$LP_1PF_1SS_1NP_1$
Hole Taper	0.0421		0.0351
HAZ Width	79.75		75.64
Grey Relational Grade (GRG)	0.74184	0.96689	0.97732
Improvement of GRG	0.23548		
Prediction Error	-0.01043		

4.7 Conclusions

Copper sheet of 0.2 mm thickness can effectively be micro-drilled with 800 µm diameter by pulsed Nd:YVO_2 laser.

It is found from main effects plot and S/N ratio plot that hole taper increases continuously with the increase of laser beam power, it increases first and then decreases with the increase of pulse frequency, scanning speed and number of pass. However, more influencing factors are the scanning speed and laser beam power. On the other hand the less influencing parameters are the pulse frequency and number of pass. From ANOVA results and confirmation test, it is observed that optimal combination of input parameters for the minimization of hole taper is obtained at laser beam power of 8.4 W, pulse frequency of 12 kHz, scanning speed of 0.2 mm/s kHz, and number of pass of 5.

It is concluded from main effects plot for Means and S/N ratio that HAZ width increases continuously with the increase of laser beam power, decreases first and then increases with the increase of pulse frequency, increases first and then decreases with the increases of scanning speed and number of pass. However, the most influencing factor is the laser beam power and the least influencing factor is the scanning speed. It is also observed that optimal combination of input parameters for minimization of HAZ width is obtained at laser beam power of 8.4 Watts, pulse frequency of 9 kHz, scanning speed of 0.6 mm/s and number of pass of 5.

Grey Relational Analysis shows that adoption of the grey-based Taguchi method leads to improvement of both the hole taper and HAZ width under certain combination of process parameters. This also indicates application feasibility of the Grey-based Taguchi technique for continuous improvement of laser micro-drilling quality in the manufacturing industry.

Chapter 5

Experimental Investigation on Micro-Channeling on Copper-Beryllium Alloy Using Diode Pumped Fiber Laser

5.1 MATERIAL CHARACTERISTICS

Copper exhibits outstanding electrical & thermal conductivity, formability & good strength. It is corrosion resistant & does not break under fatigue easily. When beryllium is added with copper, it increases its hardness & reduces its softness, fabrication become relatively easier, strength as well as machinability also increases. It is one of the newly developed and best copper alloy. Though beryllium-copper is generally an alloy of copper & beryllium but sometimes other elements like nickel, cobalt, aluminum & silicon may be added. Chemical formula is BeCu. General properties of beryllium-copper are

high fatigue strength, high mechanical strength, wear resistance, nonmagnetic, very high electrical conductivity, high corrosion resistance etc. Melting point is 865°C to 1050°C. Density at 20°C is 8.26-8.71 gm/cm^3.Specific heat at 20°C is 419 J/(kg.K). Electrical conductivity at 20°C is 25-38 % IACS [6]. The sample size for the present research work is of the dimension 50 mm × 20 mm × 1.2 mm on which the micro-channeling is to be done. Chemical composition of the selected material is represented in Table 5.1.

Table 5.1 Chemical Composition of beryllium copper alloy

Element	Copper	Beryllium	Nickel	Cobalt
Percentage	97.7 - 98	1.8 - 2.0	0.2 - 0.25	0.05- 0.06

5.2 EXPERIMENTAL SET-UP

CNC pulsed diode pumped fiber laser micro-machining system (Model - SCR1BO SLT 175, Serial Number - 2014/07/175/066) of maximum beam power 50 Watts is used to produce micro-channel. The photographic view of CNC pulsed diode pumped fiber laser machining system is showed in Fig. 5.1. Table 5.2 represents the technical specification of the laser system. The system consists of various sub-system like:

Laser Source - Active gain medium is optical fiber doped with rare-earth elements like erbium, ytterbium, neodymium, dysprosium, praseodymium, thulium and holmium. They are related to doped fiber amplifiers, which provide light amplification without lasing.

CNC Controlling System - It consists of X-Y-Z axes and controlling unit (accupos). Stepper motors are attached to each axis via this accupos through a computer. The safety shutter is located inside the laser head assembly and is attached by the toggle switch.

CCTV & CCD Camera - CCD camera together with CCTV is used for viewing the location and thereby proper focusing the surface of the workpiece.

Beam Delivery System - It consists of a beam bender and focusing lens. By changing the focal length, the power density and the depth of focus produced by the laser of given beam diameter can be adjusted. A lower focal length lens has high power density but

large depth of focus for a same beam diameter. The alignment of focusing lens is very important, because if the beam centre is not with the center of the lens, the cutting efficiency drastically decreases.

Power Supply - Q switching is an excellent method to produce very short pulse width and very high peak power of laser light from a continuous wave (CW) of lower laser power. Once the discharge in lamp is produced, then by changing the current flowing through the lamp, the intensity of the light emitted from the lamp can be controlled.

Cooling System - due to very low electro-optic efficiency a large quantity of heat is generated inside the pumping cavity when laser is produced. If heat is not removed, it will cause lamp and rod to get damaged. To avoid thermal damage, de-ionized water is used as cooling fluid.

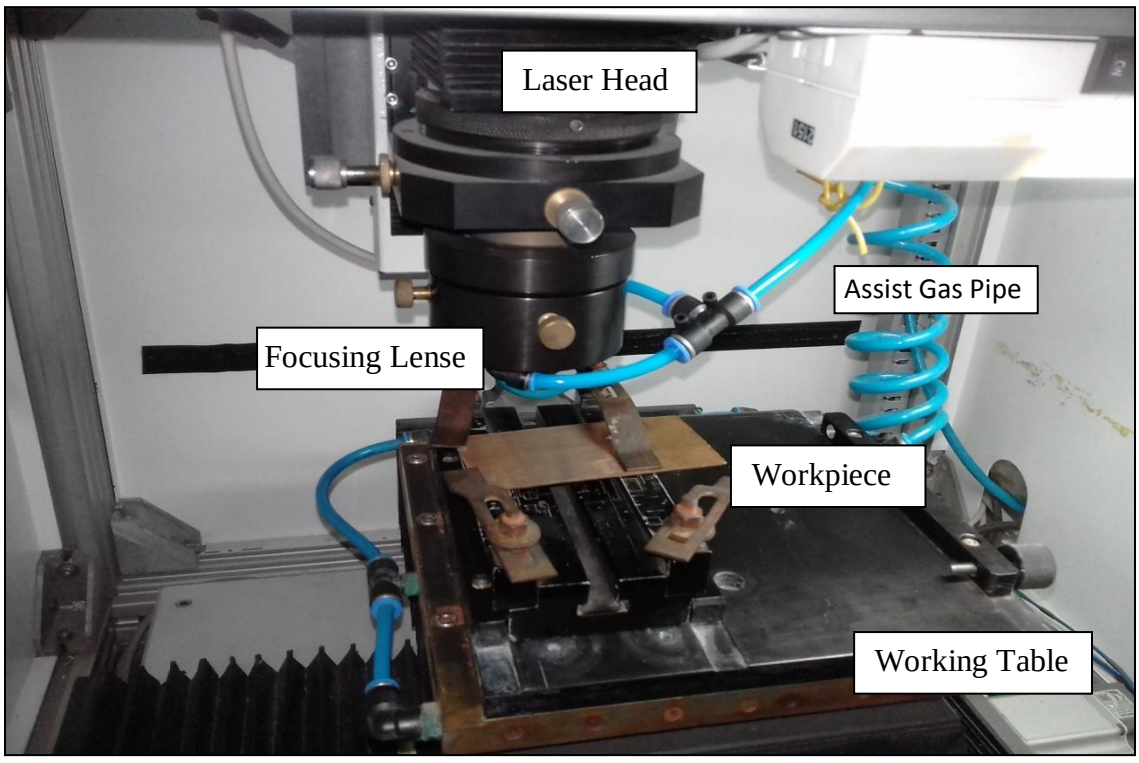

Figure 5.1 CNC Pulsed Diode Pumped Fiber Laser Micro-machining System (Production Engg. Deptt., JU)

Table 5.2 Technical specifications of diode pump fiber laser [84]

Laser Type	Diode Pumped Fiber Laser
Maximum Laser Beam Power	50 Watt
Laser Generator	IPG Laser GMBH, Germany (Model: YLP-1-120-50-50 HC
Wavelength	1064 nm
Pulse Frequency	60 - 120 kHz
Pulse Duration	120 ms
Input Voltage	230 Volt
Input Frequency	50 Hz
Input Current	4 amp
Duty Cycle	0 - 100%
Mode of Operation	Direct Power , Jog Mode
Mirror Reflectivity	Rear Mirror, 100% Front Mirror 80%
Spot Beam Diameter	21 micron
Axis Travel (X,Y Axis)	150 mm ,150 mm
Focusing Vertical Travel (Z axix)	80 mm
Focal Length	77 mm
Feed Rate	2 mm/sec (normal condition)
Control System	CNC controlled

Assist Air Supply - A coaxial flushing nozzle, connected by a pipe line from compressor, is employed with the machine to supply the assist gas during laser machining operation. A pressure gauge and controlling valve is also attached with the pipe line so that the desired pressure can be supplied. Gases are supplied around the laser source to protect the material from oxidation [83].

5.3 PLANNING FOR EXPERIMENT

Angular (90^o) shape i.e. "∟" shape of 4 mm each side is chosen as the channel shape which is to be produced on the job, maintaining 90 degree angle between the two lines. To find out the working range of process parameters, trial experiment is required. Trial experiment is done by varying a parameter keeping other parameters fixed at same value. To run the laser machine first of all it is needed to fit the program (shown in Table 5.2) in the machine through computer interfacing. After selecting the working range of process parameters, design of experiment is done.

5.3.1 Development of CNC Program for Micro-channeling Operation

The laser system is interfaced with a computer which consists of inbuilt software both for controlling and part programming. There are a set of the predefined codes & programs available into the system based on the requirement through which idea reaches to the computer. These available sets can also be modified or altered (if required specially). Programming is the language to convert theoretical & mathematical expressions into computer known language. Computer follows the instructions & moves its coordinates accordingly. Part programming for the following work is given in Table 5.3.

Table 5.3 CNC Program for Micro-channeling Operation

N0	M10		
N1	G01	X04	Y00
N2	G01	X00	X04
N3	G01	X00	Y-04
N4	G01	X-04	Y00
N5	M11		

N0,N1…N5 represent the sequence numbers. M10 means laser is on. G01 indicates linear interpolation and M11 represents laser is off.

Trial experiment is done to find out the workable range of laser beam power, pulse frequency & scanning speed so that responses can be observed easily i.e. a possibility of getting possible outcomes from the sample space.

5.3.2 Design of Experiments (DOE)

Ronald A. Fisher first proposed the technique of design of experiments in his innovative books "The Arrangement of Field Experiments" in the year of 1926 and another book "The Design of Experiments" in the year of 1935. DOE is very much helpful for designer to determine individual and interactive influence of many input factors on the output factors. DOE also helps to turn any standard design into a robust design providing a full insight interaction between design elements. Through DOE, a lot of experimental runs as well as labor, material and time can be saved without any loss of product quality characteristics of the component [80, 81].

Design of experiments is a systematic statistical method used to determine relationship between input parameters of a process and output parameters of that process. In other words, it is used to find cause-and-effect relationships. This information is needed to manage process inputs in order to optimize the output. An understanding of DOE first requires knowledge of some statistical tools and experimentation concepts. Although a DOE can be analyzed in many software programs, it is important for practitioners to understand basic DOE concepts for proper application. It has been done in MINITAB 2018 software following central composite design of response surface methodology [81].

A. Response surface methodology (RSM)

RSM explores the relationship between several explanatory variables and one or more response variable(s). The model was model was introduced by George E.P. Box and K.B. Wilson in the year of 1951. The main idea is to use a sequence of designed experiments to obtain an optimum response. RSM consists of a group of mathematical and statistical techniques used for the development of an adequate functional relationship between a response of interest, y and a number of associated control (or input) variables denoted by x_1, x_2, … x_k. In general, such a relationship is unknown but can be approximated by a low-degree polynomial model of the form

$$y = f(x)\beta + €$$ (5.1)

where $x = (x_1, x_2, \ldots x_k)$, f(x) is a vector function of p elements that consists of powers and cross-products of powers of $x_1, x_2, \ldots x_k$ up to a certain degree denoted by d (≥ 1), β is a vector of p unknown constant coefficients referred to as parameters and € is a random experimental error assumed to have a zero mean value [84].

By careful design of experiments, the objective is to optimize a response (output variable) which is influenced by several independent variables (input variables). An experiment is a series of tests, called runs, in which changes are made in the input variables in order to identify the reasons for changes in the output variables/responses. RSM can be used for the approximation of both experimental and numerical responses. Two steps are necessary, the definition of an approximation function and the design of the plan for experiments [84].

In this research, central composite design (CCD) is applied as the as the design of experiment (DOE) tool, shown in Table 5.4, to reduce the series of tests.

B. Central composite Design (CCD)

A second-order model can be constructed efficiently with central composite design (CCD). CCD are first-order (2N) designs augmented by additional centre and axial points to allow estimation of the tuning parameters of a second-order model. The design involves 2N factorial points, 2N axial points and 1 central point. CCD present an alternative to 2N designs in the construction of second-order models because the number of experiments is reduced as compared to a full factorial design. In the case of problems with a large number of design variables, the experiments may be time consuming even with the help of CCD [80, 84].

In this present experiment, the default value of $\dot{\alpha}$ is 1.682, which acts between the ranges of -1 to 1 in low to high value. In a traditional DoE, screening experiments are performed in the early stages of the processes, when it is likely that many of the design variables initially considered have little or no effect on the responses. The purpose is to identify the design variables that have large effects for further investigation. DoE of 20 sets have

been made of different combinations of input parameters. Experiments has been performed according to the set of combinations found from DOE. The levels has been selected as -ά , -1 , 0 , +1 , +ά. The DOE of 20 sets is shown in Table 5.4.

Table 5.4 DOE Through Central Composite Design of Response Surface Methodology

Std. Order	Run Order	Pt. Type	Laser Beam Power (LBP) in %	Pulse Frequency (PF) in kHz	Scanning Speed (SS) in mm/s
1	1	1	70	70	1.5
2	2	1	90	70	1.5
3	3	1	70	90	1.5
4	4	1	90	90	1.5
5	5	1	70	70	3.5
6	6	1	90	70	3.5
7	7	1	70	90	3.5
8	8	1	90	90	3.5
9	9	-1	63.1821	80	2.5
10	10	-1	96.8179	80	2.5
11	11	-1	80	63.1821	2.5
12	12	-1	80	96.8179	2.5
13	13	-1	80	80	0.81821
14	14	-1	80	80	4.18179
15	15	0	80	80	2.5
16	16	0	80	80	2.5
17	17	0	80	80	2.5
18	18	0	80	80	2.5
19	19	0	80	80	2.5
20	20	0	80	80	2.5

5.4 EXPERIMENTAL PROCEDURE

Detailed procedure is listed below:-

- Beryllium copper sheet is first polished with emery paper and then washed by acetone solution.
- Switch is put on for computer, laser & internal lights, etc.
- Program is written for the experiment on computer & saved.
- Trial experiments is performed so that workable ranges of process parameters can be selected.
- DOE is completed using RSM with the help of MINITAB-2018 software utilizing 3 process parameters within the workable range.
- Program is run for the experiment by varying the process parameters.
- Workpiece is observed with the help of microscope for the measurement of output parameters.
- Parameters like kerf depth, kerf width, HAZ, overcut, angle after experiment.
- Results are placed in the Minitab 18 software to perform ANOVA.
- Mathematical regression equations are derived from the regression analysis.
- Response Surface plots are drawn to study the combined influence of process parameters on the responses.
- Results are optimized.

5.5 ANALYSIS OF EXPERIMENTAL RESULTS AND DISCUSSIONS

After successful completion of experimental run, the workpiece is placed under a precision optical microscope (Model: Olympus STM 6, shown in Fig. 3.3), adjusting resolution at the maximum brightness & clear picture. Table 5.5 shows the detail experimental results of the responses.

Table 5.5 Experimental Results

Run Order	LBP (%)	PF (kHz)	SS (mm/s)	Kerf Depth (KD) in µm	Kerf Width (KW) in µm	HAZ (µm)	Overcut (µm)	Angle (Degree)
1	70	70	1.5	42.035	74.521	125.235	39.301	90.33
2	90	70	1.5	48.03	79.75	126.845	43.175	90.51
3	70	90	1.5	37.716	58.88	96.621	25.83	90.2
4	90	90	1.5	53.262	68.54	111.78	33.33	90.44
5	70	70	3.5	40.59	59.46	93.84	34	89.6
6	90	70	3.5	40.55	63.02	121.586	46.55	90.14
7	70	90	3.5	37.03	55.89	89.125	31.892	90.18
8	90	90	3.5	47.578	64.395	127.19	43.69	90.38
9	63.182	80	2.5	39.57	66.701	99.25	33.327	90.14
10	96.818	80	2.5	51.86	78.66	141.57	51.95	90.41
11	80	63.182	2.5	42.18	73.14	131.45	39.73	90.36
12	80	96.818	2.5	44.77	62.24	106.72	28.45	90.45
13	80	80	0.8182	43.757	63.661	99.13	32.52	89.82
14	80	80	4.1818	36.895	48.388	93.076	38.148	90.7
15	80	80	2.5	39.73	63.991	106.84	38.43	90.39
16	80	80	2.5	39.97	63.71	106.25	37.5	90.13
17	80	80	2.5	39.48	64.119	106.16	39	90.15
18	80	80	2.5	39.13	63.777	106.04	40	90.47
19	80	80	2.5	39.65	63.655	106.38	39.12	89.99
20	80	80	2.5	39.792	64.1096	106.134	38.93	90.226

Fig. 5.2 is the photograph of the channel at lowest kerf width and corresponding HAZ for run number 14 i.e. process parameters are at laser beam power of 80%, pulse frequency of 80 kHz and scanning speed of 4.18179 mm/sec. From this figure it is clear that it is very good to be acceptable for this purpose as the produced channel is regular in shape.

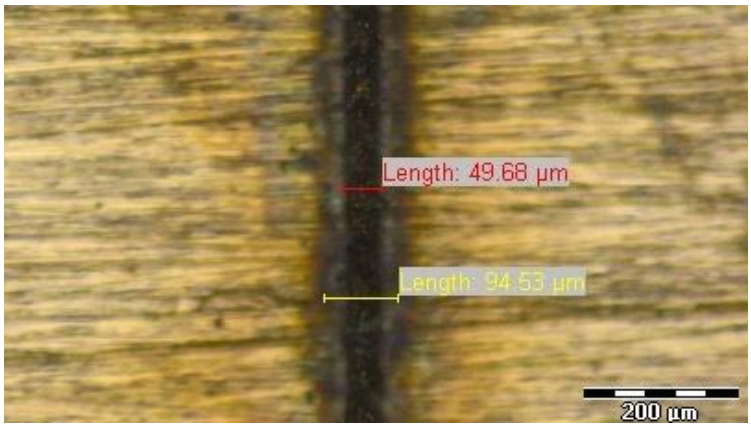

Figure 5.2 Lowest Kerf width and Corresponding HAZ (Run Number 14)

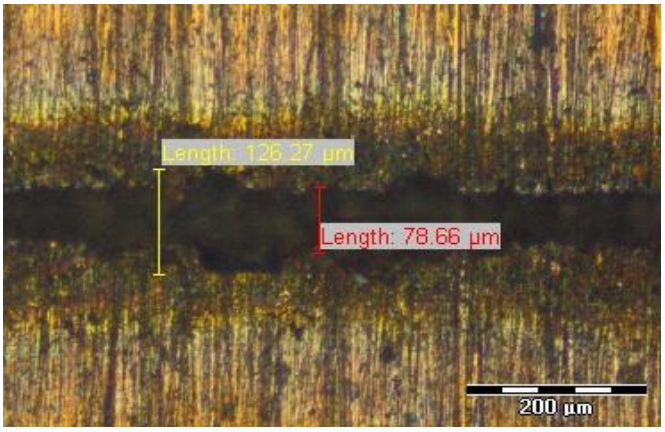

Figure 5.3 Highest Kerf width and Corresponding HAZ (Run Number 2)

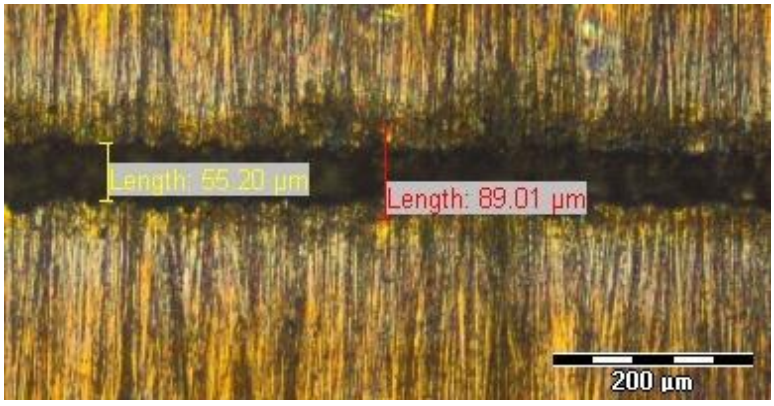

Figure 5.4 Lowest HAZ and Corresponding Kerf width (Run Number 7)

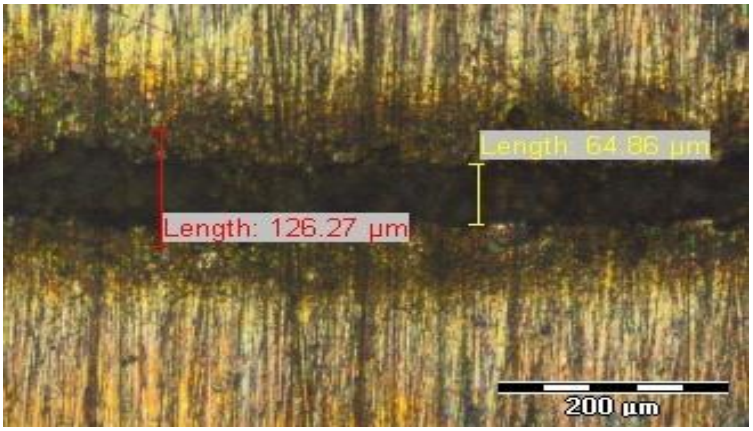

Figure 5.5 Highest HAZ and Corres-ponding Kerf width (Run Number 8)

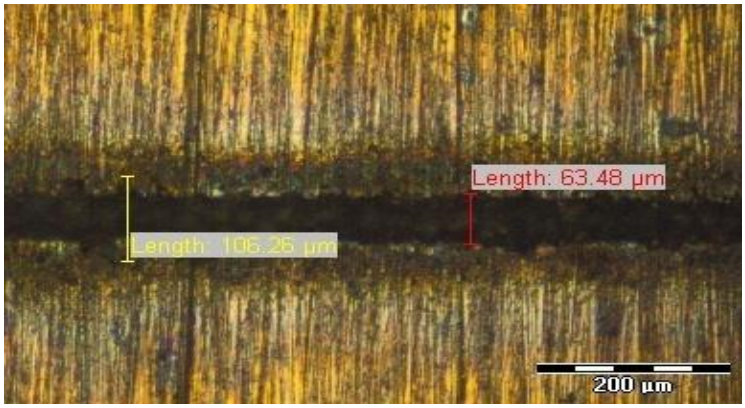

Figure 5.6 Moderate HAZ and Kerf width (Run Number 19)

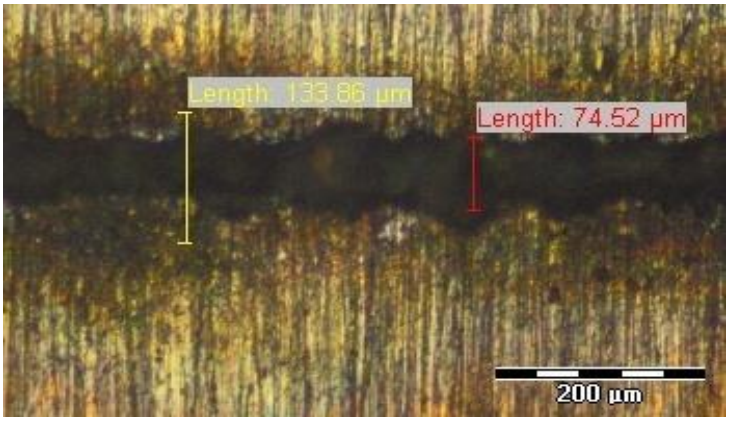

Figure 5.7 Burning case (Run Number 10)

Fig. 5.3 represents the photograph of the produced channel for highest kerf width and corresponding HAZ for run number 2, i.e. process parameters are at laser beam power of 90%, pulse frequency of 70 kHz and scanning speed of 1.5 mm/sec. It shows that kerf quality of the produced channel is not good enough and some portion has been burnt due to overheating at the surface.

Fig. 5.4 is the photograph of micro-channel at lowest HAZ and corresponding kerf width for run number 7, i.e. process parameters are at laser beam power of 70%, pulse frequency of 90 kHz and scanning speed of 3.5 mm/sec. From this figure it is clear that the kerf quality of produced channel is good enough to be acceptable.

Fig. 5.5 represents the photograph of channel for highest HAZ and corresponding kerf width for run number 8, i.e. process parameters are at laser beam power of 90%, pulse frequency of 90 kHz and scanning speed of 3.5 mm/sec. It shows that kerf quality of produced channel is bad/defective, also some portion is burnt and irregular due to overheating.

Fig. 5.6 represents the photograph for micro-channel at moderate HAZ and corresponding moderate kerf width for run number 19, i.e. process parameters are at laser beam power of 80%, pulse frequency of 80 kHz and scanning speed of 2.5 mm/sec. It shows that produced channel is very good and very regular in shape. This parametric condition may be the best for this purpose.

Fig. 5.7 represents the photograph for micro-channel at highest HAZ and corresponding highest kerf width for run number 10, i.e. process parameters are at laser beam power of 96.8179%, pulse frequency of 80 kHz and scanning speed of 2.5 mm/sec. It shows that produced channel is very bad and most of the portion is burnt, very irregular due to overheating at the surface. This parametric condition of cutting cannot be utilized for micro-channel production.

5.5.1 Analysis of the Effect of Variable Parameters on Kerf Depth

I. Analysis of Variance ANOVA) for Kerf Depth (KD)

Analysis of Variance (ANOVA) of kerf depth is done by using Minitab 18 software and result is listed in Table 5.6 where degree of freedom (DF), adjusted sum of square (adj SS), adjusted mean square (adj MS), F-value and p-value are available for process parameters based on their individual (linear), square and 2-way interaction effects. Also the Table 5.6 shows the lack-of-fit as well as total error. The most influencing parameter is LBP whereas PF may be considered as the insignificant for kerf depth observation.

Table 5.6 Analysis of Variance (ANOVA) for Kerf Depth

Source	DF	Adj SS	Adj MS	F-value	p-value
Model	9	413.857	45.984	385.35	0.000
Linear	3	261.824	87.275	731.36	0.000
LBP	1	203.503	203.503	1705.36	0.000
PF	1	5.589	5.589	46.84	0.000
SS	1	52.731	52.731	441.89	0.000
Square	3	85.305	28.435	238.28	0.000
LBP*LBP	1	66.303	66.303	555.63	0.000
PF*PF	1	26.381	26.381	221.07	0.000
SS*SS	1	0.828	0.828	6.94	0.025
2-Way Interaction	3	66.729	22.243	186.40	0.000
LBP*PF	1	50.697	50.697	424.85	0.000
LBP*SS	1	15.216	15.216	127.51	0.000
PF*SS	1	0.816	0.816	6.84	0.026
Error	10	1.193	0.119		
Lack-of-fit	5	0.769	0.154	1.81	0.265
Pure Error	5	0.425	0.085		
Total	19	415.051			

Table 5.7 Model Summary of ANOVA for Kerf Depth

S	R-sq	R-sq (Adj)	R-sq (Pred)
0.345444	99.71%	99.45%	98.39%

Regression Equation in Uncoded Units is used to calculate the kerf depth as:

KD = 373.8 - 4.715 LBP - 4.195 PF + 5.31 SS + 0.021449 LBP*LBP + 0.013530 PF*PF + 0.2396 SS*SS + 0.02517 LBP*PF - 0.1379 LBP*SS + 0.0319 PF*SS (5.2)

II. Response Surface Methodology for Kerf Depth

Fig.5.8 represents the combined effect of LBP and PF on Kerf Depth (KD) at constant SS of 2.5 mm/sec. From this surface plot it reveals that with the increase of LBP, KD decreases initially; but increases later. However the rate of increase is slower at low level of PF compared to that of high level. This due to the fact that initially with the increase of LBP, though produced heat is increased but it is utilized for melting/vaporization from top surface rather than penetrating into the surface as heat is insufficient when the PF is in the lower range. But further increase of LBP, the produced heat will be sufficient and this extra heat is utilized to penetrate enough into the surface. Whereas, KD always increases gradually with the increase of PF at all levels of LBP. Because with the increase of PF, there is an increase of interaction between the beam and sample surface; as a result KD increases gradually.

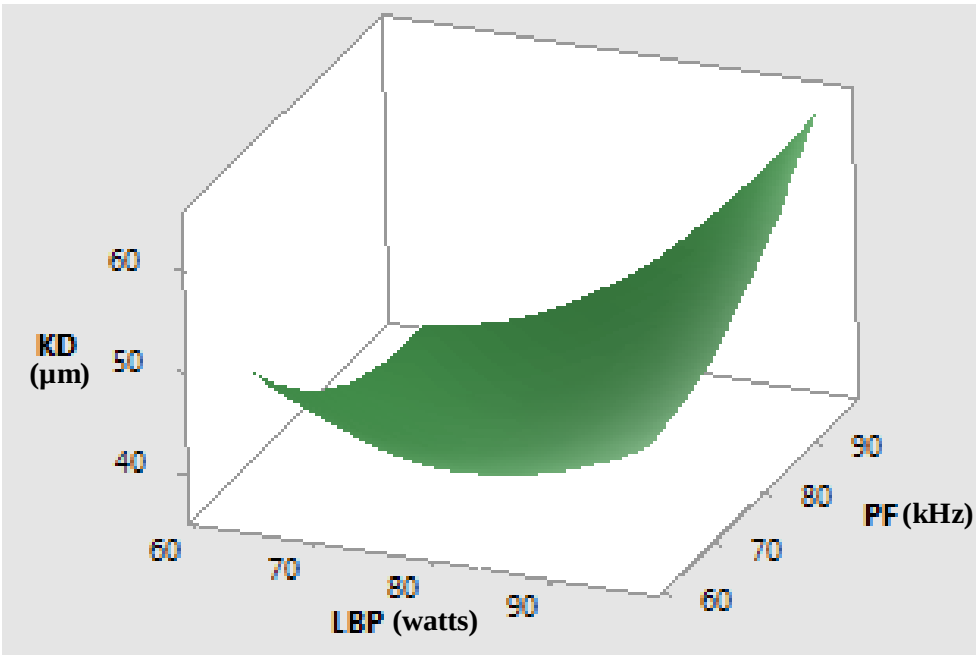

Figure 5.8 Combined Effect of LBP and PF on KD at Constant SS of 2.5 mm/sec

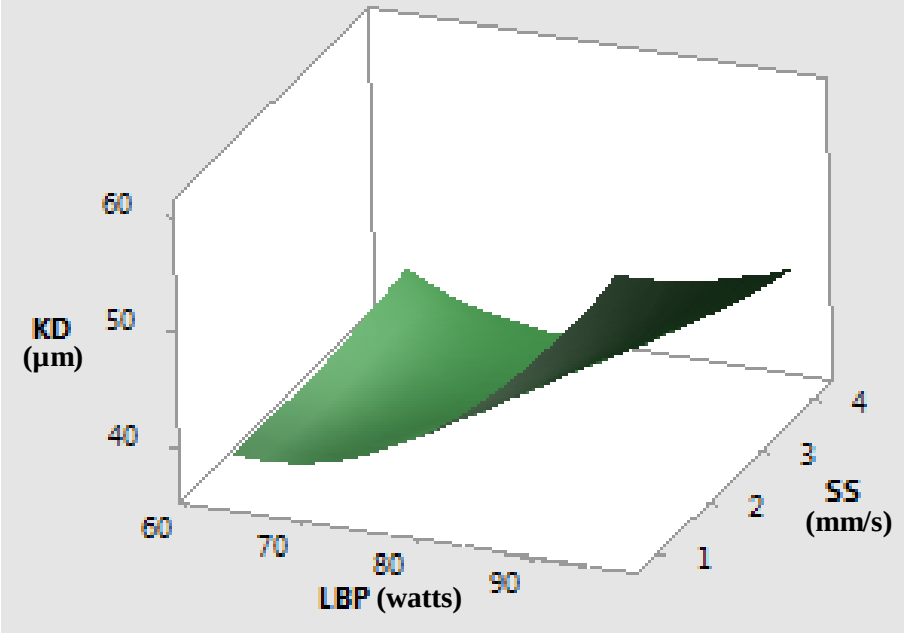

Figure 5.9 Combined Effect of LBP and SS at Constant PF of 80 kHz

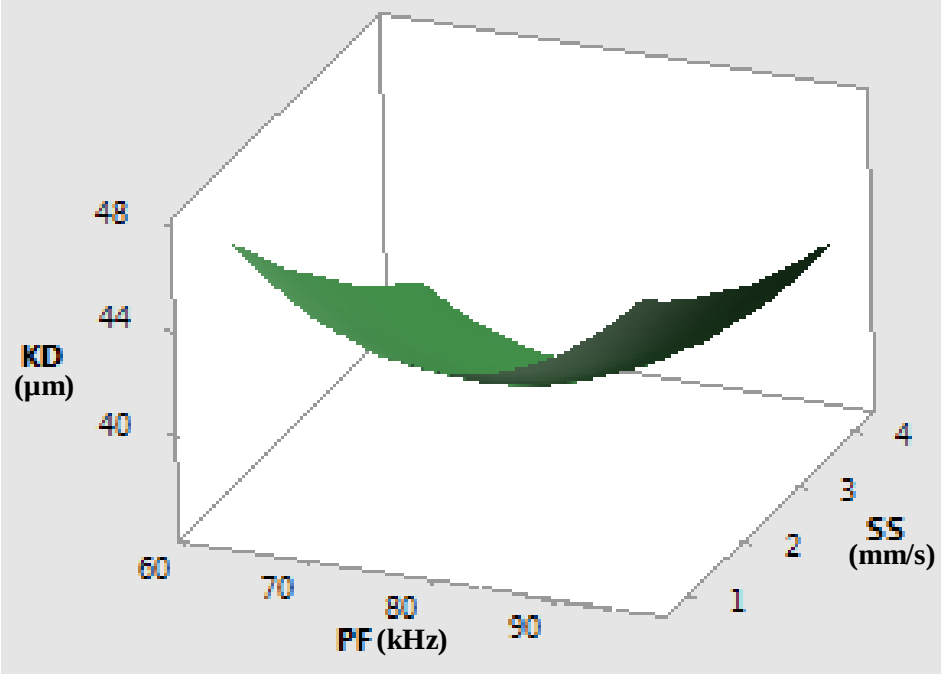

Figure 5.10 Combined Effect of PF and SS at constant LBP of 80 %

Fig. 5.9 represents the combined effect of LBP and SS at constant PF of 80 kHz. When LBP increases, KD decreases slightly at initial stage, and then increases gradually though the rate of increase is low when SS is increased. Because, initial increase of LBP will not be sufficient to penetrate well into the surface; further increase of LBP is very helpful to penetrate well. On the other hand there is little effect of SS at the lower level of LBP, but at the higher level of LBP, KD is decreased slightly with the increase of SS. The increase of SS causes the decrease of interaction time between the heat generation and the sample.

Fig. 5.10 represents the combined effect of PF and SS at constant LBP of 80 %. The plot indicates that with the increase of PF, at first KD is decreased but later increased at all levels of SS. It is due to the fact as PF increases, interaction of heat generation with the surface decreases i.e. sufficient heat cannot be penetrated into the surface; rather heat will be spread on the surface. But, further increase of PF, the heat will be penetrated well. Whereas, KD is decreased slowly with the increase of SS at all levels of PF. As SS increases, interaction of heat generation with the surface decreases as the job moves faster than the requirement i.e. sufficient heat cannot be penetrated into the surface.

5.5.2 Analysis of the Influence of Variable Parameters on Kerf Width

I. Analysis of Variance for Kerf Width (KW)

Analysis of variance (ANOVA) of kerf width is done by using Minitab 18 software and result is listed in Table 5.8 where Df, Adj SS, Adj MS, F-value and p-value are available for process parameters based on their individual (linear), square and 2-way interaction effects. Also the Table shows the lack-of-fit as well as total error. The most influencing parameter is SS.

Table 5.8 Analysis of Variance (ANOVA) for Kerf Width

Source	DF	Adj SS	Adj MS	F-Value	p-Value
Model	9	1023.61	113.734	937.11	0.000
Linear	3	632.25	210.751	1736.47	0.000
LBP	1	162.21	162.209	1336.51	0.000
PF	1	164.36	164.359	1354.23	0.000
SS	1	305.69	305.686	2518.68	0.000
Square	3	303.38	101.127	833.22	0.000
LBP*LBP	1	139.02	139.024	1145.47	0.000
PF*PF	1	25.94	25.936	213.70	0.000
SS*SS	1	111.60	111.605	919.56	0.000
2-Way Interaction	3	87.98	29.325	241.62	0.000
LBP*PF	1	10.99	10.989	90.54	0.000
LBP*SS	1	1.00	0.997	8.21	0.017
PF*SS	1	75.99	75.990	626.11	0.000
Error	10	1.21	0.121		
Lack-of-fit	5	1.00	0.200	4.75	0.056
Pure Error	5	0.21	0.042		
Total	19	1024.82			

Table 5.9 Model Summary for KW

S	R-sq	R-sq (Adj)	R-sq (Pred)
0.348379	99.88%	99.77%	99.22%

Regression Equation in Uncoded Units which can be used for calculating KW as

KW = 472.7 - 5.474 LBP - 4.201 PF - 12.65 SS + 0.031059 LBP*LBP+ 0.013415 PF*PF - 2.7828 SS*SS + 0.01172 LBP*PF - 0.0353 LBP*SS + 0.3082 PF*SS (5.3)

II. Analysis Based Response Surface Methodology for Kerf Width

Fig. 5.11 shows the combined effect of LBP and PF on KW at constant SS of 2.5 mm/sec. The surface plot says that with the increase of LBP, KW increases at all levels of PF. Because increase of LBP results more amount of heat generated at the surface which may not be penetrated well into the material. But with increase of the PF, KW is decreased for the lower value of LBP, whereas, KW is nearly constant at higher levels of LBP though PF is increased. It is due to the fact as PF increases, interaction of heat generation with the surface decreases i.e. sufficient heat cannot be penetrated into the surface; rather heat will be spread on the surface. But, further increase of PF, the heat will be penetrated well.

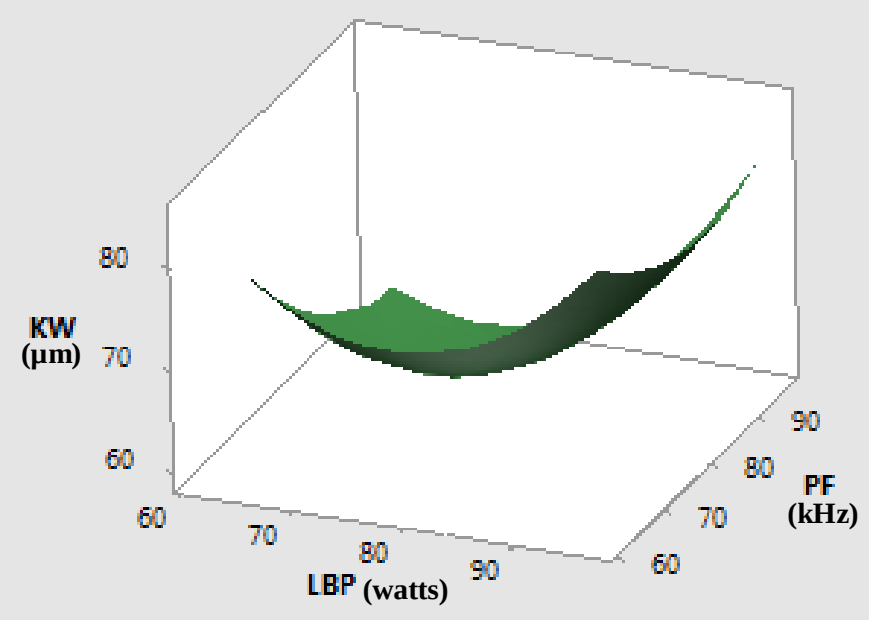

Figure 5.11 Combined Effect of LBP and PF on KW at Constant SS of 2.5 mm/sec

Fig. 5.12 represents the combined effect of LBP and SS on KW keeping constant PF at 80 kHz. The surface plot depicts that with the increase of LBP, KW decreases slightly for the initial stage and then it increases further for any change of SS. Because, initially the generated heat is sufficient to melt and penetrate into the material; but further increase of LBP results excess heat generated which is spread on the surface rather than penetration.

Whereas, with the increase of SS, KW increases for the initial stage due to spread of heat generation and then it decreases further for any changes of LBP due to well penetration.

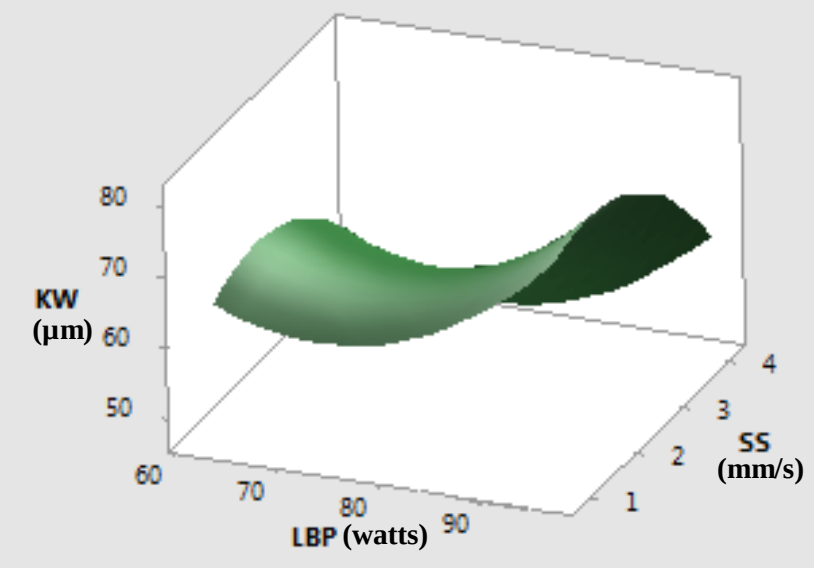

Figure 5.12 Combined Effect of LBP and SS on KW at Constant PF of 80 kHz

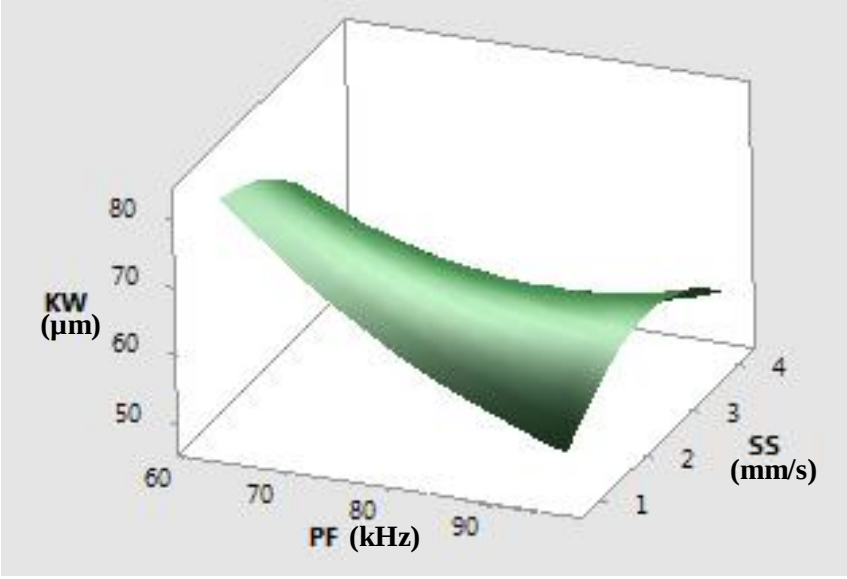

Figure 5.13 Combined Effect of PF and SS on KW at Constant LBP of 80 %

Fig. 5. 13 shows the combined effect of PF and SS on KW at Constant LBP of 80 %. This plot reveals that with the increase of PF, KW decreases gradually under lower range of SS as the interaction time decreases between surface and heat. But under the higher range of SS, KW decreases gradually for the initial stage and then it increases further slightly due to spread of heat. On the other hand, with the increase of SS, KW increases gradually at the initial stage and then decreases slightly for all levels of PF.

5.5.3 Analysis of the Effect of Process parameters on HAZ

I. Analysis of Variance for HAZ

Analysis of Variance (ANOVA) of HAZ is done by using Minitab 18 software and result is listed in Table 5.10 where DF, Adj SS, Adj MS, F-Value and p-Value are available for process parameters based on their individual (linear), square and 2-way interaction effects. Also the Table shows the lack-of-fit as well as total error. The most influencing parameter is LBP whereas SS can be considered as the insignificant for this observation.

Table 5.10 Analysis of Variance (ANOVA) for HAZ

Source	DF	Adj SS	Adj MS	F-Value	p-Value
Model	9	3850.74	427.86	97.15	0.000
Linear	3	2363.29	787.76	178.86	0.000
LBP	1	1731.01	1731.01	393.02	0.000
PF	1	521.36	521.36	118.37	0.000
SS	1	110.93	110.93	25.19	0.001
Square	3	867.31	289.10	65.64	0.000
LBP*LBP	1	338.40	338.40	76.83	0.000
PF*PF	1	276.13	276.13	62.70	0.000
SS*SS	1	202.45	202.45	45.97	0.000
2-Way Interaction	3	620.14	206.71	46.93	0.000
LBP*PF	1	71.21	71.21	16.17	0.002
LBP*SS	1	300.64	300.64	68.26	0.000
PF*SS	1	248.29	248.29	56.37	0.000
Error	10	44.04	4.40		
Lack-of-Fit	5	43.63	8.73	105.06	0.000
Pure Error	5	0.42	0.08		
Total	19	3894.79			

Table 5.11 Model Summary for HAZ

S	R-sq	R-sq (Adj)	R-sq (Pred)
2.09865	98.87%	97.85%	91.42%

Regression Equation in Uncoded Units, used for calculating HAZ as

HAZ = 1064.6 - 10.55 LBP - 11.40 PF - 77.72 SS + 0.04846 LBP*LBP + 0.04377 PF*PF - 3.748 SS*SS + 0.02984 LBP*PF + 0.6130 LBP*SS + 0.5571 PF*SS (5.4)

II. Analysis Based Response Surface Methodology for HAZ

Fig. 5.14 represents combined effect of LBP and PF on HAZ at constant SS of 80 2.5 mm/sec. This surface plot reveals that with the increase of LBP and PF, HAZ decreases upto certain range and then increases gradually for all the values. Because increase of LBP results more amount of heat generated at the surface which is be penetrated well into the material initially but later it exceed the requirement. whereas, HAZ always increases with the increase of PF at all levels of LBP. Because as PF increases, interaction of heat generation with the surface decreases i.e. sufficient heat cannot be penetrated into the surface; rather heat will be spread on the surface.

Fig. 5.15 exhibits the combined effect of LBP and SS on HAZ at constant PF of 80 kHz which shows that with the increase of LBP, HAZ is decreased slowly for the lower to middle value of SS due to well penetration of heat. However, it increases rapidly for the higher value of SS as the generated heat became too much and some of part of heat will spread on the surface. On the other hand, with the increase of SS, HAZ initially increases due spread of heat, but later it remains approximately constant or very rarely increase for the lower range of LBP value. Whereas for the higher range of LBP value, HAZ increases very rapidly due excess heat.

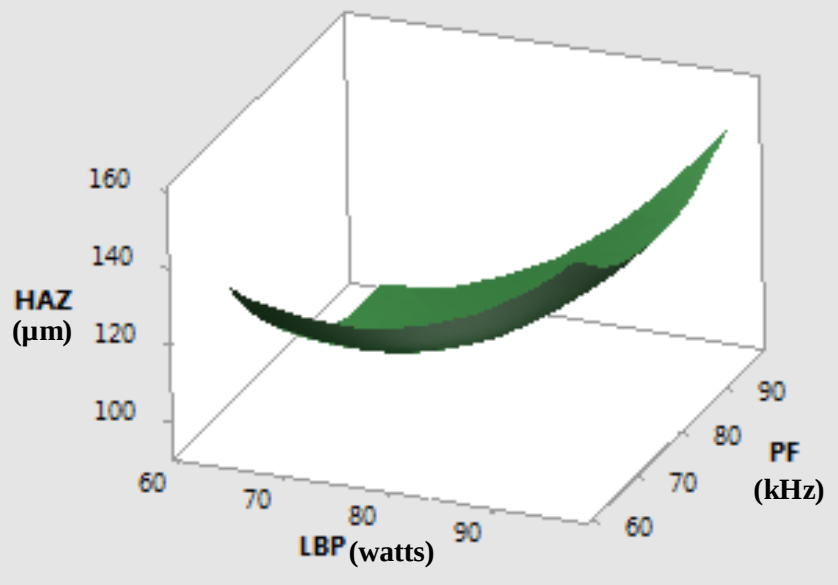

Figure 5.14 Combined Effect of LBP and PF on HAZ at Constant SS of 80 2.5 mm/sec

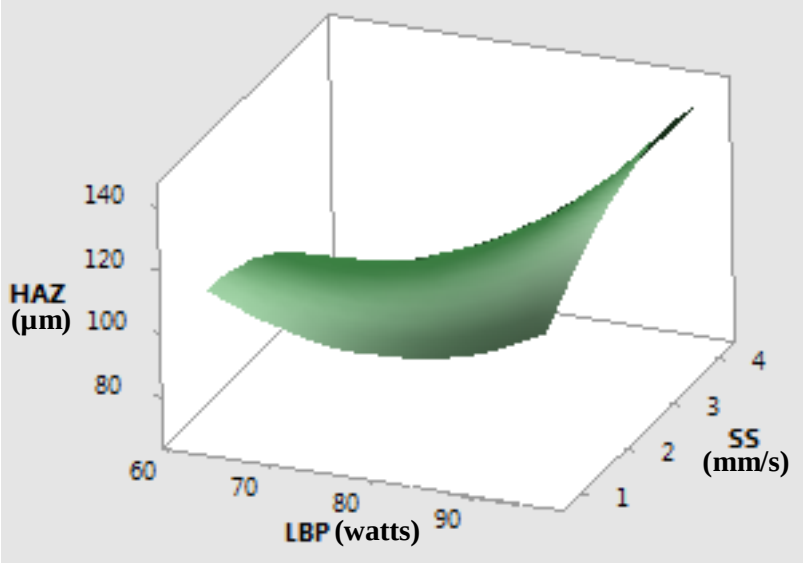

Figure 5.15 Combined Effect of LBP and SS on HAZ at Constant PF of 80 kHz

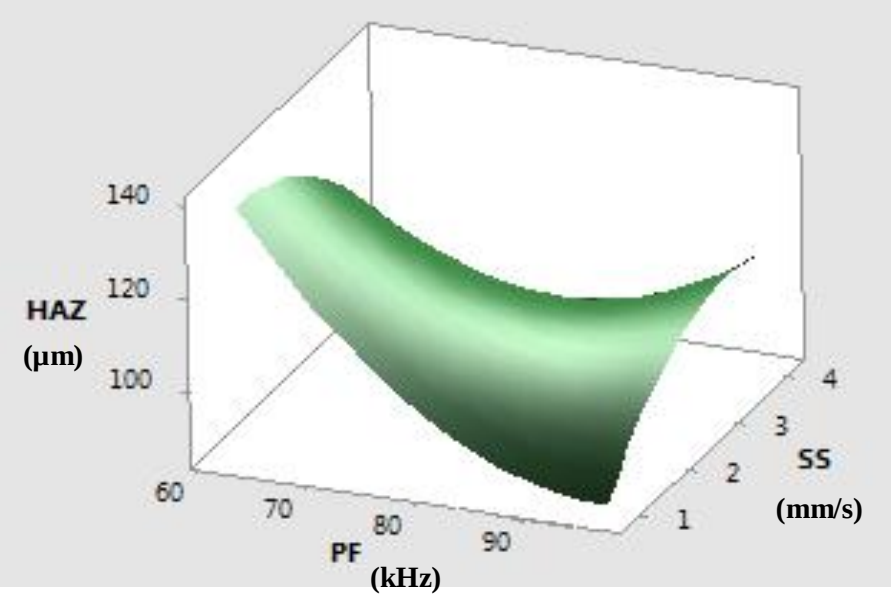

Figure 5.16 Combined Effect of P F and S S on HAZ at Constant L B P of 80 %

Fig. 5.16 indicates the combined Effect of PF and SS on HAZ at constant LBP of 80 %. This plot shows that with the increase of PF, HAZ is decreased continuously due to insufficient heat generation than the requirement under lower range of SS; but it decreases gradually and then increases further under higher range of SS because of heat spreading. On the other hand, with the increase of SS, HAZ is increased slightly because of spreading of heat on the surface rather than penetration and then decreases gradually under the lower range of PF; but it increases continuously under the higher range of PF due spread of heat as well as less interaction time between surface and heat generation.

5.5.4 Analysis of the Influence of Process Parameters on Overcut

I. Analysis of Variance for Overcut

Analysis of Variance (ANOVA) of Overcut is done by using Minitab 18 software and result is listed in Table 5.12 where DF, Adj SS, Adj MS, F-Value and p-Value are available for process parameters based on their individual (linear), square and 2-way interaction effects. Also the Table shows the lack-of-fit as well as total error. The most influencing parameter is LBP whereas SS can be considered as the insignificant for this observation.

Table 5.12 Analysis of Variance (ANOVA) for Overcut

Source	DF	Adj SS	Adj MS	F-Value	p-Value
Model	9	694.304	77.145	78.72	0.000
Linear	3	534.660	178.220	181.86	0.000
LBP	1	329.112	329.112	335.83	0.000
PF	1	163.508	163.508	166.84	0.000
SS	1	42.040	42.040	42.90	0.000
Square	3	95.490	31.830	32.48	0.000
LBP*LBP	1	25.773	25.773	26.30	0.000
PF*PF	1	40.919	40.919	41.75	0.000
SS*SS	1	22.346	22.346	22.80	0.001
2-Way Interaction	3	64.154	21.385	21.82	0.000
LBP*PF	1	1.032	1.032	1.05	0.329
LBP*SS	1	21.041	21.041	21.47	0.001
PF*SS	1	42.081	42.081	42.94	0.000
Error	10	9.800	0.980		
Lack-of-fit	5	6.379	1.276	1.86	0.255
Pure Error	5	3.421	0.684		
Total	19	704.104			

Table 5.13 Model Summary for Overcut

S	R-sq	R-sq (Adj)	R-sq (Pred)
0.989953	98.61%	97.36%	91.88%

Regression Equation in Uncoded Units, used to calculate Overcut as

Overcut = 94.1 - 2.342 LBP + 1.489 PF - 23.34 SS + 0.01337 LBP*LBP -0.01685 PF*PF - 1.245 SS*SS + 0.00359 LBP*PF + 0.1622 LBP*SS + 0.2293 PF*SS (5.5)

II. Analysis Based on Response Surface Methodology for Overcut

Fig. 5.17 depicts combined Effect of LBP and PF on overcut at constant SS of 2.5 mm/sec. From this plot it is clear that increase of LBP increases the overcut gradually at all levels of PF. Because increase of LBP, increases the amount of heat generation which may exceed the requirement and results excess material removal. On the other hand, increase of PF affects on overcut as initially increase due to spread of heat rather than penetration into the surface and then decrease for all values of LBP due well penetration of heat into the material.

Fig. 5.18 represents combined effect of LBP and SS on Overcut at constant PF of 80 kHz. It is observed that with the increase of LBP, overcut is decreased very slowly for the lower to middle value of SS as there is a less chance of spread of heat which is sufficient to melt the material. However, it increases rapidly for the higher value of SS due to spreading of heat. On the other hand, with the increase of SS, overcut initially increases gradually, but later it decrease very slowly for the lower range of LBP value as heat is not exceeded; whereas for the higher range of LBP value, HAZ increases very rapidly with the increase of SS as the generated is excess than the requirement for melting and vaporization cum spreading of heat.

Fig. 5.19 represents the combined effect of PF and SS on overcut at constant LP of 80 %. From this surface plot it is clear that with the increase of PF, overcut decreases rapidly for the lower value of SS due to less interaction time between material and heat generation; whereas for the higher value of SS, there is a very little / no change of overcut as sufficient heat is utilized. On the other hand, with the increase of SS, overcut increases rapidly for the higher value of PF due spread of heat; whereas for the higher value of PF, there is a very little / no change of overcut.

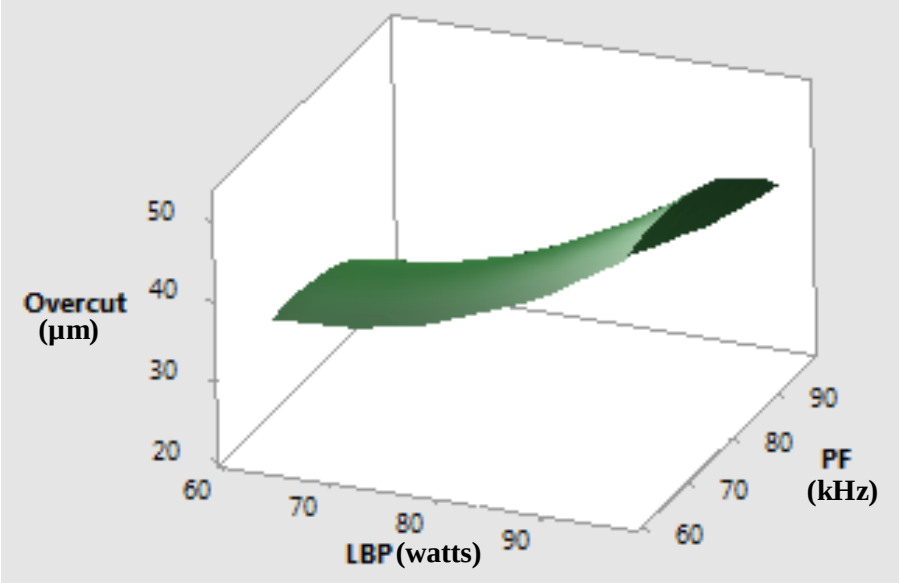

Figure 5.17 Combined Effect of LBP and PF on Overcut at Constant SS of 2.5 mm/sec

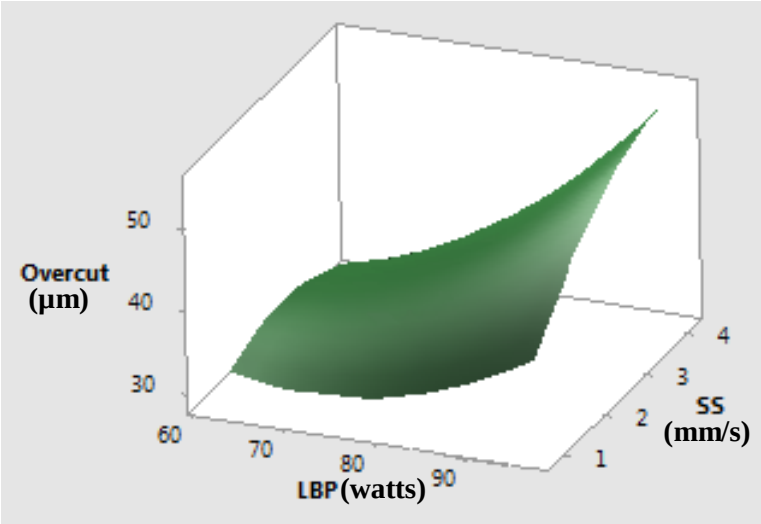

Figure 5.18 Combined Effect of LBP and SS on Overcut at Constant PF of 80 kHz

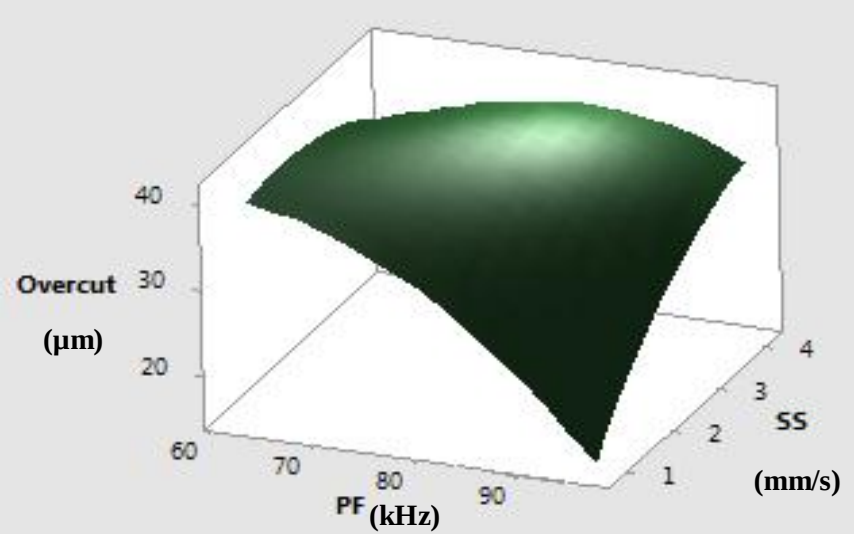

Figure 5.19 Combined Effect of PF and SS on Overcut at Constant LBP of 80 %

5.5.5 Analysis of the Effect of Variable Parameters on Angle Formed

I. Analysis of Variance for Angle Formed

Table 5.14 Analysis of Variance (ANOVA) for Angle Formed

Source	DF	Adj SS	Adj MS	F-Value	p-Value
Model	9	0.436346	0.048483	62.60	0.000
Linear	3	0.152507	0.050836	65.64	0.000
LBP	1	0.097358	0.097358	125.71	0.000
PF	1	0.019855	0.019855	25.64	0.000
SS	1	0.035294	0.035294	45.57	0.000
Square	3	0.204179	0.068060	87.88	0.000
LBP*LBP	1	0.019227	0.019227	24.83	0.001
PF*PF	1	0.088231	0.088231	113.93	0.000
SS*SS	1	0.078453	0.078453	101.30	0.000
2-Way Interaction	3	0.079660	0.026553	34.29	0.000
LBP*PF	1	0.005995	0.005995	7.74	0.019
LBP*SS	1	0.009045	0.009045	11.68	0.007
PF*SS	1	0.064620	0.064620	83.44	0.000
Error	10	0.007744	0.000774		

Lack-of-fit	5	0.002293	0.000459	0.42	0.818
Pure Error	5	0.005451	0.001090		
Total	19	0.444091			

Analysis of variance (ANOVA) of angle formed is done by using Minitab 18 software and result is listed in Table 5.14 where DF, Adj SS, Adj MS, F-Value and p-Value are available for process parameters based on their individual (linear), square and 2-way interaction effects. Also the Table shows the lack-of-fit as well as total error. The most influencing parameter is LBP.

Table 5.15 Model Summary for Angle

S	R-sq	R-sq (Adj)	R-sq (Pred)
0.0278289	98.26%	96.69%	94.20%

Regression Equation in Uncoded Units which is used for calculation of Angle as

Angle = 96.918 - 0.0365 L B P - 0.1219 P F - 0.670 S S + 0.000365 L B P*L B P
+ 0.000782 P F*P F - 0.07378 S S*S S - 0.000274 L B P*P F + 0.003362 L B P*S S
+ 0.008988 P F*S S (5.6)

II. Analysis Based Response Surface Methodology for Angle

Fig. 5.20 is the combined effects of LBP and PF on angle at constant SS of 2.5 mm/sec, which indicated that the increase of LBP increases the angle, however the rate of increase is higher under the lower ranges of PF than that under the higher ranges of PF. Because with the increase of LBP and PF, amount of heat generation is more and interaction time becomes less, as a result laser will affect at the corner i.e. angle is increases. On the other hand, with the increase of PF, angle decreases slightly and then increases gradually, though the rate of increase is higher under the lower ranges of LBP than that under the higher ranges of LBP due high rate of heat generation which affect on the corner.

Fig. 5.21 represents the combined effect of SS and PF on angle at constant LBP of 80 %. From this plot it is clear that with the increase of SS, angle first decreases very slowly, but later decreases very rapidly even below the target value i.e. 90^o for the lower ranges of PF value due to first movement of sample corner is defective. On the other hand, with the increase of PF, angle increases very rapidly for the higher values of SS.

Fig. 5.22 is the combined effect of SS and LBP on angle at constant PF of 80 kHz. It is clear from this plot that increase of SS, angle is increases slowly up to certain value and then decreases gradually though the rate of change is faster under the lower ranges of LBP than that of the higher ranges of LBP. On the other hand, with the increase of LBP, angle is decreased slightly and then increased under the lower values of SS, whereas angle is increased sharply under the higher values of SS when PBP is increased.

Actual Angle Produced at Run Number 19 i.e LBP at 80%, PF at 80 kHz and SS at 2.5 mm/sec is shown in Fig. 5.23 (a) and (b) which is the best result as the angle is very closer (90.02^o and 89.92^o, respectively) to the target angle i.e. 90^o.

Fig. 5.24 represents the optimization of all the responses simultaneously. The composite optimal value achieved is 0.8959 which is very closer to 1.0. In case of overcut and kerf depth, the optimality condition is attained fully i.e. 1.0. Whereas, the desirability for the angle is 0.84621, for HAZ is 0.96039, for kerf width is 0.70963. All these are optimizes simultaneously at parametric combination of LBP is 85.2662%, PF is 96.1384 Hz and SS is 0.8182 mm/s.

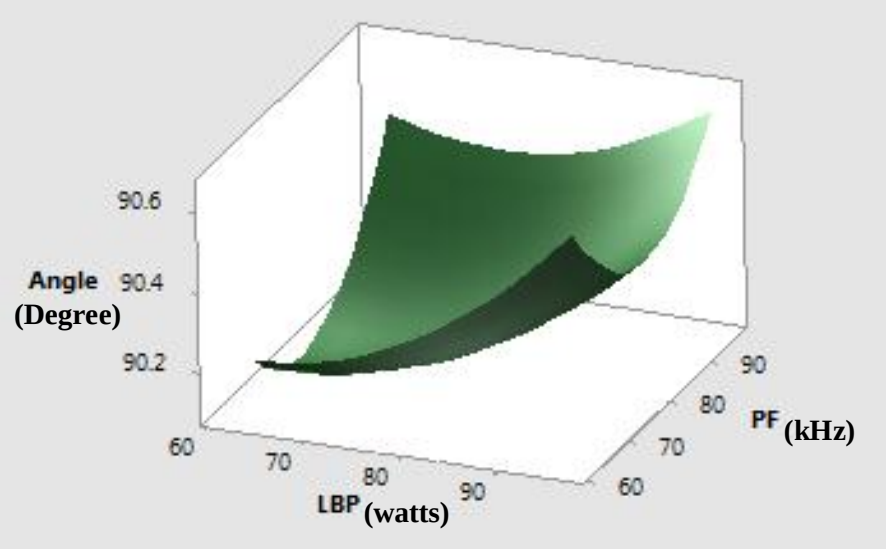

Figure 5.20 Combined Effects of LBP and PF on Angle at Constant SS of 2.5 mm/sec

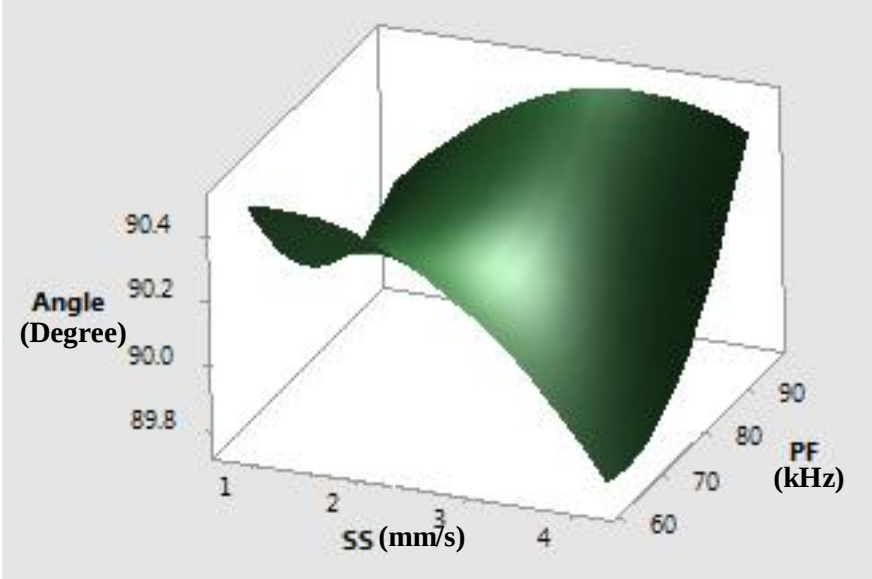

Figure 5.21 Combined Effect of SS and PF on Angle at Constant LBP of 80 %

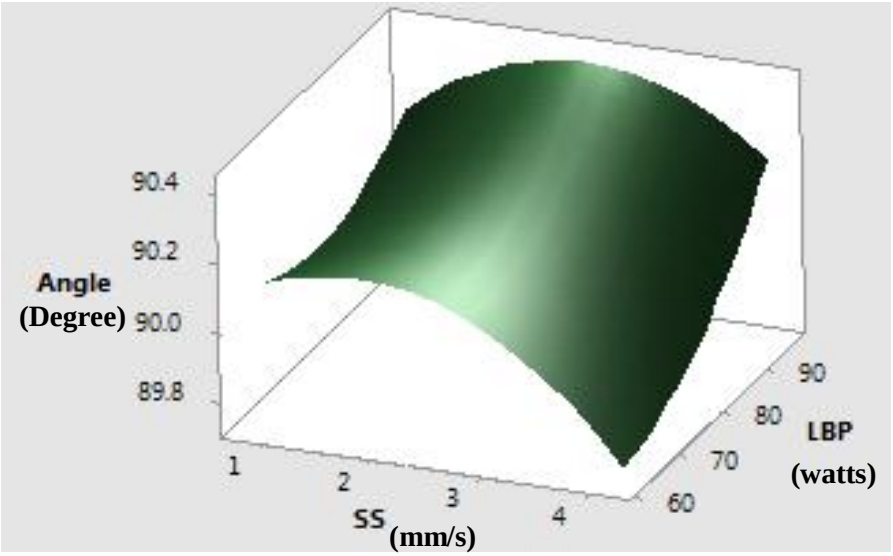

Figure 5.22 Combined Effect of SS and LBP on Angle at Constant PF of 80 kHz

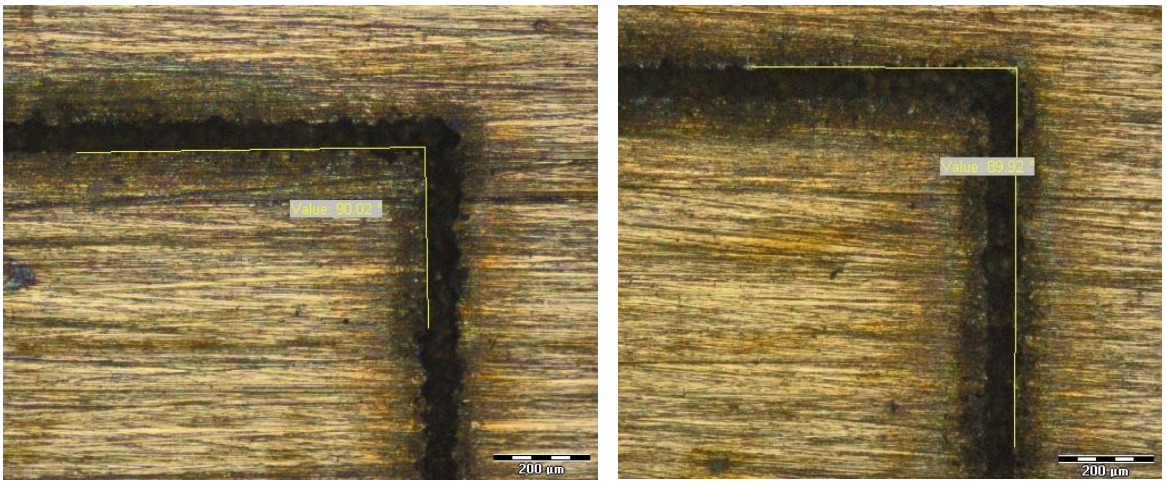

(a) (b)

Figure 5.23 Actual Angle Produced at Run Number 19

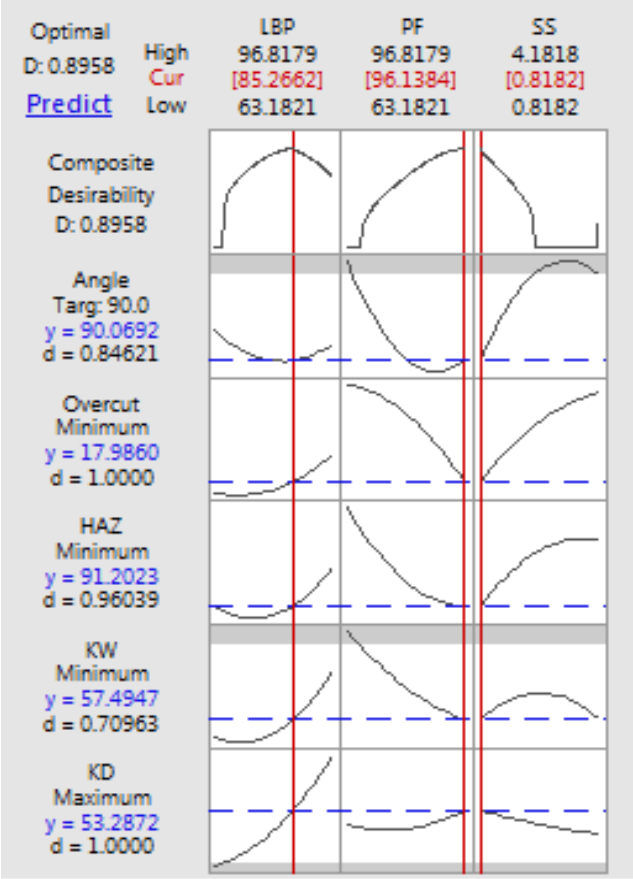

Figure 5.24 Multi-response Optimization of the Micro-channeling Process Parameters

5.6 CONCLUSIONS

i) Basic material removal mechanism of laser micro-channeling on BeCu is studied.

ii) Effect of different input parameters such as, laser beam power, pulse frequency and scanning speed on the responses like kerf depth, kerf width, HAZ, Overcut and angle formed are observed on BeCu alloy sheet.

iii) Analysis of experimental results has been performed through response surface plots and ANOVA.

iv) Mathematical (regression) model has been developed to get responses at any levels of input parameters.

v) Graphical relationship between process parameters & responses are critically analyzed and discussed on combined effects

vi) Optimization of the parametric combination has been performed simultaneously. It is observed that multi-optimization of the process parameters are obtained at LBP of 85.2662%, PF of 96.1384 Hz and SS of 0.8182 mm/s where optimal composite desirability is achieved 0.8959.

Chapter 6

INVESTIGATION ON SURFACE CHARACTERISTICS OF AL 7075 ALLOY BY USING ND:YVO_4 LASER

6.1 EXPERIMENTAL SET-UP AND MATERIAL SELECTION

In this present experimental work, pulsed Nd:YVO_4 laser is sued to perform laser micro-machining operation on Al 7075 alloy to study the surface characteristics. Details of the experimental set-up and material selection is discussed in Chapter 3. In this chapter, numbers of parameters and their working ranges are differently selected.

6.2 PROCESS PARAMETER SELECTION

In this research work, three influencing parameters e.g. laser beam power (LBP), pulse frequency (PF) and scanning speed (SS) with three levels each are selected. Here, the effect of these process parameters on surface roughness during micro-machining of Al 7075 alloy is observed and analyzed. Workable ranges of these influencing parameters are identified through trial/pilot experiments. For better performance and more accurate experimental results, a square geometrical patter of 4 mm each side is chosen for investigation. It is observed from trial experiments that number of pass has very little effect as compared to other processing parameters on the surface roughness. However, relatively best result is investigated for a number of passes of 3. Ranges of processing parameters after a successful trial is identified which are tabulated in Table 6.1. Table 6.2 represents the L9 orthogonal array using Taguchi's.

Table 6.1 Ranges of Process Parameters

Parameters	Laser Beam Power (LBP) in Watt	Pulse Frequency (PF) in kHz	Scanning Speed (SS) in mm/s
Lower Value	7	2	0.2
Higher Value	9	6	0.6

Table 6.2 L9 Orthogonal Array (Taguchi Methodology)

Parameters	LBP (Watt)	PF (kHz)	SS (mm/s)
Level 1	7	2	0.2
Level 2	8	4	0.4
Level 3	9	6	0.6

6.3 EXPERIMENTAL PROCEDURE

- Nd:YVO_4 laser system is set to perform micro-machining operation on Al 7075 alloy.
- Sample is polished by emery paper and cleaned by acetone.
- Pilot/Trial Experiment has been performed to identify the working range of the parameters.
- DOE is established to get the parameter combination for experimentation .
- Laser micro-machining operation is performed by varying the combination.
- Surface roughness is observed and measured by Automic Force Microscope (AFM); (Model: Nanosurf Easyscan 2).
- Signal-to-Noise Ratio (S/N) graph (based on their optimization criteria) is used to identify the ideal parametric combination for optimum response.
- ANOVA is performed to identify the most significant and non-significant parameter.
- Confirmation experiment has been performed to verify the optimum parametric combination.
- SEM photographs are observed for the surface characteristic property changes.

6.4 ANALYSIS OF EXPERIMENTAL RESULTS

After successful completion of experimental work, the response i.e. surface roughness is measured by atomic force microscope (AFM) of model: Nanosurf Easyscan 2, at several locations/positions of micro-machined surface; average is calculated and noted down. Details of experimental result and corresponding S/N ratios are shown in Table 6.3. S/N ratio is calculated based on the smaller-the-better criteria by using the formula as given in Eq. 3.1 and Eq. 3.2. Same can be done by using Minitab 18 software.

Table 6.3 Experimental Results

Expt. No.	LBP (W)	PF (kHz)	SS (mm/sec)	Surface Roughness	
				(nm)	S/N Ratio
1	7	2	0.2	454.22	-53.145
2	7	4	0.4	307.29	-49.751
3	7	6	0.6	203.35	-46.165
4	8	2	0.4	345.67	-50.773
5	8	4	0.6	302.83	-49.624
6	8	6	0.2	509.71	-54.147
7	9	2	0.6	396.30	-51.961
8	9	4	0.2	936.19	-59.427
9	9	6	0.4	464.93	-53.348

Few SEM photographs are captured to observe the surface characteristics of machined zone. Hence, Joel SEM of model, JSM 6360, is used. Fig. 6.1 is the SEM photographs captured under best machining or very good kerf quality condition i.e. optimum parametric combination at which surface roughness is minimum. From this Figure it can be stated that the quality of the produced micro-channel is very good though very less dross formation and recast layer is observed. This SEM photograph is captured under the combination at level $LBP_1PF_3SS_3$.

Whereas, Fig 6.2 exhibits another SEM photographs at a certain moderate machined condition or nearly good kerf quality i.e. surface roughness is good enough. Under this condition, the micro-channel contains few dross formation and recast layer. Also, the cutting edge is not regular. This SEM photograph is captured under the combination at $LBP_3PF_1SS_3$.

While, Fig. 6.3 represents the SEM photographs at worst machining condition or very bad kerf quality i.e. surface produced with highest surface roughness. The micro-channel is full of dross formation and recast layer. Even the cutting edges are not visible clearly because of extreme machining condition. This photographs is taken at the parametric combination of $LBP_3PF_2SS_1$.

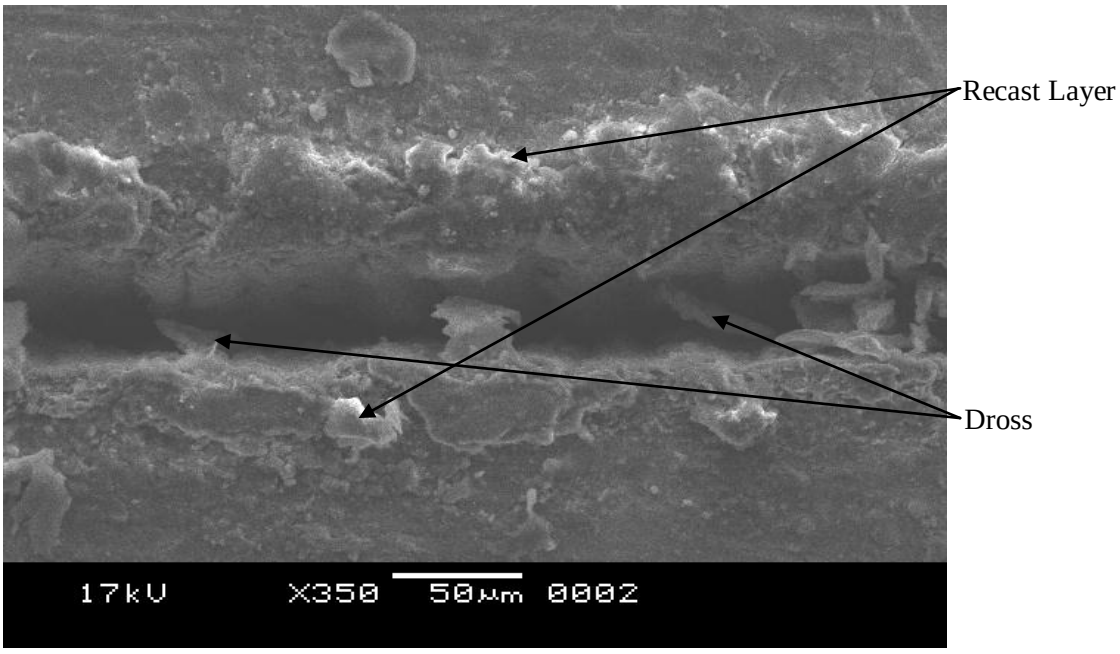

Figure 6.1 SEM Photograph Under Best Surface Roughness Condition ($LBP_1PF_3SS_3$)

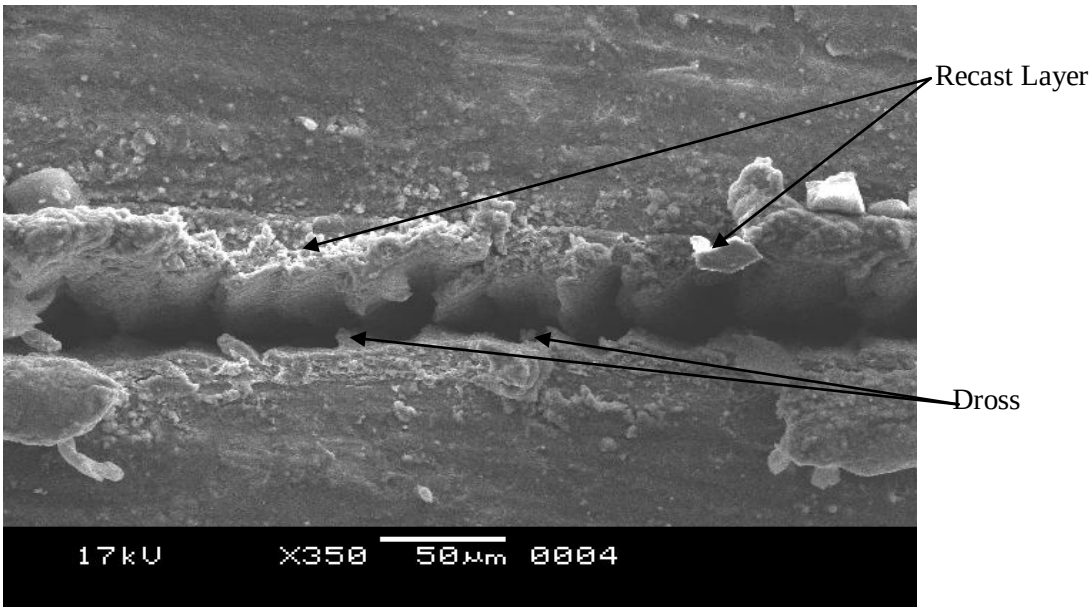

Figure 6.2 SEM Photograph Under Moderate Surface Roughness Condition ($LBP_3PF_1SS_3$)

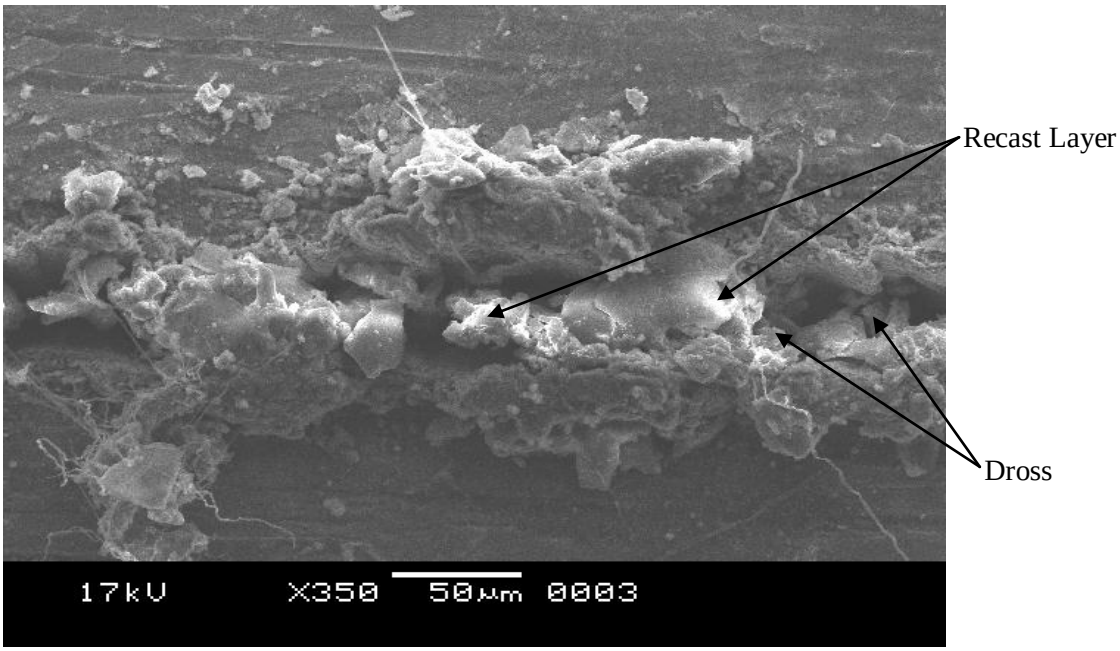

Figure 6.3 SEM Photograph Under Worst Surface Roughness Condition ($LBP_3PF_2SS_1$)

6.4.1 Analysis Based on S/N Ratio Plots

Fig. 6.4 represents S/N ratio plot for surface roughness Vs processing parameters, shows that surface roughness decreases at faster rate due to increase of laser beam power. Because, increase of laser beam power results more heat generation which is not utilized fully for removing the material through penetration; rather some part of heat is spread over the surface and creates poor surface. In case of pulse frequency, it is quite interesting. Initially, with the increase of pulse frequency, interaction time between generated heat and job surface decreases which results insufficient penetration of heat rather heat is spread over the surface. Later, further increase of pulse frequency results sufficient time of heat generation and penetration into the surface. As a result surface roughness is decreased. While, S/N ratio increases due to increase of scanning speed. Because, increase of scanning speed results reduction of part of spread heat over the job surface and thereby increases the penetrating heat part. Also, the plot reveals that optimum parametric combination is observed at $LBP_1PF_3SS_3$ i.e. laser beam power of 7 W, pulse frequency of 6 kHz and scanning speed of 0.6 mm/s.

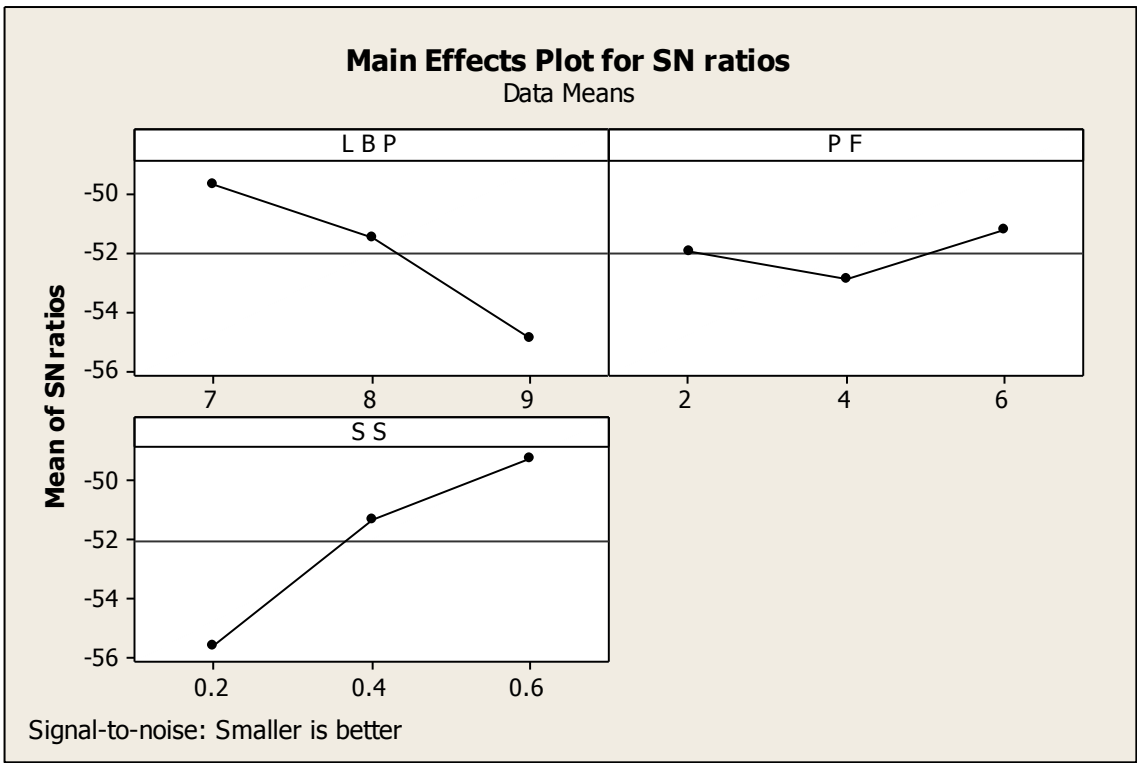

Figure 6.4 S/N Ratio Plot for Surface Roughness

6.4.2 Analysis Based on Analysis of Variance (ANOVA)

ANOVA of surface roughness is done by using the Minitab 18 software which is represented in Table 6.4. It is stated that scanning speed affects mostly (57.25%) on surface roughness, then after laser beam power (38.65%) and pulse frequency (4.06%).

Table 6.4 ANOVA of Surface Roughness

Parameters	Degree of Freedom	Sum of Squares	Mean Squares	F-Value	Percentage Contribution	p-Value
LBP	2	42.17952	21.08976	984.123	38.65	0.001
PF	2	4.43602	2.21801	103.5	4.06	0.01
SS	2	62.4876	31.2438	1457.947	57.25	0.001
Error	2	0.04285	0.02143		0.04	
Total	8	109.14606				

where, S = 0.1465, R-sq = 100% and R-sq(adj) = 99.8%.

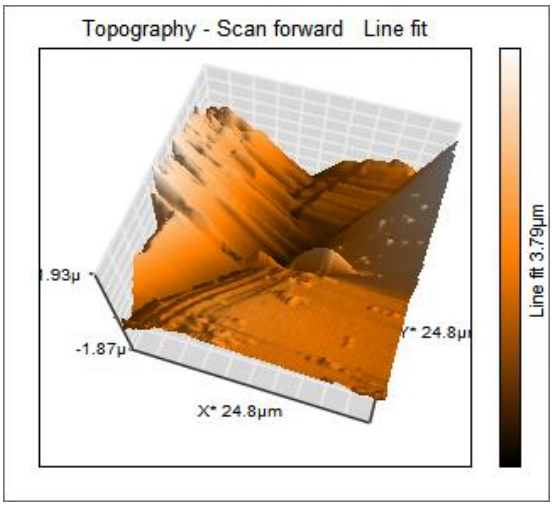

(a) $LBP_1\ PF_3\ SS_3$

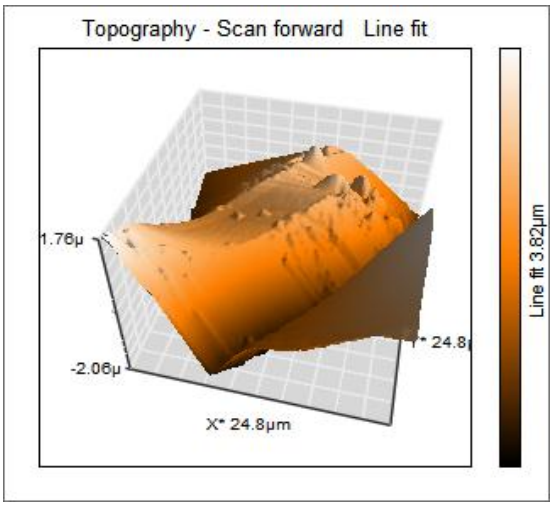

(b) $LBP_3\ PF_3\ SS_2$

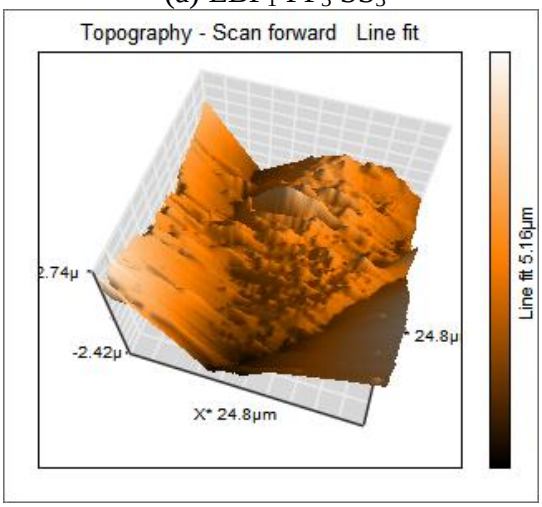

(c) $LBP_1\ PF_2\ SS_2$

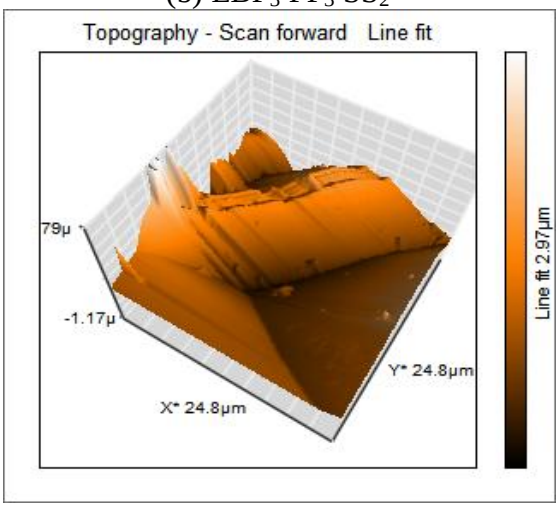

(d) $LBP_3\ PF_1\ SS_3$

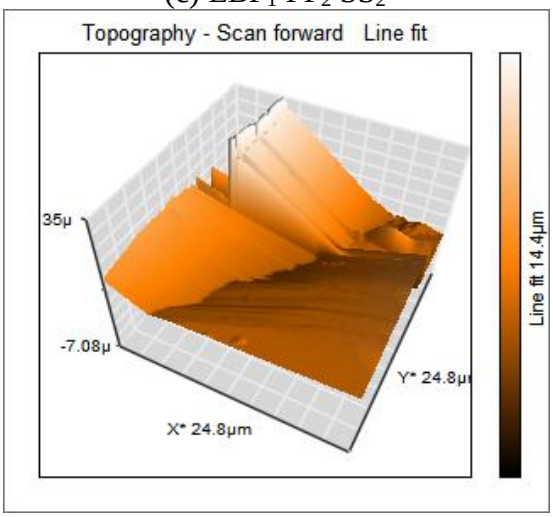

(e) $LBP_2\ PF_1\ SS_2$

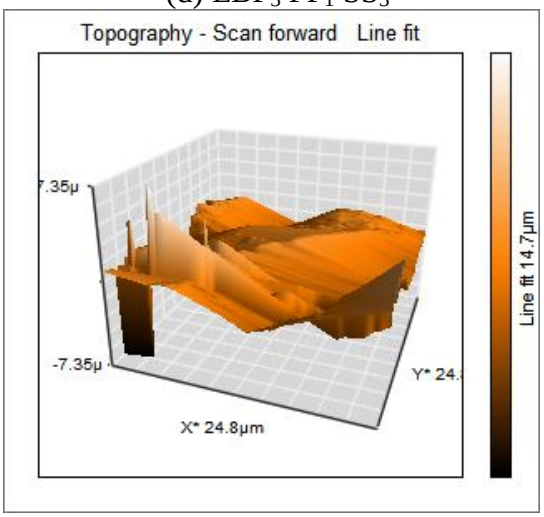

(f) $LBP_3\ PF_2\ SS_1$

Figure 6.5 AFM Photographs for Surface Roughness of Laser Machined Kerf

Fig. 6.5 represents photographs of surface roughness captured from AFM at six different parametric combinations as mentioned in (a), (b), (c), (d), (e) and (f), respectively. A suitable scanning area of 24.8 µm × 24.8 µm has been selected. Fig. 6.5 (a) represents the best quality surface with surface roughness value of 203.35 nm. Fig. 6.5 (b), (c), (d) and (f) represent four different photographs at different levels which shows moderate surface quality with surface roughness values 464.93 nm, 307.29 nm, 396.30 nm and 345.67 nm, respectively. Whereas, Fig. 6.5 (d) represents the AFM photograph at highest surface roughness value of 936.19 nm.

6.4.3 Confirmation Test Based on Taguchi methodology and S/N Ratio Plots

After identifying the optimum condition from the S/N ratio plot and predicting the surface roughness theoretically, it is required to verify this with an additional experimental run, called as confirmation test. The result of confirmation test and predicted values are represented by Table 6.5. It proves the reliability and feasibility of the model. The adequacy of the model for predicting the optimum value is also verified.

Table 6.5 Confirmation Test Result for Surface Roughness

	Initial Parameter Setting	Optimum Parameter Setting	
		Predicted	Experimental
Level	$LBP_1PF_3SS_3$	$LBP_1PF_3SS_3$	$LBP_1PF_3SS_3$
Surface Roughness (nm)	203.35	201.393	195.342
S/N Ratio (dB)	-46.1649	-46.0809	-45.8159
Predicted Error of S/N Ratio		0.265	
Confidence Limits		± 0.2928	

6.6 CONCLUSIONS

Following conclusions can be made based on the experimental result:

(i) From the S/N ratio plot, it is observed that surface roughness increases with the increase of laser beam power, but it decreases due to increase of scanning speed. While with the increase of pulse frequency, initially surface roughness increases up to certain value, then decreases.

(ii) The optimum parametric combination for minimum surface roughness is observed at level $LBP_1PF_3SS_3$ i.e. laser beam power of 7 W, pulse frequency of 6 kHz and scanning speed of 0.6 mm/s.

(iii) ANOVA shows that scanning speed is the most significant (contribution is 57.25%) parameter to affect surface roughness and effect of pulse frequency (contribution is only 4.06%) can be neglected.

(iv) Confirmation test agreed well with the predicted optimized result.

(v) AFM photographs shows the comparative studies of surface roughness and kerf quality at different parametric combination. The best and worst result in terms of surface roughness are observed at $LBP_1PF_3SS_3$ and $LBP_3PF_2SS_1$, respectively.

(vi) SEM photographs reflects the quality of the surface (kerf) produced. They includes recast layer as well as presence of dross. The best and worst kerf quality analysis in terms of surface roughness are observed at their corresponding parametric combinations of i.e. $LBP_1PF_3SS_3$ and $LBP_3PF_2SS_1$, respectively [76].

Chapter 7

GENERAL CONCLUSIONS& FUTURE SCOPE OF WORK

7.1 GENERAL CONCLUSIONS

Within the limited resources, extensive experimental observation, parametric analysis, mathematical modeling, single-objective as well as multi-objective optimization, prediction of responses, surface characteristics of micro-machining, micro-drilling and micro-channeling operation on light metal alloys have been carried out by using Nd:YVO_4 and diode pumped fiber laser. The experimental works will help technologically, in the development of the different industries, working with light metal alloys. The following conclusions can be made from the extensive experimental research carried out by the author:

(i) Literature survey is done for acquiring state-of-art knowledgeof research on micro-machining of light metal alloys. A large number of past research work have been studied for this purpose.

(ii) Study of the in-depth material removal mechanism of light metal alloys by using$Nd:YVO_4$and diode pumped fiber laserand has been performed successfully.

(iii) In-depth study, analysis and optimization of process parameters namely, laser beam power, pulse frequency, scanning speed and repetition rate on kerf width, heat affected zone and angular deviation for laser micro-machining of Al 7075 alloy using $Nd:YVO_4$ laser following L9 OA is made.ANOVA shows that repetition rate has most significance on kerf width, whereas pulse frequency has very little significance. ANOVA also represents that repetition rate hast most significance on HAZ, whereas scanning speed has very little significance. On the other side, scanning speed is the most significant parameter to affect on angular deviation, whereas pulse frequency has very little significance. Confirmation experiment is performed to verify the predicted values at optimum levels.

The corresponding optimized parametric combinations for minimum kerf width of 66.2907 µm is $LBP_2PF_1SS_1RR_1$,i.e. laser beam power of 8.5 W, pulse frequency of 2kHz, scanning speed of 0.2 mm/s and repetition rate of 1. Similarly, optimized parametric combinations for minimum HAZ of 112.193 µm is $LBP_2PF_1SS_3RR_1$, i.e. laser beam power of 8.5 W, pulse frequency of 2 kHz, scanning speed of 0.6 mm/s and repetition rate of 1 and optimized parametric combinations for minimum angular deviation of $-0{,}0233^o$is $LBP_1PF_1SS_2RR_2$,i.e. laser beam power of 7.5 W, pulse frequency of 2 kHz, scanning speed of 0.4 mm/s and repetition rate of 3, respectively.

When Kerf width, HAZ and angular deviations are optimized simultaneously using a single character called grey relational grade for all the experiment as well as at all the levels and verified by confirmation, the optimized parametric condition is observed at $LBP_1PF_1SS_1RR_1$ i.e. laser beam power of 7.5 W, pulse frequency of 2 kHz, scanning speed of 0.2 mm/s and repetition rate of 1. At this condition, minimum values of kerf width is found as 65.66 µm, HAZ as 111.21 µm and

angular deviation as 0.03^{o}Confirmation experiment for both the cases improved the machining quality sufficiently compared to the initial machining parameter setting. However, there is no improvement of angular deviation.

(iv) The effect of process parameters namely, laser beam power, pulse frequency, scanning speed and number of pass on hole taper andHAZ width during laser micro-drilling of copper sheetusing Nd:YVO_4laser by L9 OA has been performed through proper study,analysis and optimization.

It is observed that more influencing factors on hole taper are the scanning speed and laser beam power and less influencing parameters are the pulse frequency and number of pass. From ANOVA results and confirmation test, it is observed that optimal combination of input parameters for minimization of hole taper (of 0.0334 rad)is obtained at LP_1 PF_3 SS_1 NP_1 i.e. laser beam power of 8.4 W, pulse frequency of 12 kHz, scanning speed of 0.2 mm/s kHz, and number of pass of 5.

It is also observed that most influencing factor on HAZ width is the laser beam power and the least influencing factor is the scanning speed and optimal combination of input parameters for minimization of HAZ width (of 67.1902 µm) is obtained at$LP_1PF_2SS_3NP_1$i.e. laser beam power of 8.4 Watts, pulse frequency of 9 kHz, scanning speed of 0.6 mm/s and number of pass of 5.

Grey Relational Analysis shows improvement of both the hole taper and HAZ width under $LP_1PF_1SS_1NP_1$ i.e. laser beam power of 8.4 Watts, pulse frequency of 6 kHz, scanning speed of 0.2 mm/s and number of pass of 5 combination of process parameters. This also indicates application feasibility of the Grey-based Taguchi technique for continuous improvement of laser micro-drilling quality in the manufacturing industry.

(v) In-depth analysis of the influence of laser beam power, pulse frequency and scanning speed on kerf width, kerf depth, HAZ, overcut and angle formed in micro-channeling on copper-beryllium alloy sheet by using diode pumped fiber laser following central composite design of response surface methodologyhas been completed successfully.

Mathematical model for achieving the desired responses is developed and optimized the process parameters individually as well simultaneously by Taguchi methodology and response surface methodology.

Optimization of the responses/output parameters and thereby the optimized parametric combination by using Taguchi methodology, grey relational analysis are performed.

(vi) Surface characteristic of Nd:YVO_4laser machined Al 7075 alloy following L9 OAconsidering laser beam power, pulse frequency and scanning speed as the influencing parameters are performed and analyzed.Statistical model has been developed for predicting the responses at any parametric combination during micro-machining operation for all the experimental observation.

ANOVA shows that scanning speed is the most significant and pulse frequency is the least significant parameter on surface roughness. The optimum parametric combination for minimum surface roughness of 195.392 µm is observed at level $LBP_1PF_3SS_3$ i.e. laser beam power of 7 W, pulse frequency of 6 kHz and scanning speed of 0.6 mm/s.

Characteristics of the micro-machined surfaceproduced are discussed by using optical and scanning electron microscope. It is observed that at a certain parametric condition surface quality is very good compared to other case; though in all the cases surface roughness values are in nm ranges.

7.2 FUTURE SCOPE OF WORK

The present research work have been carried out with the limitations of resource & time. However, few more studies, analysis, optimization and prediction can be conducted in future.

It is observed that during light metal thin alloy processing, there is a chance of bending of the workpiece due to heating effect. So, to avoid this bending some precaution may be required; like pre-strain or pre-heat treatment of the workpiece, proper job holding fixture, etc.

(i) Experimental investigation may be conducted by using other laser sources.

(ii) Micro-machining operation can be extended for any other profile cutting.

(iii) Artificial neural network, genetic algorithm, etc. can be utilized for prediction and optimization of the process parameters.

(iv) Temperature distribution andthermal stress distribution patterns can also be analyzed.

REFERENCES

1. A. J. Dolata, M. Dyzia, "Light Metal and their Alloys III: Technology, Microstructure and Properties", 2014, Transtech Publication, Verlag.
2. I. Polmar, "Light Alloys: From Traditional to Nanocrystals", 2006, 4th Ed. Elsevier, UK.
3. John C. Ion, "Laser processing of Engineering Materials: Principles, Procedure and Industrial Application", 2005, 1st Ed, Elsevier, Oxford.
4. J. F. Reddy (Chief Editor), "LIA, Handbook of Laser Materials Processing", 2011, Mongolia Publishing Inc., Mongolia.
5. I. Shikawa et al , “Beryllium copper alloy excellent in strength, workability& heat resistant & method for producing the same”, United states patent ,no-5824167, oct-20, 1998.
6. T. Masuzawa, "State of art of micro-machining", 49/2 (2000) 473 - 486.
7. L. Li, "The challenges ahead for laser macro, micro and nano manufacturing, 2010, 1st Ed. Elsevier, Canbridge
8. J. Wilson, J.F.B. Hawkers, "Laser Principles and Applications", 1987, Prentice-Hall, New Delhi, India.
9. W. M. Steen, "Laser Material Processing", 1991, Springer, Verlag, New York.
10. P.W. Milonni, J.H. Eberly, "Lasers", 1988, Willey, New York.
11. G. Chryssolouris, "Laser Machining: Theory and Practice", 1991, Springer, Berlin.
12. K. A. Elijah Jr., "Principles of Laser Material Processing", 2009, John Willey & Sons Inc., Hoboken, New Jersy.
13. G. G. Gladush, I. Smurov, "Physics of Laser Materials Processing: Theory and Experiment", 2011, Springer, Berlin.
14. E. Hecht, "Optics", 1998, 3rd Ed, Addison-Weslay, New York.
15. P. K. Das, "Lasers and Optical Engineering", 1991, 1st Ed, Springer, New York.
16. K.J. Kuhn, "Laser Engineering", 1998, 1st Ed, Prentice Hall, New York.

17. M. Mitsuishi, N. Sugita, I. Kono, S. Warisawa, "Analysis of laser micromachining in silica glass with an absorbent slurry", CIRP Annals - Manufacturing Technology, 57 (2008), 217 - 222.
18. A. Grigoryants, "Basics of Laser Material Processing", 1994, Mir Pulishers, Mosco.
19. X. Zhu, D. M. Villeneuve, A. Tu. Naumov, S. Nikumb, P. B. Corkum, "Experimental study of drilling sub-10 μm holes in thin metal foils with femtosecond laser pulses", Applied Surface Science, 152 (1999) 138 - 148.
20. D. Arau´jo, F. J. Carpio, D. Me´ndez, A. J. Garcı´a, M. P. Villar, R. Garcı´a, D. Jime´nez, L. Rubio, "Microstructural study of CO2 laser machined heat affected zone of 2024 aluminium alloy" Applied Surface Science, 208 - 209 (2003) 210 - 217.
21. J. Meijer, "Laser beam machining (LBM), state of the art and new opportunities", Journal of Materials Processing Technology, 149 (2004) 2 - 17.
22. W. Perriea, M. Gill, G, Robinson, P. Fox, W. O'Neill, "Femtosecond laser micro-machining of aluminium under helium", Applied Surface Science, 230 (2004) 50 - 59.
23. L. Tunna, W. O'Neill, A. Khan, C. Sutcliffe, "Analysis of laser micro drilled holes through aluminium for micro-manufacturing applications", Optics and Lasers in Engineering, 43 (2005) 937 - 950.
24. K. Salonitis, A Stoumaras, G. Tsoukantas, P. Stavropoulos, G. Chryssolouris, " A theoretical and experimental investigation on limitations of pulsed laser drilling", Journal of Materials Processing Technology, 183 (2007) 96 - 103.
25. A. K. Dubey, V. Yadava, "Experimental study of Nd:YAG laser beam machining - An overview", Journal of Materials Processing Technology, 195 (2008) 15 - 26.
26. S. K. Dhara, A. S. Kuar, S. Mitra, "An artificial neural network approach on parametric optimization of laser micro-machining of die-steel". International Journal of Advanced Manufacturing Technology, 39 (2008) 39 - 48.
27. Y. Kuo, T. Yang, G. W. Huang, "The use of grey relational analysis in solving multiple attribute decision-making problems", Computers and Industrial Engineering, 55 (2008) 80 - 93.

28. A. K. Dubey, V. Yadava, Multi-objective optimization of Nd:YAG laser cutting of nickel-based superalloy sheet using orthogonal array with principal component analysis", Optics and Lasers in Engineering, 46 (2008) 124 - 132.
29. A. Riveiro, F. Quintero, F. Lusquiños, J. Pou, M. Perez-Amor, "Laser cutting of 2024-T3 aeronautic aluminium alloy", Journal of Laser Applications, 20 (2008) 230 - 235.
30. A. K. Dubey, V. Yadava, "Robust parameter design and multi-objective optimization of laser beam cutting for alumunium alloy sheet", International Journal of Advanced Manufacturing Technology, 38 (2008) 268 - 277.
31. A. K. Dubey, V. Yadava, "Optimization of kerf quality during pulsed laser cutting of aluminium alloy sheet", Journal of Materials Processing Technology, 204 (2008) 412 - 418.
32. A. K. Dubey, V. Yadava, "Laser beam machining - A review", International Journal of Machine Tools & Manufacture, 48 (2008) 609 628.
33. U. Caydas, A Hascalik, "Use of grey relational analysis to determine optimum laser cutting parameters with multi-performance characteristics", Optics & Laser Technology, 40 (2008) 987 - 994.
34. A. Stournaras, P. Stavropoulos, K. Salonitis, G. Chryssolouris, "An investigation of quality in CO2 laser cutting of aluminium", CIRP journals of Manufacturing Science and Technology, 2 (2009) 61 - 69.
35. M. J. Tsai, C. HaoLi, "The use of grey relational analysis to determine laser cutting parameters for QFN packages with multiple performance characteristics", Optics & Laser Technology, 41 (2009) 914 - 921.
36. S. M. Karazi, A Issa, D. Brabazon, "Comparison of ANN and DoE for the prediction of laser-machined micro-channel dimensions", Optics and Laser in Engineering, 47 (2009) 956 - 964.
37. R. Biswas, A. S. Kuar, S. Sarkar, S. Mitra, "A parametric study of pulsed Nd:YAG laser micro-drilling of gamma-titanium aluminide", Optics & Laser Technology, 42 (2010), 23 - 31.

38. B. S. Yilbas, S. Khan, K. Raza, O. Keles, M. Ubeyli, T. Demir, M. S. Karakas, "Laser cutting of 7075 Al alloy reinforced with Al_2O_3 and B_4C composites", International Journal of Advanced Manufacturing Technology, 50 (2010) 185 - 193.
39. K. Huehnlein, K. Tschirpke, R. Hellmann, "Optimization of laser cutting processes using design of experiments", Physics Procedia, 5 (2010) 243 - 252.
40. A. Sharma, V. Yadava, R. Rao, Optimization of kerf quality characteristics during Nd:YAG laser cutting of nickel based superalloy sheet for straight and curved cut profiles", Optics and Lasers in Engineering, 48 (2010) 915 - 925.
41. A. Riveiro, F. Quintero, F. Lusqui˜nos, R. Comesa˜na, J. Pou, "Parametric investigation of CO_2 laser cutting of 2024-T3 alloy", Journal of Materials Processing Technology, 210 (2010) 1138 - 1152.
42. S. A. A. A. Mousavi, S. T. Niknejad, "Study on the microstructure and mechanical properties of Nd:YAG pulsed laser beam weld of UNS-C17200 copper beryllium alloy", Journal of Materials Processing Technology, 210 (2010) 1472 - 1481.
43. A. Riveiro, F.Quintero, F. Lusquiños, R. Comesaña, J. D. Val, J. Pou, "The role of assist gas nature in laser cutting of aluminium alloy", Physics Procedia, 12 (2011) 548 - 554.
44. B. Adelmann, R. Hellmann, " Fast laser cutting Optimization algorithm" Physics Procedia, 12 (2011) 591 - 598.
45. L. Li, M. Hong, M. Schmidt, M. Zhong, A. Malshe, B. Huisin'tVeld, V. Kovalenko, "Laser nano-manufacturing - State of the art and challenges", CIRP Annals - Manufacturing Technology, 60 (2011) 735 - 755.
46. A. Riveiro, F. Quintero, F. Lusqui˜nos, R. Comesa˜na, J. Pou, "Effects of processing parameters on laser cutting of aluminium-copper alloys using off-axial supersonic nozzles", Applied Surface Science, 257 (2011) 5393 - 5397.
47. D. ganguly, B. Acherjee, A. S. Kuar, S. Mitra, "Hole characteristics optimization in Nd:YAG laser micro-drilling of zirconium oxide by grey relational analysis", International Journal of Advanced Manufacturing Technology, 61 (2012) 1255 - 1262.

48. A. Sharma, V. Yadava, "Modelling and optimization of cut quality during pulsed Nd:YAG laser cutting of thin Al-alloy sheet for straight profile", Optics & Laser Technology, 44 (2012) 159 - 168.
49. P. Kurylo, Property examination of surface layer of copper alloy casts on the example of MO59 alloy", Procedia Engineering, 48 (2012) 312 - 319.
50. A. S. Kuar, B. Acherjee, D. Ganguly, S. Mitra, "Optimization of Nd:YAG laser parameters for microdrilling of alumina with multiquality characteristics via Grey-Taguchi method", Materials and Manufacturing Processes, 27 (2012) 329 - 336.
51. K. Hock, B. Adelmann, R. Hellmann, "Comparative study of remote fiber laser and water-jet guided laser cutting of thin metal sheets", Physics Procedia, 39 (2012) 225 - 231.
52. S. L. Campanelli, G. Casalino, N. Contuzzi, "Multi-objective optimization of laser milling of 5754 aluminium alloy", Optics & Laser Technology, 52, (2013) 48 - 56.
53. A. Sharma, V. Yadava, "Modelling and optimization of cut quality during pulsed Nd:YAG laser cutting of thin Al-alloy sheet for curved profile", Optics and Lasers in Engineering, 51 (2013) 77 - 88.
54. R. Khettabi, L. Fatmi, J. Masounave, V. Songmene, "On the micro and nanoparticle emission during machining of titanium and aluminium alloys", CIRP Journal of Manufacturing Science and Technology, 6 (2013) 175 - 180.
55. G. Tiranda, C. Arvieua, E. Lacostea, J. M. Quenisset, "Control of aluminium laser welding conditions with the help of numerical modeling", Journal of Materials Processing Technology, 213 (2013) 337 - 348.
56. S. Mishra, V. Yadava, "Modeling and optimization of laser beam percussion drilling of thin aluminium sheet", Optics & Laser Technology, 48 (2014-3) 461 - 474.
57. S. Mishra, V. Yadava, "Modeling and optimization of laser beam percussion drilling of nickel-based superalloy sheet using Nd:YAG laser", Optics and Lasers in Engineering, 51, (2013) 681 - 695.
58. S. Kasman, "Impact of parameters on the process response: A Taguchi orthogonal analysis for laser engraving", Measurement, 46 (2013) 2577 - 2584.

59. G. Selvakumar, G. Sornalatha, S. Sarkar, S. Mitra, "Experimental investigation and multi-objective optimization of wire electrical discharge machining (WEDM) of 5083 aluminium alloy", Transaction of Nonferrous Material Society, China, 24 (2014) 373 - 379.
60. B. Acherjee, S. Prakash, A. S. Kuar, S. Mitra, "Grey relational analysis based optimization of underwater Nd:YAG laser micro-channeling on PMMA", Procedia Engineering, 97 (2014) 1406 - 1415.
61. C. Leone, S. Genna, A. Caggiano, V. Tagliaferrid, R. Molitierno, "An investigation on Nd:YAG laser cutting of Al 6061 T6 alloy sheet", Procedia CIRP, 28 (2015) 64 - 69.
62. R. Adalarasan, M. Santhanakumar, M. Rajmohan, "Optimization of laser cutting parameters for Al6061/SiCp/Al_2O_3 composite using grey based response surface methodology (GRSM)", Measurement, 73 (2015) 596 - 606.
63. R. Biswas, A. S. Kuar, S. Mitra, "Process optimization in Nd:YAG laser microdrilling of alumina-aluminium interpenetrating phase composite", Journal of Material Research Technology, 4 (2015) 322 - 332.
64. C. Chen, M. Gao, X. Zeng, "Relationship between temperature at cut front edge and kerf quality in fiber laser cutting of Al-Cu aluminum alloy", International Journal of Machine Tools & Manufacture, 109 (2016) 58 - 64.
65. Q. Wang, S. Luo, Z. Chen, H. Qi, J. Deng, Z. Hu, "Drilling of aluminum and copper films with femto second double-pulse laser", Optics & Laser Technology, 80 (2016) 116 - 124.
66. J. Li, C. Lua, A. Wanga, Y. Wua, Z. Maa, X. Fanga, L. Tao, "Experimental investigation and mathematical modeling of laser marking two-dimensional barcodes on surface of aluminum alloy", Journal of Manufacturing Processes, 21 92016) 141 - 152.
67. S. G. Irizalp, N. Saklakoglu, "High strength and high ductility behavior of 6061-T6 alloy after laser shock processing", Optics and Lasers in Engineering, 77 (2016) 183 - 190.

68. H. Rao, S. Giet, K. Yang, X. Wu, C. H. J. Davies, "The influence of processing parameters on aluminium alloy A357 manufactured by selective laser melting", Materials and Design, 109 (2016) 334 - 346.
69. M. L. M. Sistiagaa, R. Mertensb, B. Vranckena, X. Wanga, B. V. Hoorewederb, J. P. Kruthb, J. V. Humbeeck, "Changing the alloy composition of Al7075 for better processability by selective laser melting", Journal of Materials Processing Technology, 238 (2016) 437 - 445.
70. K. K. Mandal, B. Chatterjee, A. S. Kuar, S. Mitra, "Parametric study of hole taper in laser micro-drilling of copper sheet", International Journal of Emerging Trends in Science and Technology, 3 (2016) 393 - 397.
71. Md. Antar, D. Chantzis, S. Marimuthu, "High speed EDM and laser drilling of aerospace alloys", Procedia CIRP, 42 (2016) 526 - 531.
72. A. M. Alahmari, S. Darwish, N. Ahmed, "Laser beam micro-milling (LBMM) of selected aerospace alloys", International Journal of Advanced Manufacturing Technology, 36 (2016) 2411 - 2431.
73. B. Chatterjee, K. K. Mandal, A. S. Kuar, S. Mitra, "Parametric study of heat affected zone (HAZ) width in laser micro-drilling of copper sheet", ELK Asia Pacific Journals, Special Issue.
74. A. Bharatish, H. N. Narasimhamurthy, B. Anand, K. N. Subramanya, M. krishna, P. V. Srihari, "Assesment of drilling characteristics of alumina coated on aluminium using CO_2 laser", Measurement, 100 (2017) 164–175.
75. G. D. Gautam, A. K. Pandey, "Pulsed Nd:YAG laser beam drilling: A review", Optics and Laser Rechnology, 100 (20180 183 - 215.
76. K. K. Mandal, A. S. Kuar, S. Mitra, "Experimental investigation on laser micro-machining of Al7075 alloy", Optics and Laser Technology, 107 (2018), 260–267.
77. A Sharma, V. Yadava, "Experimental analysis of Nd:YAG laser cutting of sheet materials - A review", Optics and Laser Technology, 98 (2018) 264 - 280.
78. D. J. Kotadiya, JM. Kapopara, A,R. Patel, C.G. Dalwadi, D.H. Pandyac, "Parametric analysis of process parameters for laser cutting process on SS-304", Materials Today: Procedings, 5 (2018) 5384 - 5390.

79. Laser manual for pulsed Nd:YVO_4 laser, Electrox, Lasers for Industry, Japan.

80. D. C. Montgomery, "Design and Analysis of Experiments", 2011, Fifth Edition, John Willet & Sons Inc, New York.

81. W. G. Cochram, G. M. Cox, "Experimental Design", 1997, Asia Publishing House, 2nd Ed., India.

82. H.C.T. Ricardo, D. Kalyanmoy, F.W. Elizabeth, G. Salvatore, "Evolutionary Multi-criterion Optimization", 2011, Springer, Singapore.

83. Laser manual for CNC pulsed diode pumped fiber laser, Sahajanand Laser Technology, Ahmedabad, India.

84. A.I. Khuri and S. Mukhopadhyay, "Response Surface Methodology", 2010, John Wiley & Sons Inc., WIREs Comp Stat , Volume 2, 128–149.